ISSN: 2161-4954 Volume 6, Number 2, June 2016

Scientific Research Publishing

World Journal of Nano Science and Engineering

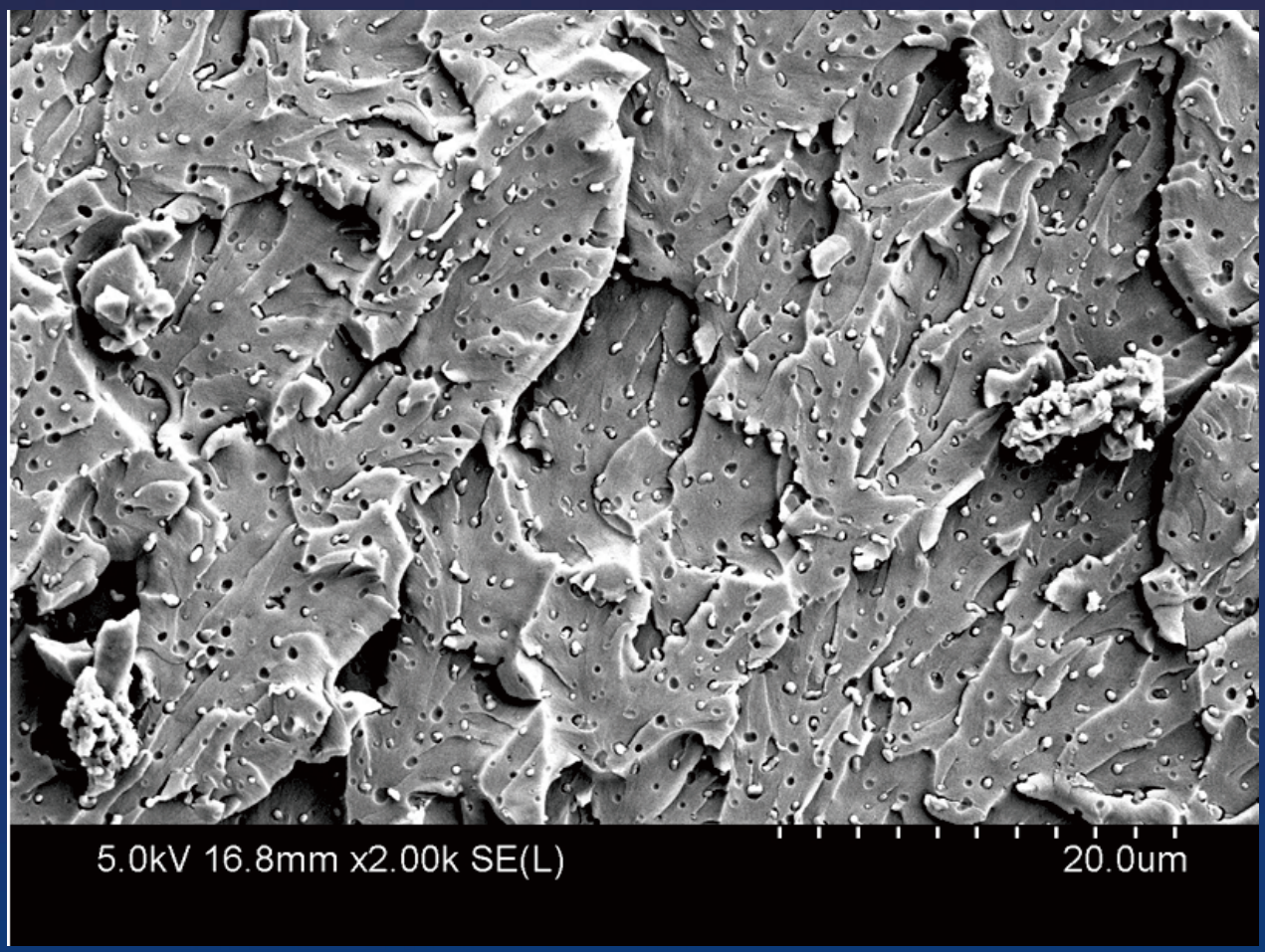

ISSN: 2161-4954

www.scirp.org/journal/wjnse

Journal Editorial Board

ISSN 2161-4954 (Print) ISSN 2161-4962 (Online)
http://www.scirp.org/journal/wjnse

Editor-in-Chief

Editorial Board

World Journal of Nano Science and Engineering, 2016, 6, 45-110
Published Online June 2016 in SciRes. http://www.scirp.org/journal/wjnse

Table of Contents

Volume 6 Number 2 June 2016

The figure on the front cover is from the article published in World Journal of Nano Science and Engineering, 2016, Vol. 6, No. 2, pp. 58-63 by Salwan Al-Assafi, Nils de Bruijn, Ahmed M. Al-Jumaily.

World Journal of Nano Science and Engineering (WJNSE)

Journal Information

SUBSCRIPTIONS

The *World Journal of Nano Science and Engineering* (Online at Scientific Research Publishing, www.SciRP.org) is published quarterly by Scientific Research Publishing, Inc., USA.

Subscription rates:

Print: $69 per issue.
To subscribe, please contact Journals Subscriptions Department, E-mail: sub@scirp.org

SERVICES

Advertisements
Advertisement Sales Department, E-mail: service@scirp.org

Reprints (minimum quantity 100 copies)
Reprints Co-ordinator, Scientific Research Publishing, Inc., USA.
E-mail: sub@scirp.org

COPYRIGHT

PRODUCTION INFORMATION

For manuscripts that have been accepted for publication, please contact:
E-mail: wjnse@scirp.org

World Journal of Nano Science and Engineering, 2016, 6, 45-50
Published Online June 2016 in SciRes. http://www.scirp.org/journal/wjnse
http://dx.doi.org/10.4236/wjnse.2016.62005

Electrospinning and Electrospun Nanofibers

Lefayet Sultan Lipol, Md. Moshiur Rahman

University of Borås, Borås, Sweden
Email: lefayetbd@gmail.com

Received 31 December 2015; accepted 12 April 2016; published 15 April 2016

Abstract

Electro-spinning is a very modern process which can be used in various purposes. We did this experimental work at Swerea IVF in Sweden during M. Sc in Textile Technology programme at University of Borås. We should especially thank our supervisor—Anna Thorvaldsson and course teacher—Ioannis S. Chronakis. In this report, we have tried to explain the basic manufacturing techniques of the electrospun nanofiber by the electro-spinning, how one can characterize it by SEM (Scanning Electron Microscopy) and its various applications in the practical field, e.g wound healing, Tissue Engineering Scaffold. The experimental work helped us a lot to gather sufficient knowledge about the electro-spinning process which we wanted to share with all.

Keywords

Nano-Fibers, Tissue Engineering Scaffold, Nano-Collagen, Cartilage and Bones, Bladder and Kidney, SEM (Scanning Electron Microscopy)

1. Background

Electro-spinning is a best way of producing fibers in nano and micro size scale. A polymer solution is fed through a syringe with a metal needle. A high voltage is connected between the needle and a grounded collector, creating an electric field in which the fiber is immensely stretched upon its way to collector. The stretching together with evaporation of the solvent renders fibers in nano to micro size to be collected on the collector. Applications of the nanofibers are sound absorption, filters, sensors and biomedicine.

1.1. Factors Are Affecting Electro-Spinning Process

Viscosity, pressure of the pump, distance between plate and needle, the electric field, type of fiber and solution, temperature, different kind of plate, drying the fabric after fabrication [3].

1.2. Key Dimensions

Polymeric nano-fibers: 50 nm to 1 micro; blood cell: 5 micro; human hair: 20 - 30 micro [3].

How to cite this paper: Lipol, L.S. and Rahman, Md.M. (2016) Electrospinning and Electrospun Nanofibers. *World Journal of Nano Science and Engineering*, **6**, 45-50. http://dx.doi.org/10.4236/wjnse.2016.62005

1.3. Remarkable Features

1) Technological Motivation;
2) High surface area per unit mass;
3) (diam. of 100 nm - 1000 m^2/g);
4) Small and specific pore size;
5) Extremely long length (kilometers);
6) 3D continuous structures (unlike CNT, nanorods);
7) High axial strength combined with extreme flexibility;
8) Mixture of polymers is feasible;
9) Alignment of nanofibers (nanotubes & nanowires) is feasible;
10) Nanoparticles can be encapsulated;
11) Variety of cross-sectional shapes & sizes;
12) Various routes for functionalization (PVD, CVD etc.);
13) Cost effective top-down nanomanufacturing process (compared to bottom up) [3].

2. The Basic Set Up for Electro-Spinning

In **Figure 1**, It consists of three major components: a high voltage power supply, a spinneret (a metalic needle), and a collector (a grounded collector).

The spinneret is connected to a syringe in which the polymer solution (or melt) is hosted. With the use of a syringe pump, the solution can be fed through the spinneret at a constant and controllable rate. When a high voltage (usually in the range of 1 to 30 kV) is applied, the pendent drop of polymer solution at the nozzle of the spinneret will become highly electrified and the induced charges are evenly distributed over the surface. As a result, the drop will experience two major types of electrostatic forces: the electrostatic repulsion between the surface charges; the coulombic forces exerted by the external electric field.

Under the action of these electrostatic interactions, the liquid drop will be distorted into a conical object commonly known as Taylor cone. Once the strength of the electric field has surpassed a threshold value, the electrostatic force can overcome the surface tension of the polymer solution and thus force the ejection of a liquid jet from the nozzle. The electrified jet then undergoes a stretching and whipping process, leading to the formation of a long and thin thread. As the liquid jet is continuously elongated and the solvent is evaporated, its diameter can be greatly reduced from hundreds of micrometer to as small as tens of micrometers. Attracted (opposite charge) by the grounded collector placed under the spinneret, the charged fiber is often deposited as a randomly oriented, non-woven mat [1].

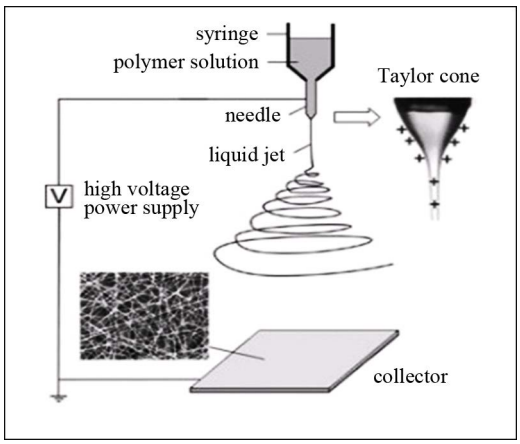

Figure 1. Schematic illustration of the basic set up for the electro-spinning [1].

2.1. How Does the Fibers Become So Thin

a) Bending instability so every loop grows larger and larger;

b) The jet streches and becomes thinner;
c) The jet can be sterched untill the diameter is about 100 nm [3].

2.2. Control of Electro-Spun Nanofibers

a) Control of Morphology and Diameter;
b) Control of Chemical Composition: (Functional Polymers & Blends, Encapsulation of Functional Nanomaterials, Modification of Nanofibers);
c) Control of Secondary Structures: (Core/Sheath Nanofiber Structures, Hollow Interiors Nanofibers, Porous Nanofiber Structures) [3].

2.3. Examples of Polymer-Solvents System

In Table 1, we mention here names of the some polymers and the solvents are used for producing electro-spun nano-fibers.

Table 1. Polymer-solvent system [3].

Sl. No.	Polymers	Solvents
01	Nylon 6 and nylon 6, 6	Formic acid
02	Polyacrylonitrile	Dimethyl Formaldehyde
03	PET	Trifluroacetic acid/Dimethyl chloride
04	PVA	Water
05	Polystyrene	DMF/Toluene
06	Nylon-6-co-polyamide	Formic acid
07	Polybenzimidazole	Dimethyl acetamide
08	Polyramide	Sulfuric acid
09	Polyamides	Phenol

2.4. Nanofiber with Core/Sheath Structure

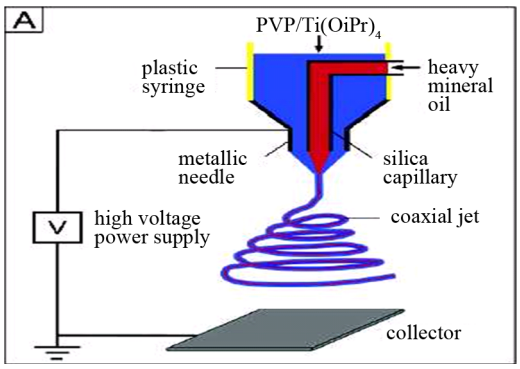

Figure 2. Nanofibers with core/sheath structure [1].

From the above shown process in Figure 2, we can make the nanofibers with hollow interiors, nanofibers with porous structures.

The spinneret has two coaxial capillaries. The silica capillary contains mineral oil while the solution in the plastic syringe is containing poly (vinyl pyrrolidone)/(PVP) and titanium tetraisopropoxide/$Ti(OiPr)_4$ were simultaneously ejected to form a compound jet [1].

3. Sputtering in SEM

- In Figure 3, the electro-spun nanofiber with the coating of the gold is used. The gold is used for more visibility

of the electro-spun nanofibers under Scanning Electron Microscopy (SEM). The fiber is set over a slide before putting under SEM.

- The polymer was used Eudragit (Methacrylic acid)—15% with Solvent: 1:1 Ethanol/Formic acid to form the electro-spun nanofibers which was observed under SEM to predict the characteristics.

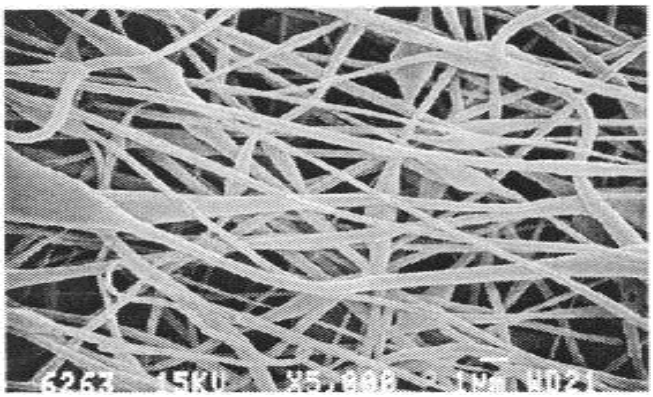

Figure 3. Nanofibers on SEM [2].

We can evaluate the fiber performance by using scanning electron microscopy (SEM) and contact angle measurements. If the contact angle of the fiber surface with liquid is high, the fiber is hydrophobic. Sessile drop can be used as liquid [2].

4. Application of Nanofibers

The applications of nanofibers are mentioned in **Table 2** (summary of the application of the Nanofibers).

Table 2. Application of nanofibers [3].

Sl. No.	The area of the applications	Applications
01	**Nanosensors**	Nanoelectronics, optical devices, nanowires, interconnect.
02	**Coating**	Protective clothing, sound absorption.
03	**Biomedical applications**	Wound healing, artificial skin, scaffolding, tissue engineering.
04	**Nano filter media**	nano membranes
05	**Other industrial applications**	Nanocomposites, nanoceramics, nano catalysts

4.1. Wound Healing

Polyurethane dressing: EVOH electro spun directly onto a human hand. EVOH is just a medical application polymer (Ethylene-vinyl alcohol copolymer) [3].

4.2. Features of Material Use as Tissue Engineering Scaffold

Various specific shape for specific applications, porosity of membranes for skin, hydrophillicity, biodegradation property, conductivity, filtration, binding ability, flexibility, tolerate sudden force, cell adhesion and migration. Tengion is one of very few companies making business of tissue engineered products. They produced tissue engineered bladders. Because it is very simple tissue to manufacture, it is easy to biomimic the bladder. Liver is complicated to imitate [2].

4.2.1. Important Features to Consider for Selecting Scaffold

It must tolerate certain force; it must have resiliency, high tear tension, elasticity, work of rupture [1].

4.2.2. Basic of Working of a Tissue Engineering Scaffold

The mixture of the cell and the salt (solution) on nanofibers surface increases attraction power of the cell because of salt and there may be some porosity as well on the cell. Salt gives away the cell in solution. Then these cells attract other cells to adjust with it [3].

4.2.3. Important Notes

Nanofiber is used to produce bladder commercially. The bladder is used to pass urine that comes from the kidney [2].

Water + dirt → Kidney (pure liquid) → Bladder (pass urine).

4.2.4. Difference between Injection and Implantation

If we inject something that is injection, making two layers and then insert scaffold is implantation [2].

4.3. Drug Delivery

It can be observed porosity or hole in the nanofibers under Scanning Electron Microscopy (**Figure 3**). One can insert drug in that specific regions. After that one will implant it in the patient's body. Because of porosity, drug can move from the fiber as well as they have hydrophillicity. This is the reason why drugs are dispersed in the blood and in that way the fiber can be used to deliver drug in the fiber. In addition, the fibers are biodegradable so they will not create any problem in the human body.

When doctors make operation of a patient, they need to put medicine on a specific region. This is the reason why they need one carrier to hold the medicine on the exact place. The electrospun nanofibers are used for this purpose. The fibers do not create any problem in the human body in the long run as it is biodegradable [2].

4.4. Difference between Cartilage and Bones

In cartilage has no blood vessels but in bone has blood vessels. Cartilage is a soft bone found in ear, nose. Cartilage absorbs the forces that bones applied so the bone can recover to a large extent if it is forced by external objects.

We can make a hole over the bones or cartilage as well as insert the blood in holes, coagulate the blood. And this blood attracts other cells and helps to the cells grow over it. In a word, blood work like a scaffold there [2].

4.4.1. Nanocollagen

It is used to replace damaged blood vessels [2].

4.5. Air Filtration

Air filtration by nanofiber is cheaper than commercial air filtration process as well as it is more effective.

Moreover, nanofibers can be used for the liquid filtration and to for the acoustic insulation [4] [5].

5. Discussion

Electro-spun fibers are produced according to **Figure 1**. It is necessary to use polymer and solvent together for producing nanofibers. When a high voltage is applied, the pendent drop of polymer solution at the nozzle of the spinneret will become highly electrified and the induced charges are evenly distributed over the surface. As a result, the drop will experience two major types of electrostatic forces. Under the action of these electrostatic interactions, the liquid drop will be distorted into Taylor cone. When the fibers will be formed, the solvent will be evaporated to the environment. The electro-spun nanofibers with porous structure can be formed according to **Figure 2**. We can insert required substances in the porous structure. The characteristics of the electro-spun nanofibers can be identified by Scanning Electron Microscopy. These fibers can be used for various purposes. For instance-wound healing, tissue engineering scaffold, drug delivery, air filtration etc.

6. Conclusion

Electro-spinning is the way to produce nanofibers which have various prolific applications. From this research

work, we have understood the manufacturing process of the electro-spun nanofibers and its characteristics and applications. This is the reason why we hope that the practical experience should help us in the future.

References

[1] Li, D. and Xia, Y.N. (2004) Electro-Spinning of Nanofibers: Reinventing the Wheel. Advanced Materials.

[2] (2009) Laboration Work at Swerea IVF (Supervisor-Anna Thorvaldsson). 5 March 2009, M. Sc in Textile Technology Program at University of Boras, Textile Fiber Material Course.

[3] (2009) Ioannis, S., Chronakis, Swerea IVF, M. Sc in Textile Technology Program, University of Boras, Lecture Materials of Textile Fiber Material Course.

[4] (2015) Elmarco Nano for Life. Date: 2015-07-14. http://www.elmarco.com/application-areas/air-filtration/

[5] (2015) Electro-Spun Nano-Fibers for Air Filtration. Date: 2015-07-14. http://www.sciencedirect.com/science/article/pii/S1877705813018092

About Authors

Author-1: I have completed B. Sc in Textile Technology from College of Textile Technology, Tejgaon, Dhaka-1208 under Dhaka University. My specialization was in wet processing technology.

In Sweden, I have completed three M. Sc degrees from Boras University. The degrees are-Textile Engineering, Applied Textile Management and Industrial engineering. I have published six international journals and 3 magazine papers. I worked in Sweden as Researcher at SP Technical Research Institute of Sweden. Presently, I work as Lecturer and Program coordinator of the Textile Engineering department at Fareast International University, Bangladesh.

Author-2: I have completed B. Sc in Textile Technology from Bangladesh University of Textiles (BUTEX), Tejgaon, Dhaka-1208. My specialization was in yarn manufacturing technology and obtained the 1st class.

I started my career as a Trainee Merchandiser at COTTON GROUP and then switched to EPYLLION GROUP as an Assistant Merchandiser. Then I worked at Matin Spinning Mills Ltd. (a sister concern of DBL GROUP) as an Executive in the department of Quality Control. Finally I joined at Northern University Bangladesh as a Lecturer in the department of textile engineering. At present, I am a permanent employee and attend at different programs arranged by this university.

World Journal of Nano Science and Engineering, 2016, 6, 51-57
Published Online June 2016 in SciRes. http://www.scirp.org/journal/wjnse
http://dx.doi.org/10.4236/wjnse.2016.62006

Technology of Porous Tantalum Production

Yu. Zh. Tuleushev, V. N. Volodin, E. A. Zhakanbaev, V. N. Lisitsin, A. A. Migunova, A. S. Suleymenova

Institute of Nuclear Physics, Almaty, Republic of Kazakhstan
Email: yuriy.tuleushev@mail.ru

Received 8 April 2016; accepted 6 June 2016; published 9 June 2016

Abstract

Ion-plasma sputtering and codeposition of ultrafine Ta and Cd particles on a moving substrate were used to prepare the solid solutions, in particular, the alloys with up to 66.2 at.% Cd in the form of coatings. In vacuum heat treatment cadmium evaporates at 700˚C from cadmium based solid solutions resulting in formation of a porous tantalum with a highly developed surface. The prepared tantalum-based materials assume the technological application of the investigation results.

Keywords

Tantalum, Cadmium, Porous Structures, Specific Surface

1. Introduction

The methods for preparing of porous metals, known to date, are multi-staged and complicated [1] [2]. The authors find it tempting to find an alternative method of preparing a porous refractory metal in the coating using the technique of magnetron sputtering with two magnetrons [3]-[6]. For this purpose, the most promising seems the preparation of a mixture of refractory metal (tantalum) with metal characterized by high vapor pressure at a relatively low temperature, cadmium.

It is known that tantalum and cadmium can't form the intermetallic compounds and alloys [7]. Tantalum has two modifications: α-Ta with a body-centered cubic lattice a = 0.3305 nm and β-Ta with a tetragonal lattice (a = 1.0194 and c = 0.5313 nm). It is known [8], that β-Ta is produced in the form of fine-grained powder using electrolysis of salt melts. The papers [9] [10] report about β-Ta thin films preparation by dc-magnetron sputtering. Subsequent heating to 1000˚C is accompanied by an irreversible β-Ta to α-Ta transition that confirms the meta-stability of the β-phase. The mechanism of β-Ta formation and the features of the crystal lattice belonging to this phase are described in [11].

Our preliminary studies related to the preparation of tantalum coatings by ion-plasma sputtering showed that the change of tantalum modification may be due to the concentration of dissolved metal [3], as well as the size

How to cite this paper: Tuleushev, Yu.Zh., Volodin, V.N., Zhakanbaev, E.A., Lisitsin, V.N., Migunova, A.A. and Suleymenova, A.S. (2016) Technology of Porous Tantalum Production. *World Journal of Nano Science and Engineering*, **6**, 51-57.
http://dx.doi.org/10.4236/wjnse.2016.62006

of ultra dispersed particles.

The potential application of film tantalum in the form of porous coating, prepared as an alloy and followed by removal of the second metal, has determined the interest towards possible preparation of tantalum-cadmium solid solutions and their structure. The peculiarity of this system is the absence of cadmium solubility in tantalum under normal conditions and the high pressure of cadmium vapor at relatively low temperatures (boiling temperature at atmospheric pressure is 766.3˚C), which determines the possibility to transfer cadmium from solutions into the vapor at relatively low temperatures [9] with the pores remaining in the tantalum matrix.

In this regard, the aim of the completed investigation was to study the morphology, the phase composition, depending on metals concentration, and the thermal resistance of the tantalum-cadmium coatings.

2. Experimental

We studied the tantalum-cadmium films prepared by codeposition of ultrafine particles of the metals, which were obtained by ion-plasma sputtering on cols substrates made from monocrystalline silicon.

We used tantalum with 99.96 mas.% of main element and cadmium (99.99 mas.%) in the form of targets 40 mm in diameter and 4 mm thick for application of film coatings. Argon was used as the plasma-forming gas, purified with a sputtered titanium getter.

Samples of coatings were prepared by the procedure implying ion-plasma sputtering of tantalum and cadmium and cooperative deposition of ultra dispersed particles on the substrates moving with respect to plasma flows in the form of short period (with a low number of crystal lattice periods) sublayers that form films of 0.7 - 3.1 μm total thickness. The velocity of substrate movement was 5×10^{-2} m·s^{-1} with respect to metal containing plasma flow. The sputtering was performed with the simultaneous use of two magnetrons located opposite one another; the spacing between magnetrons was separated by a unit for the substrates movement.

The composition of coatings was controlled by varying the powers supplied to magnetrons sputtered tantalum and cadmium targets. The concentration of deposited metals was verified by the weighing method, *i.e.* the amounts of each metal sputtered and deposited during the formation of coating were determined [3]-[6]. The film thickness was determined by Rutherford proton back-scattering spectrometry using UKP-2-1 tandem accelerator in the Institute of Nuclear Physics (Republic of Kazakhstan) and was calculated using the amounts of deposited metals. Electron-microscopic studies were performed using a JEM-8230 (JEOL) electron-microprobe analyzer. The X-ray diffraction studies were performed using a D8 Advance (Bruker) diffractometer with copper irradiation $\lambda_{k\alpha} = 0.154051$ nm and graphite monochromator in the Θ-2Θ mode. The lattice parameters were determined by averaging of the magnitudes obtained using all diffraction reflections of the identified phase.

High-temperature annealing was performed in a vacuum high-temperature furnace that was designed based on URVT-2500 unit.

3. Results and Discussion

The samples of tantalum-cadmium films containing 0.7 - 87.6 at.% Cd were prepared and the phase composition of the coatings was determined. To study the thermal stability of the prepared tantalum-cadmium coating, the isochronous (1 h) vacuum annealing at 300˚C - 700˚C (with 100˚C step) were performed.

The phases identified in the film coating and the calculated parameters of the lattice in the initial state are shown in **Table 1**.

The phase analysis of the samples showed that, as the cadmium content in the Ta-Cd coatings changes, the following four concentration ranges can be distinguished: 0 - 44.0 at.% Cd range corresponding to existence of β-Ta phase; 48.8 - 56.6 at.% Cd range corresponding to existence of β-Ta and α-Ta phases; 59.6 - 66.2 at.% Cd range, corresponding to α-Ta only; 74.4 - 100 at.% Cd corresponding to the presence of cadmium and amorphous tantalum. At cadmium content of 48.8 at.% the β-Ta phase is highly grain-orientated (001), therefore it is not possible to determine the lattice parameters a and b. The parameters of β-Ta lattice slightly linearly decrease with cadmium concentration increase in the coating in accordance with the dependencies: a [nm] = $1.0186 - 3 \times 10^{-6} x_{Cd}$; c [nm] = $0.5319 - 3 \times 10^{-5} x_{Cd}$, hereinafter x_{Cd} is the cadmium concentration, at.%.

It is known from [9] that the atomic radius of Ta and Cd is 0.1626 nm and 0.1727 nm, respectively. Considering these values, formation of a substitute solid shall be accompanied by the increase in the β-Ta lattice parameter during placing of the impurity atoms in the basal planes of the unit cell. The opposite variations in the cell parameters indicate the presence of cadmium atoms in the internal channels of β-tantalum unit cell [10], as

Table 1. Identified phases and parameters of their lattices in the tantalum-cadmium films.

Cd concentration in the coating, at.%	β-Ta, tetragonal lattice, nm		α-Ta, cubic lattice, nm	Cd, hexagonal lattice, nm	
	a	*c*	*a*	*a*	*c*
6.7	1.0095 ± 0.0018	0.5333 ± 0.0018	-	-	-
9.9	1.0213 ± 0.0010	0.5307 ± 0.0010	-	-	-
13.9	1.0214 ± 0.0011	0.5310 ± 0.0011	-	-	-
17.0	1.0207 ± 0.0007	0.5306 ± 0.0007	-	-	-
17.3	1.0204 ± 0.0005	0.5307 ± 0.0005	-	-	-
22.9	1.0224 ± 0.0011	0.5301 ± 0.0011	-	-	-
25.3	1.0199 ± 0.0012	0.5335 ± 0.0012	-	-	-
30.4	1.0145 ± 0.0007	0.5319 ± 0.0007	-	-	-
38.0	1.0215 ± 0.0009	0.5300 ± 0.0009	-	-	-
44.0	1.0153 ± 0.0002	0.5343 ± 0.0002	-	-	-
48.8	-	0.5334	0.3343 ± 0.0001	-	-
56.6	1.0740	0.5338	0.3340 ± 0.0038	-	-
61.3	-	-	0.3361 ± 0.0002	-	-
66.2	-	-	0.3351 ± 0.0001	-	-
74.4	-	-	-	0.29769	0.56154
75.4	-	-	-	0.29772	0.56136
87.6	-	-	-	0.29785	0.56114

for Ta-Cu system [2].

Formation of cadmium solid solution in α-Ta is accompanied by a slight increase in the size of the body-centered cubic lattice within the concentration range of the phase existence according to the dependence: a [nm] = $0.3305 + 8 \times 10^{-5} x_{Cd}$, enabling us to suggest the formation of a substitution solid solution.

The opposite variations of the lattice parameters a [nm] = $0.2968 + 1 \times 10^{-5} x_{Cd}$ and c [nm] = $0.5633 - 3 \times 10^{-5} x_{Cd}$ allow us to assume the interstitial arrangement of tantalum atoms in the basal plane of cadmium hexagonal crystal lattice of coatings corresponding to the mentioned concentration range of coatings composition.

SEM studies of the morphology of the coating in the initial state and after annealing were performed for the compositions with 30.4, 56.6 and 74.4 at.% Cd.

The electron-microscopic studies showed that, in the initial state with 30.4 at.% Cd (see **Figure 1**) the coating is characterized by a flat surface with fine projected crystallites of 300 - 400 nm maximal size.

After annealing at 700˚C the sizes of projected formations decreases; between some crystallites small pores less than 100 nm in lateral size are present, which result from the evaporation of cadmium from the solid solution.

Figure 2 provides the diffraction patterns of the coating with 30.4 at.% Cd in the initial state (spectrum a) and after annealing at 300˚C (spectrum b), 600˚C (spectrum c) and 700˚C (spectrum d).

In the initial state and after annealing at 400˚C, 500˚C and 600˚C the coating is represented by β-tantalum phase (**Figure 2**, spectra a-c). At the increase of annealing temperature up to 700˚C the coating is represented by a mixture of α- and β-Ta phases (**Figure 2**, spectrum d). The parameter of the body-centered cubic lattice α-Ta is $a = 0.3311 \pm 0.0001$ nm.

With increase of vacuum heat treatment temperature from 300˚C to 700˚C, accompanied with cadmium evaporation from its solid solution with tantalum, the parameters of the β-Ta lattice increases relatively to those determined in the initial sample. If the parameter c of the tetragonal lattice approaches the tabular value, the parameter a significantly exceeds it. In our opinion, this can be explained by thermally initiated process of cadmium atoms replacement from the internal channels of the unit cell of β-tantalum into the nodes, located in the basal plane ab. It follows that in the internal channels the impurity atoms have a lower energy than those in the nodes,

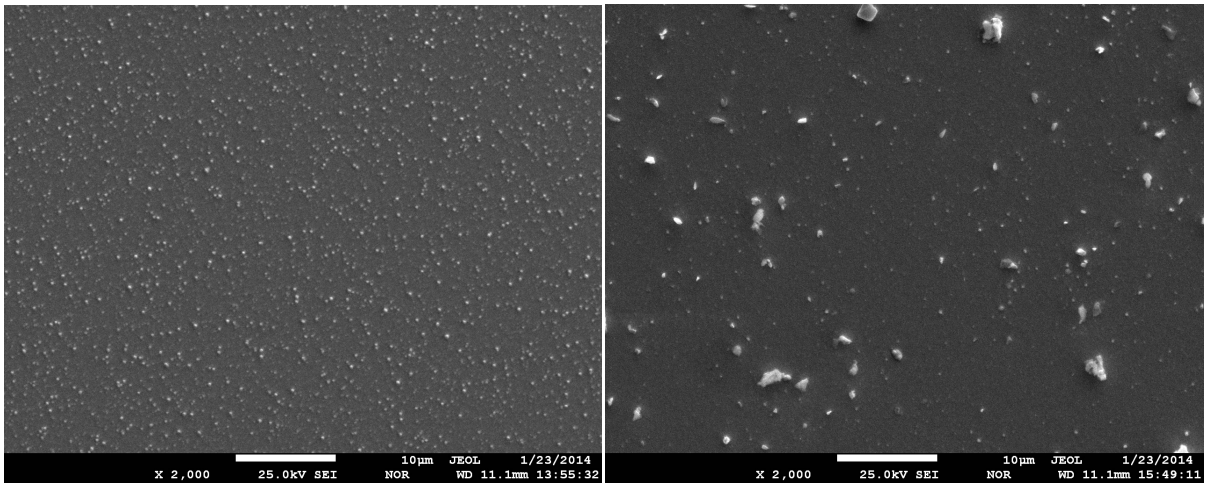

(a) (b)

Figure 1. SEM micrographs of the coating with 30.4 at.% Cd before (a) and after annealing at 700˚C (b).

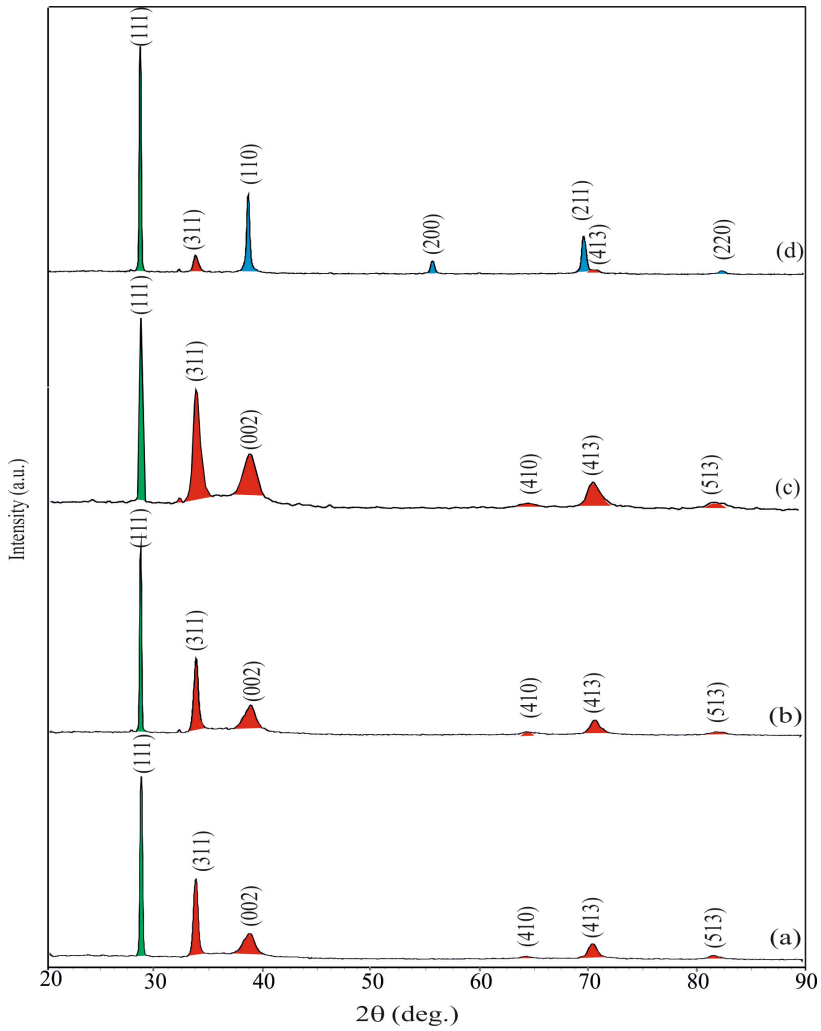

Figure 2. X-ray diffraction patterns of the coating with 30.4 at.% Cd: 1—in the initial state, 2—after annealing at 300˚C; 3—the same at 600˚C; 4—the same at 700˚C; —β-Ta; —α-Ta; —Si (substrate).

located in the basal plane *ab*.

The annealing of the sample with 56.6 at.% Cd, which in the initial state, consists of the fine-grained mixture of α- and β-Ta phases, showed their stability up to the temperature 600˚C, while at 700˚C the major portion of β-Ta modification transforms into α-tantalum. The electron-microscopic study of this sample (**Figure 3**) enabled us to find the existence of a great amount of through pores after annealing at 700˚C compared with the sample with 30.4 at.% Cd.

The phase composition of coating with 74.4, 75.4 and 87.6 at.% Cd is represented by cadmium with a hexagonal lattice and amorphous tantalum (**Figure 4**), the amount of which (according to halo) decreases with increasing of cadmium content in the coating. In this case, the lattice parameters of cadmium slightly vary irregularly from a = 0.29769 nm and c = 0.56154 nm at 74.4 at.% Cd to a = 0.29785 nm and c = 0.56114 nm at 87.6 at.% Cd, respectively.

This fact allows us to state that the coating contains the solid solution of tantalum in cadmium with the hexagonal lattice. Since a portion of tantalum precipitates in the form of individual amorphous phase, it was impossible to calculate the amount of tantalum dissolved in cadmium.

SEM studies of the morphology of the coating with 74.4 at.% Cd showed that the coating in the initial state is represented by the conglomerate of closely adjoining crystallites of the round shape (**Figure 5(a)**). After vacuum annealing at 700˚C the surface of the coating is characterized by the presence of elements with similar shape to that of crystallites in the initial sample (**Figure 5(b)**), free of cadmium according to the X-ray diffraction analysis. The microprobe analysis of the same sample after annealing showed cadmium concentration in the coating at the detection limit. That is, the thermal stability of the coatings with high cadmium content is very low at low pressures the temperature increase is accompanied by almost complete evaporation of the latter.

This behavior of the tantalum-cadmium film coating makes it possible to prepare a porous tantalum with the developed surface by forming the film with Ta concentration less than 30 at.% (Cd is remaining) and subsequent distillation of volatile metal.

The assessment of the specific surface area of the film tantalum and porous tantalum coating, performed by BET method, revealed the increase in the specific surface area by at least 277.5 m^2/g Ta only because of pore 10 nm in diameter.

4. Conclusions

The performed studies have shown that magnetron preparation of coatings from a mixture of tantalum and cadmium, and subsequent removal of cadmium from the coating by vacuum annealing can be used to prepare the coatings from a porous tantalum with a very developed surface area. It is shown that porous tantalum has a body-centered cubic lattice, *i.e.*, it is α-tantalum and formed by recrystallization of the amorphous tantalum.

The obtained results of the study may be applied for other binary systems consisting of metals and materials

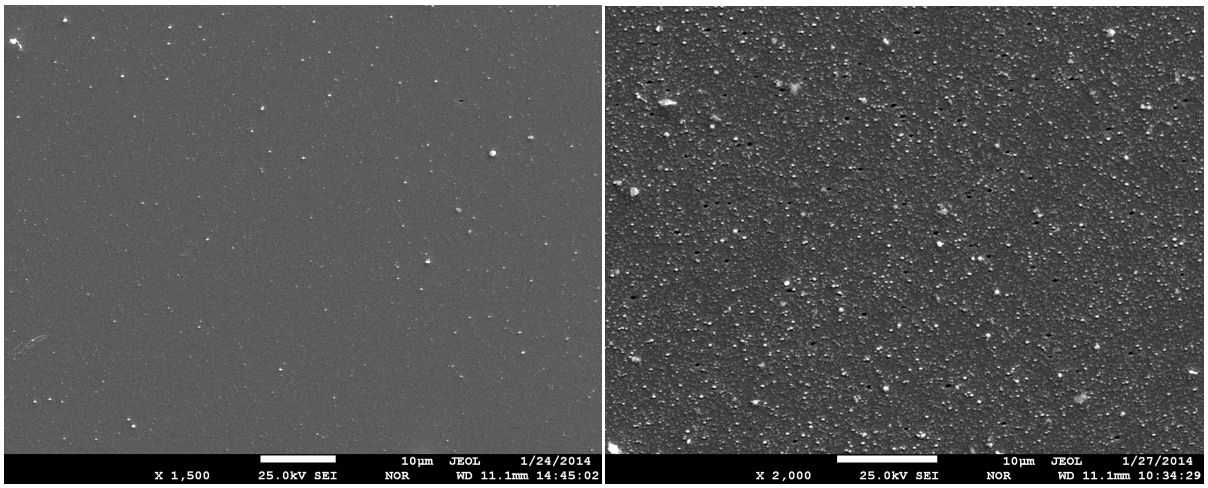

(a) (b)

Figure 3. SEM micrographs of the coating with 59.6 at.% Cd before (a) and after annealing at 700˚C (b).

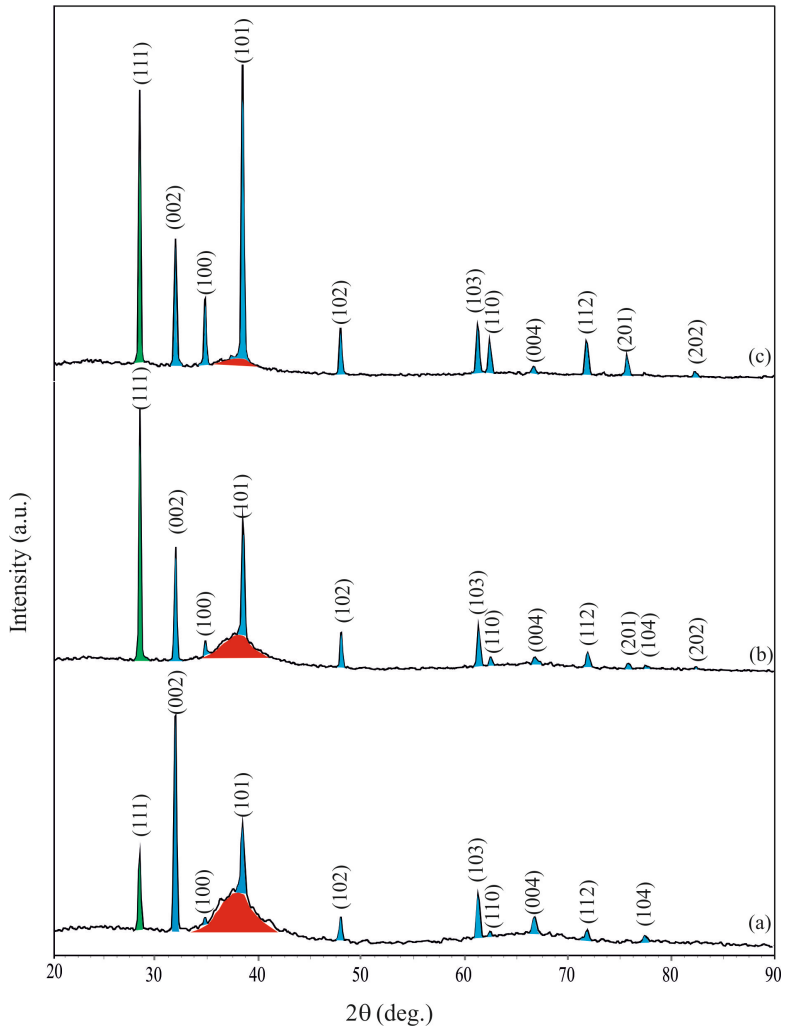

Figure 4. X-ray diffraction patterns of the Ta-Cd coatings with at.% Cd: 1—74.4; 2—75.4; 3—87.6; —Cd; —amorphous Ta; —Si (substrate) with orientation (111).

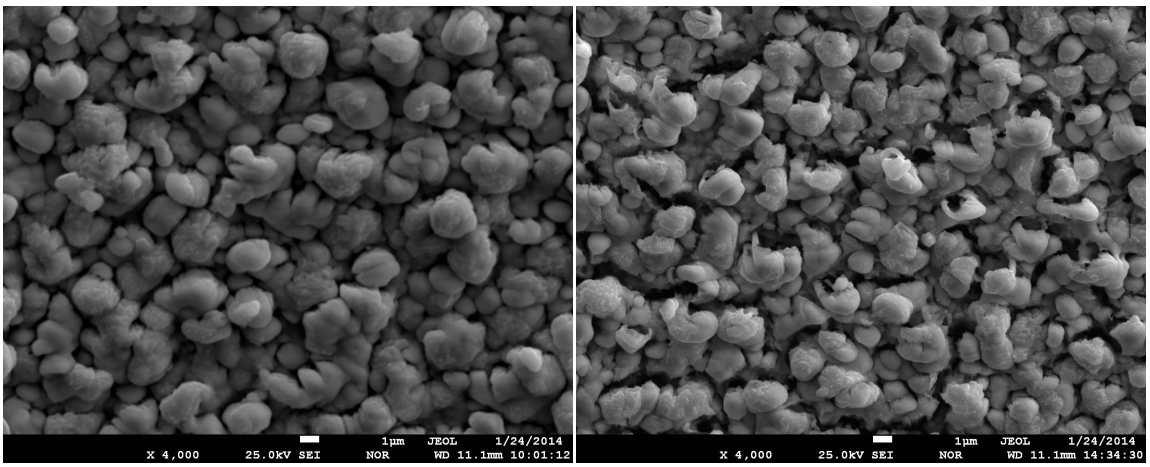

(a) (b)

Figure 5. SEM micrographs of the coating with 74.4 at.% Cd in the initial state (a) and after annealing at 700˚C for 1 hour (b).

with similar properties.

Acknowledgements

This study was supported by the Committee for Science of the Ministry of Education and Science of the Republic of Kazakhstan, grant No. 1457/GF4.

References

[1] Fife, J.A. (1991) Fibrous Tantalum and Capacitors Made Therefrom. Patent US 5306462 A.

[2] Dobrusin, S.Y., Obgolts, O.J., Kachalov, N.A., Frolova, N.M., Chernikov, I.I. and Berezko, V.I. (2011) The Method for Preparation of Fibrous Tantalum Powder and Fibrous Powder of Tantalum. Patent RU 2349423.

[3] Tuleushev, Yu.Zh., Volodin, V.N. and Zhakanbaev, E.A. (2013) Nanosize β-Tantalum Coatings: Formation, Structure, and Properties. *The Physics of Metals and Metallography*, **114**, 573.

[4] Volodin, V.N., Tuleushev, Yu.Zh. and Zhakanbaev, E.A. (2014) Structure of Niobium-Tungsten Alloy Films Produced by Metal Sputtering. *Journal of Surface Investigation*. *X-Ray*, *Synchrotron and Neutron Techniques*, **8**, 1146-1151. http://dx.doi.org/10.1134/s1027451014060160

[5] Volodin, V.N., Tuleushev, Yu.Zh. and Zhakanbaev, E.A. (2013). Structure of Sputter-Deposited Films of β-Tantalum-Aluminum Alloys. *The Physics of Metals and Metallography*, **114**, 935-939. http://dx.doi.org/10.1134/S0031918X13110136

[6] Volodin, V.N., Tuleushev, Yu.Zh. and Zhakanbaev, E.A. (2015) Structure and Phase Composition of Niobium-Copper Deposited Films. *Journal of Surface Investigation*. *X-Ray*, *Synchrotron and Neutron Techniques*, **9**, 178-183. http://dx.doi.org/10.1134/S1027451015010371

[7] Barabash, O.M. and Koval. Yu.N. (1986) The Crystal Structure of Metals and Alloys. Sciences, Kiev, Dumka.

[8] Moseley, P.T. and Seabrook, C.J. (1973) The Crystal Structure of β-Tantalum. *Acta Crystallographica*, **B29**, 1170.

[9] Kwon, K.-W., Ryu, C., Sinclair, R. and Wong, S.S. (1997) Evidence of Heteroepitaxial Growth of Copper on Beta-Tantalum. *Applied Physics Letters*, **71**, 3069. http://dx.doi.org/10.1063/1.119439

[10] Lee, S.L., Doxbeck, M., Mueller, J., Cipollo, M. and Cote, P. (2004) Texture, Structure and Phase Transformation in Sputter Beta Tantalum Coating. *Surface and Coatings Technology*, **177-178**, 44-51. http://dx.doi.org/10.1016/j.surfcoat.2003.06.008

[11] Arakcheeva, A., Chapius, G. and Grinevich, V. (2002) The Self-Hosting Structure of β-Ta. *Acta Crystallographica*, **B58**, 1-7. http://dx.doi.org/10.1107/S0108768101017918

World Journal of Nano Science and Engineering, 2016, 6, 58-63
Published Online June 2016 in SciRes. http://www.scirp.org/journal/wjnse
http://dx.doi.org/10.4236/wjnse.2016.62007

Processing and Characterization of PMMA Nanofiber Reinforced Epoxy Composites

Salwan Al-Assafi[1*], Nils de Bruijn[2], Ahmed M. Al-Jumaily[1]

[1]Institute of Biomedical Technologies, Auckland University of Technology, Auckland, New Zealand
[2]Academie for Technology, Health and Environment, Avans University of Applied Sciences, Breda, Netherlands
Email: *Salwan.alassafi@aut.ac.nz

Received 2 May 2016; accepted 13 June 2016; published 16 June 2016

Abstract

Growing demand for high-performance materials is driving the development of composites with nano material reinforcement. The use of nano reinforcement can provide a distinct advantage due to high surface area of the material. There are still many challenges in achieving the full potential of nanocomposites. In this paper, we investigate the performance of epoxy nanocomposites reinforced with short polymethyl methacrylate (PMMA) nanofibers. PMMA nanofibers were chopped and mixed with the epoxy resin and then the mixture was poured into a mould. Samples were cut to an appropriate size after cure and mechanical testing was carried out. Tensile and flexural strength and modulus were evaluated for samples with various fiber volume fractions to determine changes in mechanical performance. Also Scanning Electron Microscopy was utilized to investigate fracture surface and fiber-matrix interface. Results indicated that mechanical performance dropped as volume fraction of fibers increased, namely poor fiber-matrix adhesion and presence of porosity resulted in deterioration in strength and modulus. Further research is required to develop fiber coating system to enhance performance of the nanocomposite by improving fiber-matrix adhesion and fiber wet-out.

Keywords

Nanocomposite, Nanofiber, Epoxy, Electrospinning, PMMA, Polymer, Composites

1. Introduction

There is a growing interest in using nanofibers as reinforcement for composites. The high surface area of nano-

*Corresponding author.

How to cite this paper: Al-Assafi, S., de Bruijn, N. and Al-Jumaily, A.M. (2016) Processing and Characterization of PMMA Nanofiber Reinforced Epoxy Composites. *World Journal of Nano Science and Engineering*, **6**, 58-63.
http://dx.doi.org/10.4236/wjnse.2016.62007

fibers coupled with good fiber-matrix bonding offers exceptional properties due to the high fiber-matrix interface area [1]. One of the common techniques to produce nanofibers is electrospinning [2]-[6]. This process is recognised as an efficient technique to produce nanofibers from polymer solutions or melts and it dates back to the early 1930s [2] [3]. In this technique, an electric field is used to produce an electrically charged jet of polymer solution or polymer melt flowing out of pendant or sessile droplet [4]. Electrical forces stretch and thin the jet as it flows away from the droplet producing nanofibers in the range of 100 nm or less. Many applications have been reported for electrospun fibers, such as drug delivery, filtration, energy generation, and other applications [5]. The focus of this study is on the use of nanofibers in the reinforcement of composites.

Several studies have been conducted on utilizing nanofibers in the reinforcement of composites [7]-[15]. Song Lin *et al*. investigated reinforcement of 2,2-bis-[4-(methacryloxypropoxy)-phenyl]-propane (Bis-GMA) dental resin system with PAN core-PMMA shell nanofiber fabric prepared by electrospinning method [12]. Strong adhesion was reported between the nanofibers and the matrix, and consequently the mechanical performance was significantly improved. Compared to neat resin, flexural strength, flexural modulus and work of fracture improved by 18.7%, 14.1% and 64.8% respectively, after adding 7.5 wt% PAN-PMMA nanofibers.

Alejandro J. Rodriguez *et al*. studied reinforcement of polymer composites using multiscale-reinforcement fabrics (MRFs) [8]. The MRFs were fabricated by electrophoretic deposition of carbon fibers on the surface of carbon fiber layers. Improvements of 12% in interlaminar shear strength and 13% in compressive strength were reported. It was observed that failure mechanism was a combination of matrix detachment from the surface of the fiber and matrix failure.

The use of short electrospun polymeric nanofibers as reinforcement for nanocomposites has also been investigated [10] [11]. Nylon-6 and polyimide electrospun nanofiber mats were cut and dispersed for nanocomposite films at various nanofiber weight fractions. Results showed an improvement of 185% in the elastic modulus after adding 3.5 wt% short nylon-6 nanofibers to a matrix of thermoplastic urethane. This significant increase was attributed to strong nanofiber-matrix adhesion due to hydrogen bonding, however, lower improvement was reported when the nylon-6 nanofibers were used to reinforce PMMA matrix due to poor nanofiber-matrix adhesion caused by absence of hydrogen bonding. Shaohua Jiang *et al*. showed that the use of short nanofibers could be more efficient than long nanofibers [11]. The addition of 2 wt% polyimide nanofibers to polyimide matrix helped in improving tensile strength and modulus by 53% and 87% respectively. However, to achieve performance similar to that for the 2 wt% nanofiber composites, 38 wt% of continuously long fibers were required. The superior performance of the short nanofiber was attributed to the improved dispersability of the short nanofibers in the matrix polymer.

In this study, the use of short electrospun PMMA nanofibers in reinforcing epoxy resin has been assessed. Flexural and tensile properties were determined for epoxy samples with various nanofiber weight fractions. Furthermore, scanning electron microscopy (SEM) was utilized to examine fracture surface of the nanocomposite samples.

2. Experimental Protocol

2.1. Materials

Electrospun PMMA nanofibers in mat form were supplied by Revolution Fibres Ltd, Auckland, New Zealand. Average diameter range for the nanofibers was 150 nm - 200 nm, and nanofiber deposition weight was 0.5 - 15 g/m^2. The matrix system used for this study was R180 Bisphenol A epoxy resin and H180 amine hardener supplied by Nuplex Industries Ltd, Auckland, New Zealand.

2.2. Sample Preparation

The PMMA nanofiber mat was cut into 10 mm × 10 mm squares and fibres were mixed manually with epoxy resin at fibre weight fractions of 0 wt%, 0.5 wt%, 2 wt% and 5. The fibre-epoxy mix was then placed under vacuum for 24 hours to remove air bubbles. The hardener was added at 1:5 hardener to epoxy weight ratio and was mixed thoroughly. Following this, the mixture was poured into silicone moulds and was allowed to cure under vacuum at room temperature for 24 hours.

Cured samples were removed from moulds and cut using a rotating blade saw to sample size of 40 mm × 4.5 mm × 4.5 mm for the 3-point bend test measurement. A rotating blade saw and a CNC machine were used to

prepare samples for tensile strength test. Dimensions of the samples were 40 mm in length, 10 mm gage length, 2.5 mm width, and thickness of 4 mm.

2.3. Mechanical Testing

Tensile and 3-point bend tests were carried out on a universal testing machine to evaluate performance of nanocomposites with various fibre weight fractions. Cross-head speed of 2.5 mm/min was used for the tensile test and 0.5 mm/min for the 3-point bend test. A span of 30 mm was used for the 3-point bend test.

2.4. Data Analysis

Data collected from the tensile and 3-point bend tests were analyzed using IBM SPSS Statistics 22. A One-way ANOVA with an alpha of 0.05 was used to compare data for Young's modulus, tensile strength and work of fracture (WOF) for samples with fiber content of 0 wt%, 0.5 wt%, 2 wt% and 5 wt%. WOF values were calculated by measuring area under stress-strain curve for tensile tests.

3. Results and Discussion

Scanning electron microscope (SEM) Hitachi SU-70 FEG-SEM was utilized to evaluate nanofibers and nanocomposite fracture surfaces. **Figure 1** shows an SEM micrograph of PMMA nanofibers used in this study prior to mixing with epoxy resin.

Young's modulus of elasticity and flexural modulus of all samples were determined from tensile and 3-point bend test results respectively. **Figure 2(a)** and **Figure 2(b)** illustrate Young's and flexural modulus results for the neat resin control sample and for samples with nanofiber content of 0.5 wt%, 2 wt%, and 5 wt%. Young's modulus results showed no noticeable change in modulus after adding PMMA nanofibers. Flexural modulus results, on the other hand, showed an initial drop in modulus for the 0.5 wt% nanofiber samples, followed by an increase in modulus for the 2 wt% and 5 wt% nanofiber samples.

Tensile and flexural strength results are illustrated in **Figure 3**. While there was no statistically significant difference between the samples with various nanofiber content in the case of flexural strength test, tensile strength results indicate a drop in tensile strength with increasing nanofiber content. Drops of 35% and 33% in tensile strength average values were recorded for 2 wt% and 5 wt% nanofiber content respectively. Similar results were achieved when measuring WOF for the various samples, as shown in **Figure 4**. Drops of 41% and 48% in average values for WOF were recorded for 2 wt% and 5 wt% nanofiber content respectively. Results achieved in this study were not in agreement with results reported in other studies that showed significant improvement in mechanical performance with the addition of nanofibers [10]-[12]. These studies attributed the improvement in mechanical performance to strong fiber/matrix adhesion. In order to assess fiber/matrix adhesion in our study, SEM was utilized to examine fracture surfaces to help determine cause in drop of tensile

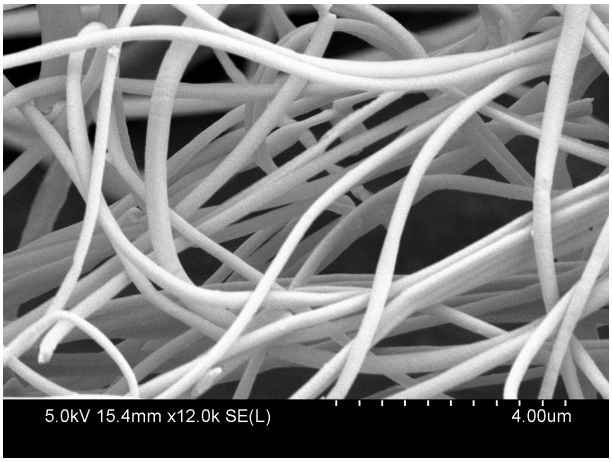

Figure 1. SEM micrograph of PMMA nanofibers at a magnification of 12 k.

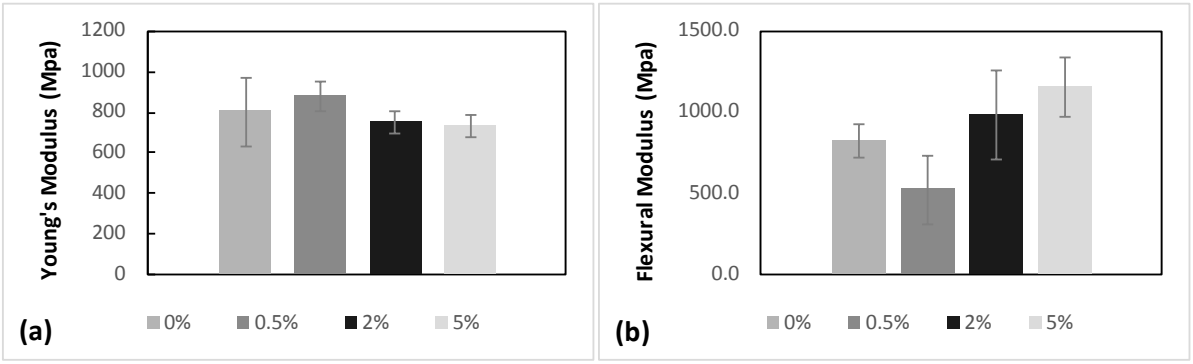

Figure 2. (a) Young's modulus and (b) Flexural modulus of epoxy resin reinforced with different amounts of PMMA nanofibers.

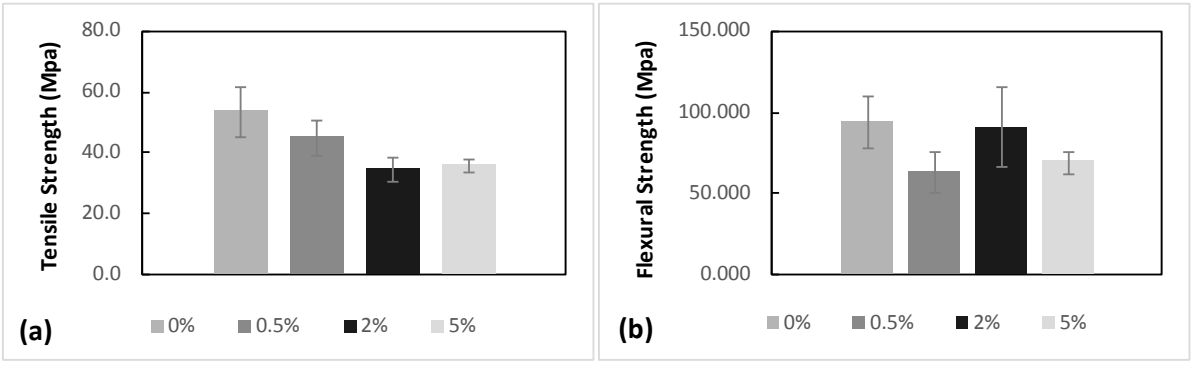

Figure 3. (a) Tensile strength and (b) Flexural Strength of epoxy resin reinforced with different amounts of PMMA nanofibers.

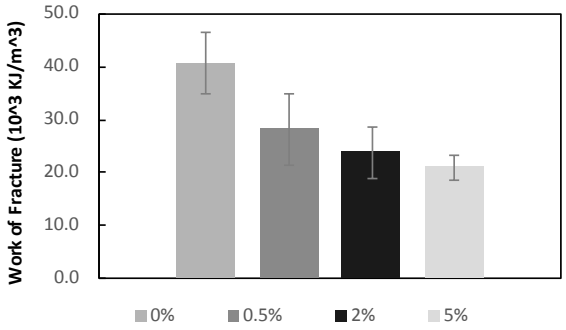

Figure 4. Work of fracture of epoxy resin reinforced with different amounts of PMMA nanofibers.

strength and WOF with increasing nanofiber content. **Figure 5** and **Figure 6** show SEM micrographs of 3-point bend test fracture surfaces for nanocomposite samples with 5 wt% PMMA at magnification of 2 k and 20 k respectively. **Figure 5** shows presence of porosity throughout the fracture surface. It appears that there was air entrapment during mixing of the fibers with the resin, and the use of vacuum during curing was not sufficient to release the air. Furthermore, **Figure 6** shows clean fiber-matrix interface in locations where fibers were pulled out during the test. This clean interface indicates poor fiber/matrix bonding. Also, an examination of the fracture surface indicates absence of fiber toughening behavior due to lack of long lengths of fiber pullout [16].

The results of this study are limited to the type of resin and nanofiber used, as fiber/matrix adhesion can be improved by using more compatible materials [10] [11]. Also, the use of functional coatings to enhance adhesion can enhance fiber/matrix adhesion and result in improved mechanical performance. For future work, we

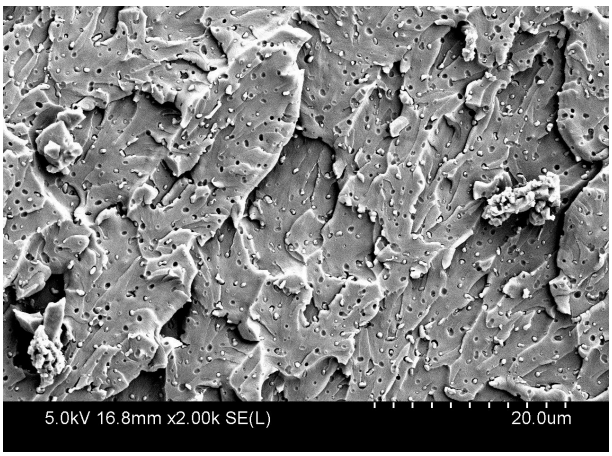

Figure 5. SEM micrograph of 3-point bend test fracture surface for sample with 5 wt% PMMA nanofibers at a magnification of 2 k.

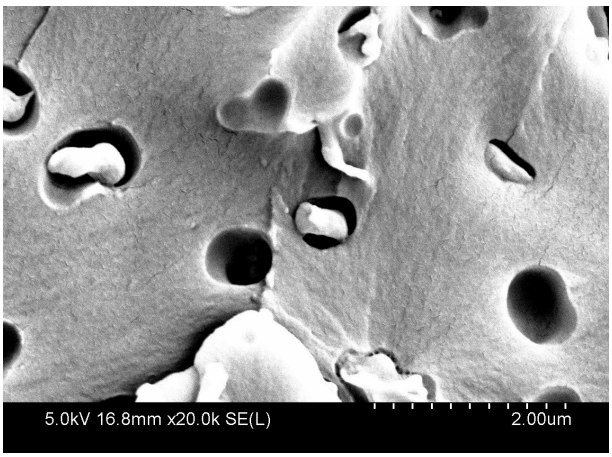

Figure 6. SEM micrograph of 3-point bend test fracture surface for sample with 5 wt% PMMA nanofibers at a magnification of 20 k.

will study various types of coatings to improve fiber/matrix interface. We will also modify resin mix and processing method to eliminate air entrapment in the cured nanocomposites. This could be achieved by the addition of air release and wetting agents, in addition to applying vacuum for a longer period of time after every mixing step.

4. Conclusion

Effect of uncoated PMMA nanofiber content in epoxy nanocomposites was determined in this study. Results showed drop in tensile strength and WOF with the increase in PMMA nanofiber content. Young's modulus results showed no noticeable change in modulus after adding PMMA nanofibers. SEM micrographs of fracture surfaces showed presence of porosity and poor fiber/matrix bonding. In addition, SEM micrographs showed poor fiber toughening behaviour due to lack of long lengths of fiber pullout. This work shows the need to develop functional coatings for PMMA nanofibers for various matrices to improve mechanical behaviour of the nanocomposite.

Acknowledgements

The authors would like to thank Revolution Fibres Ltd. and Nuplex Industries Ltd. for providing materials for

this project. The author would also like to thank Patrick Conor for his valuable assistance on the SEM.

References

[1] Alubaidy, A., Venkatakrishnan, K. and Tan, B. (2013) Nanofibers Reinforced Polymer Composite Microstructures. In: Maguire, R., Ed., *Advances in Nanofibers*, InTech, Croatia, 166.

[2] Huang, Z.-M., Zhang, Y.-Z., Kotaki, M. and Ramakrishna, S. (2003) A Review on Polymer Nanofibers by Electrospinning and Their Applications in Nanocomposites. *Composite Science and Technology*, **63**, 2223-2252. http://dx.doi.org/10.1016/S0266-3538(03)00178-7

[3] Subbiah, T., Bhat, G.S., Tock, R.W., Parameswaran, S. and Ramkumar, S.S. (2005) Electrospinning of Nanofibers. *Journal of Applied Polymer Science*, **96**, 557-569. http://dx.doi.org/10.1002/app.21481

[4] Reneker, D.H., Yarin, A.L., Zussman, E. and Xu, H. (2007) Electrospinning of Nanofibers from Polymer Solutions and Melts. *Advances in Applied Mechanics*, **41**, 43-195. http://dx.doi.org/10.1016/S0065-2156(07)41002-X

[5] Bhardwaj, N. and Kundu, S.B. (2010) Electrospinning: A Fascinating Fiber Fabrication Technique. *Biotechnology Advances*, **28**, 325-347. http://dx.doi.org/10.1016/j.biotechadv.2010.01.004

[6] Teo, W.-E., Inai, R. and Ramakrishna, S. (2011) Technological Advances in Electrospinning of Nanofibers. *Science and Technology Advanced Materials*, **12**, 1-19. http://dx.doi.org/10.1088/1468-6996/12/1/013002

[7] Lozano, K. and Barrera, E.V. (2001) Nanofiber-Reinforced Thermoplastic Composites. I. Thermoanalytical and Mechanical Analyses. *Journal of Applied Polymer Science*, **79**, 125-133. http://dx.doi.org/10.1002/1097-4628(20010103)79:1<125::AID-APP150>3.0.CO;2-D

[8] Rodriguez, A.J., Guzman, M.E., Lim, C.-S. and Minaie, B. (2011) Mechanical Properties of Carbon Nanofiber/Fiber-Reinforced Hierarchical Polymer Composites Manufactured with Multiscale-Reinforcement Fabrics. *Carbon*, **49**, 937-948. http://dx.doi.org/10.1016/j.carbon.2010.10.057

[9] Li, B., Yuan, H. and Zhang, Y. (2013) Transparent PMMA-Based Nanocomposite Using Electrospun Graphene-Incorporated PA-6 Nanofibers as the Reinforcement. *Composite Science and Technology*, **89**, 134-141. http://dx.doi.org/10.1016/j.compscitech.2013.09.022

[10] Jiang, S., Greiner, A. and Agarwal, S. (2013) Short Nylon-6 Nanofiber Reinforced Transparent and High Modulus Thermoplastic Polymeric Composites. *Composites Science and Technology*, **87**, 164-169. http://dx.doi.org/10.1016/j.compscitech.2013.08.011

[11] Jiang, S., Duan, G., Schobel, J., Agrawal, S. and Greiner, A. (2013) Short Electrospun Polymeric Nanofibers Reinforced Polyimide Nanocomposites. *Composites Science and Technology*, **88**, 57-61. http://dx.doi.org/10.1016/j.compscitech.2013.08.031

[12] Lin, S., Cai, Q., Ji, J., Sui, G., Yu, Y., Yang, X., Ma, Q., Wei, Y. and Deng, X. (2008) Electrospun Nanofiber Reinforced and Toughened Composites through *in Situ* Nano-Interface Formation. *Composites Science and Technology*, **68**, 3322-3329. http://dx.doi.org/10.1016/j.compscitech.2008.08.033

[13] Vidotti, H.A., Manso, A.P., Leung, V., do Valle, A.L., Ko, F. and Carvalho, R.M. (2015) Flexural Properties of Experimental Nanofiber Reinforced Composite Are Affected by Resin Composition and Nanofiber/Resin Ration. *Dental Materials*, **31**, 1132-1141. http://dx.doi.org/10.1016/j.dental.2015.06.018

[14] Yao, J., Li, G., Bastiaansen, C.W.M. and Peijs, T. (2015) High Performance Co-Polyimide Nanofiber Reinforced Composites. *Polymer*, **76**, 46-51. http://dx.doi.org/10.1016/j.polymer.2015.08.054

[15] Ahmadi, M., Masoomi, M. and Safi, S. (2015) Mechanical Property Characterization of Carbon Nanofiber/Epoxy Nanocomposites Reinforced by GMA-Grafted UHMWPE Fibers. *Composites Part B*, **83**, 43-49. http://dx.doi.org/10.1016/j.compositesb.2015.08.006

[16] Bansal, N.P. and Eldridge, J.I. (1999) Effects of Fiber/Matrix Interface and Its Composition on Mechanical Properties of Hi-Nicalon/Celsian Composites. NASA/TM-1999-209057, *Proceedings of ICCM*-12 *Conference*, Paris, 5-9 July 1999, 147.

World Journal of Nano Science and Engineering, 2016, 6, 64-69
Published Online June 2016 in SciRes. http://www.scirp.org/journal/wjnse
http://dx.doi.org/10.4236/wjnse.2016.62008

Effect of Nanoparticles Reinforced Adhesive Layers on Microleakage of Tooth Restorations

Mohamed I. Ebrahim[1], Mohamed Ashour Ahmed[2], Nayef H. Felemban[3]

[1]Department of Restorative Dentistry, Faculty of Dentistry, Taif University, Taif, Saudi Arabia
[2]Department of Prosthodontics, Faculty of Dentistry, Taif University, Taif, Saudi Arabia
[3]Department of Orthodontics, Faculty of Dentistry, Taif University, Taif, Saudi Arabia
Email: m.ismail@tudent.org, m.ashour@tudent.org, nfelemban@tudent.edu.sa

Received 26 May 2016; accepted 13 June 2016; published 16 June 2016

Abstract

Adhesive layer is an essential part of tooth colored restorations which play an important role in decreasing the microleakage between the tooth and restoration material after polymerization shrinkage. The purpose of this study was to evaluate the effect of deferent adhesive system of bonding agent on microleakage of nanocomposite resin in class II cavities. Two different types of adhesive systems: universal adhesive (ExciTE) and a newly developed adhesive (Nano-Bond) and one type of light-cured resin restorative material (nanocomposite resin) were used in this study. These adhesives were applied to prepared tooth cavities by either manufactures' instructions or by an experimental method (single or double application). Nanocomposite resin was then placed and light-cured for 40 seconds. Teeth were subjected to 500 thermal cycles between 5˚C and 55˚C and were immersed in 3% methylene blue solution for 24 hours; microleakage was observed microscopically. The data were analyzed by a two-way ANOVA. For comparison between groups, Tukey's post-hoc test was used. Nanoparticles reinforced adhesive system shows low microleakage in compare with universal adhesive system, and application of two adhesive layers also can decrease the microleakage. The ability of stress absorption by adhesive layer after polymerization shrinkage of restoration material will reduce the microleakage.

Keywords

Adhesive Layer, Tooth Colored Restorations, Nanoparticles, Microleakage

1. Introduction

A major shortcoming of light-cured composite resin is polymerization shrinkage. This shrinkage produces con-

How to cite this paper: Ebrahim, M.I., Ahmed, M.A. and Felemban, N.H. (2016) Effect of Nanoparticles Reinforced Adhesive Layers on Microleakage of Tooth Restorations. *World Journal of Nano Science and Engineering*, **6**, 64-69.
http://dx.doi.org/10.4236/wjnse.2016.62008

traction stress in a confined structure such as tooth cavity [1]. The contraction stress in resin composite plays an important role in marginal adaptation [2]. When the stress generated by the polymerization shrinkage exceeds the bond strength of adhesive resin to cavity walls and floor, a contraction gap of microleakage is formed [3] [4]. The linear shrinkage of microfilled composites ranged from 2% - 3% after curing. Hybrid composites and micro-hybrid composite shrank from 0.6% - 1.4% [5]. Such shrinkage caused microleakage, a well-known effect of contraction gaps on the interface of resin and tooth. Saliva, fluid, food residue, and microorganism strapped in the gaps lead to decayed teeth and damaged enamel which is a major problem in current restorative and esthetic dentistry so as to provide a material with high mechanical properties and low polymerization shrinkage. It was anticipated that composites with epoxy resin and nanosilica filler could fulfill these requirements [6] [7].

There have been many efforts at reducing the polymerization shrinkage in resin composites. One approach is through control of components of the composite itself such as the amount and type of matrix resin [8], the filler level [9], the curing chemistry [10], the initiator level [11] and the addition of non-bonded micro-filler particles [12]. The other approach is performed technically and includes a modified application technique [13] [14], the sandwich restoration with glass ionomer [15], the use of resin inlay [16], and controls the restoration rate by altering light energy [17] [18].

One practical approach to reducing the effects of composite contractions is to place a flexible and low-viscosity intermediate layer of a bond agent or a lining material between the composite and cavity walls [19] [20]. This layer acts as an elastic buffer at the resin-dentin interface and gives the total restoration the flexibility required to compensate for the part of the polymerization contraction. As a result, the adhesive bond will remain intact and marginal integrity will be preserved. This observation supports the stress-absorbing theory [21] [22]. Such stress can also be reduced significantly by a relatively thin layer of Scotch bond™ Multi-purpose adhesive and additional adhesive layers in the marginal area to reduce the overall degree of microleakage [20].

The purpose of this study was to evaluate the effect of deferent adhesive system of bonding agent on microleakage of nanocomposite resin in class II cavities.

2. Material and Methods

Two different types of adhesive available systems, ExciTE (Ivoclar, Vivadent, Schaan, Liechtenstein, Swiss, lot #K41832) and Nano-Bond adhesives (Pentron Clinical Technologies, USA, lot #183421) and one type of nanofilled composite (Artiste Nanocomposite, Pentron Clinical Technologies LLC, USA, lot #182066-185215) were used in this study. ExciTE is a fourth-generation universal adhesive system and Nano-Bond is fourth-generation newly developed adhesive system.

Twenty freshly extracted caries-free human molar teeth were collected for the purpose of this study. The teeth were cleaned by an ultrasonic scaler and stored in distilled water at 37˚ C before testing.

Standardization class II cavities were prepared in the selected teeth. Cavities were prepared with 330 carbide burs at high speed with air-water coolant. The buccoligual width was 2 mm and 1.5 mm deep. The proximal boxes were prepared with No. 557 carbide burs. The proximal box margins were placed 2 mm above the cementoenamel junction. The depth of the box from the cavosurface margin to the axial wall was almost 2 mm and the occlusal was almost 4 mm. The interproximal walls, floor, and marginal ridge area were beveled to approximately 1 mm long with No. 7901 carbide burs.

The prepared teeth were divided into two main groups (of 10 each) according to the type of adhesive system. Group A: ExciTE adhesive and Group B: Nano-Bond adhesive system. Each group was further subdivided into two subgroups (of five each) according to the layers of the adhesive system. Subgroup 1 (A1 & B1): one layer of adhesive systems and subgroup 2 (A2 & B2): two layers of adhesive systems.

The cavity of each tooth was acid etched using 37% phosphoric acid gel for 15 seconds. Then the teeth were rinsed with water spray and dried with oil-free stream for five seconds. The adhesives were applied on the cavities by either the manufactures' instructions or by an experimental method (single or double application). The adhesives were applied to the entire surface of the cavity and air thinned for 15 seconds. A gentle stream of dry air was applied to disperse the material into a thin, uniform, shiny appearing surface. The adhesive was then light-cured for 10 seconds with light emitting diodes (LED). Specimens with thick adhesive layers were produced by the application of one additional coat of adhesive. Additional coats were applied only to the marginal areas of the cavity to avoid pooling. Each layer was light-cured separately for 10 seconds.

Cavities were then filled with nanofilled composite. Resin composite was placed in two separately light-cured increments; each increment was light-cured for 40 seconds with the tip as close to the surface as possible. Cur-

ing radiometer equipment was used to ensure steady light intensity throughout the polymerization of all specimens. All restorations were finished and polished with a set of solfex discs (3 M Company, St. Paul, MN, USA).

Teeth were prepared for microleakage evaluation by sealing the root apices with sticky wax. All other surfaces, except the restorations and 1 mm from the margins, were coated with two layers of nail varnish to avoid dye penetration. Teeth were stored in distilled water for 48 hours and then subjected to 500 thermal cycles between 5˚C and 55˚C water baths.

Dwell time was one minute with a 10-second transit time between baths. After thermocycling, teeth were immersed in a 3% methylene blue solution for 24 hours. Subsequently, all teeth were sectioned into two halfmesiodistally sections with a low-speed diamond disc* under water coolant.

Dye penetration was measured under a stereomicroscope (Olympus SZ-PT-Japan) at 10x magnifications. Linear dye penetration (in microns) of each specimen in different groups was automatically calculated used the image analysis software (Image Ware, Image J 1.3lb, USA). Linear dye penetration was measured along the gingival floor as well as the axial wall. The ratio of linear dye penetration to the total measure of the gingival floor or axial wall was calculated and the percentage of dye penetration obtained for each specimen. Data analysis was performed by a two-way ANOVA. Tukey's post-hoc test was used for a pairwise comparison between the means when the ANOVA test was significant.

3. Results

The mean percentage of microleakage for the tested adhesives (ExciTE and Nano-Bond) with different interactions at the gingival floor is presented in **Table 1**. The microleakage (%) of ExciTE adhesive applied in one layer (A1) at the gingival floor had the statistically significant highest mean microleakage (%). This was followed by application of the ExciTE adhesive in two layers (A2), then Nano-Bond adhesive in one layer (B1). The statistically significant lowest mean microleakage (%) was found with the Nano-Bond adhesive in two layers (B2). There were significant differences ($P < 0.05$) between study groups. Microleakage was decreased for the specimens receiving two layers.

The mean percentage of microleakage for the tested adhesives with different interactions at the axial wall is presented in **Table 2**. ExciTE adhesive of group A1 showed the highest microleakage while Nano-Bond adhesive of group 2 had the lowest microleakage. In a similar manner as presented in **Table 2**, the application of two layers of adhesive to the cavity wall reduced significantly ($P < 0.001$) the microleakage (%) at axial walls. Between the specimens receiving one and two adhesive layers, there were significant differences between the gingival floor and the axial wall. The microleakage (%) at gingival floors was higher than those at the axial wall of each specimen.

4. Discussions

In many dentin-bonding systems, dentin preparation is a multistage process involving three steps: 1) etching with an acidic conditioner; 2) priming with hydrophilic resin in solvent; and 3) bonding with an unfilled or lightly filled resin [23].

The major goals of using dentin-bonding systems are to enhance the bonding strength between resin and the tooth structure, increase the retention of restoration, reduce the microleakage across dentin-resin interface, and scatter the occlusal stress [24].

Marginal leakage of composite restorations may be influenced by external stress produced during chewing and internal stress produced by polymerization contraction. These stresses may compromise the material's

Table 1. Comparison between microleakage of the tested adhesives with different interactions at gingival floor.

Material	Adhesive Layer	Mean (%)	SD	Rank	P-value
ExciTE (Group A)	one layer (A1)	67	2.7	A	0.003*
	two layers (A2)	47.9	4.4	B	
Nano-Bond (group B)	one layer (B1)	24.8	1.7	C	
	two layers (B2)	14.8	1.5	D	

*Significant at $P \leq 0.05$; means with different letters are statistically significantly different according to Tukey's post-hoc test.

Table 2. Comparison between microleakage of the tested adhesives with different interactions at axial wall.

Material	Adhesive Layer	Mean (%)	SD	Rank	*P*-value
ExciTE (group A)	one layer (A1)	34.9	2.5	A	0.003*
	two layers (A2)	25	2.4	B	
Nano-Bond (group B)	one layer (B1)	16.7	1	C	
	two layers (B2)	7.9	1.1	D	

*Significant at $P \leq 0.05$; means with different letters are statistically significantly different according to Tukey's post-hoc test.

properties, creating marginal openings and deform the tooth substrate [25] [26]. The contraction stress of composite depends upon the type and level of filler included. Generally, an increased filler level should contribute to a reduce polymerization shrinkage, since the overall polymerization shrinkage depends on the amount of polymer matrix [9]. On the other hand, the stiffness of the composite is also increased at high filler levels. The high stiffness leads to increased stress for a given contraction strain, according to Hooke's law; therefore, the composite stiffness and the amount of contraction both play important roles in the generation of stress in dental composite restorations [27].

Adhesive layer acts as an elastic intermediate layer (elastic cavity wall) between the cavity walls and the adjacent composite. This layer could resist the polymerization shrinkage stress of the resin composites and absorb the shock produced by occlusal loads and thermal cycling [19].

According to many investigators [29] [30], the uses of filled adhesive resin increases the mechanical properties and improves marginal and internal seals of composite restoration.

This study demonstrated that increasing the adhesive thickness by means of additional layering on the cavity walls should lead to an improvement of the marginal integrity and, as a consequence, may prolong the life of a restoration; however, a thick layer of low stiffness (unfilled or lightly filled) adhesive resin at the margins of restoration may lead to reduction in contraction stress and enhanced wear at this location.

The result of the present study also showed less microleakage in Nano-Bond adhesive (one and two layers). This may be contributed to increased filler levels and decreased particle sizes in Nano-Bond adhesives over the ExciTE adhesive.

The findings from this study supports many previous studies which demonstrate that gingival margins are potentially a greater source of marginal leakage in class II composite restorations compared to occlusal margins and axial walls [31]-[33]. Neme, *et al*. [34] have suggested that the absence of enamel at the gingival cavosurface margin of the proximal box results in low-bond strength between material and substrate. This lack of enamel requires adhesion of the restorative material to cementum/dentin, a less reliable, more complex substrate than enamel. A third hypothesis proposed for increased cervical or gingival leakage compared to that of occlusal margins or axial walls, as it relates the distance of the light source from the material at the proximal box base to the axial or occlusal surface. It has been hypothesized that the resulting higher polymerization stresses at the gingival floor cause increased dimensional changes, leading to gap formation [33]. Further laboratory studies and long-term clinical evaluations are needed before definite conclusions could be drawn.

5. Conclusion

In this study, Nanoparticles reinforced adhesive system shows low microleakage in compare with universal adhesive system, and application of two adhesive layers also can decrease the microleakage.

References

[1] Alster, D., Feilzer, A., de Gee, A. and Davidson, C. (1997) Polymerization Contraction Stress in Thin Resin Composite Layers as a Function of Layer Thickness. *Dental Materials Journal*, **13**, 146-150. http://dx.doi.org/10.1016/S0109-5641(97)80115-7

[2] Uno, S. and Shimokobe, H. (1994) Contraction Stress and Marginal Adaptation of Composite Restorations in Dentinal Cavity. *Dental Materials Journal*, **13**, 19-24. http://dx.doi.org/10.4012/dmj.13.19

[3] Cincchi, B., Bonillagent, S., Delaloye, M. and Holz, J. (1997) Volume of Internal Gap Formed under Composite Restorations *in Vitro*. *Journal of Dentistry*, **25**, 305-312. http://dx.doi.org/10.1016/S0300-5712(96)00032-2

[4] Kinomoto, Y. and Tarri, M. (1998) Photoelastic Analysis of Polymerization Contraction Stresses in Resin Composite Restoration. *Journal of Dentistry*, **26**, 165-171. http://dx.doi.org/10.1016/S0300-5712(96)00083-8

[5] Power, J. and Sakguch, R. (2006) Craig's Restorative Dental Materials. Mosby, Inc., St Louis, 203-205.

[6] Frank, C., Miller, R., *et al.* (2002) Structure and Interaction of Organic/Inorganic Hybrid Nanocomposites for Microelectronic Applications. 1. MSSQ/P (MMA-*co*-DMAEMA) Nanocomposites. *Chemistry of Materials*, **14**, 3676-3685. http://dx.doi.org/10.1021/cm020014z

[7] Giannelis, E. (1996) Polymer Layered Silicate Nano Composites. *Advanced Materials*, **8**, 29-35. http://dx.doi.org/10.1002/adma.19960080104

[8] Eick, J., Byerley, T., Chappell, R., Chen, G., Bowles, C. and Chappelow, C. (1993) Properties of Expanding Soc/Epoxy Copolymers for Dental Use in Dental Composites. *Dental Materials Journal*, **9**, 123-127. http://dx.doi.org/10.1016/0109-5641(93)90088-8

[9] Munksgaard, E., Hansen, E. and Kato, H. (1987) Wall-to-Wall Polymerization Contraction of Composite Resins versus Filler Content. *Scandinavian Journal of Dental Research*, **95**, 526-531. http://dx.doi.org/10.1111/j.1600-0722.1987.tb01970.x

[10] Feilzer, A., de Gee, A. and Davidson, C. (1993) Setting Stresses in Composites for Two Different Curing Modes. *Dental Materials Journal*, **9**, 2-5. http://dx.doi.org/10.1016/0109-5641(93)90095-8

[11] Venhoven, B., de Gee, A. and Davidson, C. (1996) Light Initiation of Dental Resins: Dynamics of the Polymerization. *Biomaterials*, **17**, 2313-2318. http://dx.doi.org/10.1016/S0142-9612(96)00074-9

[12] Condon, J. and Ferracane, J. (1998) Reduction of Composite Contraction Stress through Non-Bonded Microfiller Particles. *Dental Materials Journal*, **14**, 256-260. http://dx.doi.org/10.1016/S0109-5641(98)00036-0

[13] Kemp-Scholte, C.M. and Davidson, C. (1988) Marginal Sealing of Curing Contraction Gaps in Class V Composite Resin Restorations. *Journal of Dental Research*, **67**, 841-845. http://dx.doi.org/10.1177/00220345880670050901

[14] Krejci, I. and Lutz, F. (1991) Marginal Adaptation of Class V Restorations Using Different Restorative Techniques. *Journal of Dentistry*, **19**, 24-32. http://dx.doi.org/10.1016/0300-5712(91)90032-t

[15] Davidson, C. (1994) Glass Ionomer Bases under Posterior Composites. *International Journal of Esthetic Dentistry*, **6**, 223-424. http://dx.doi.org/10.1111/j.1708-8240.1994.tb00863.x

[16] Liberman, R., Ben-Amar, A., Herteanu, L. and Judes, H. (1997) Marginal Seal of Composite Inlays Using Different Polymerization Techniques. *Journal of Oral Rehabilitation*, **24**, 26-29.

[17] Davidson-Kaban, S., Davidson, C., Feilzer, A., de Gee, A. and Eerdilek, N. (1997) The Effect of Curing Light Variations of Bulk Curing and Wall-to-Wall Quality of Two Types and Various Shades Resin Composites. *Dental Materials Journal*, **13**, 344-352. http://dx.doi.org/10.1016/S0109-5641(97)80105-4

[18] Sakaguchi, R. and Berge, H. (1998) Reduced Light Energy Density Decreases Post-Gel Contraction While Maintaining Degree of Conversion in Composites. *Journal of Dentistry*, **26**, 695-700. http://dx.doi.org/10.1016/S0300-5712(97)00048-1

[19] Kemp-Scholte, C.M. and Davidson, C. (1990) Marginal Integrity Related to Bond Strength and Strain Capacity of Composite Resin Restorative Systems. *Journal of Prosthetic Dentistry*, **64**, 658-664. http://dx.doi.org/10.1016/0022-3913(90)90291-J

[20] Choi, K., Condon, J. and Ferracane, J. (2000) The Effects of Adhesive Thickness on Polymerization Contraction Stress of Composite. *Journal of Dental Research*, **79**, 812-817. http://dx.doi.org/10.1177/00220345000790030501

[21] Kemp-Scholte, C.M. and Davidson, C. (1990) Complete Marginal Seal of Class V Resin Composite Restorations Effected by Increased Flexibility. *Journal of Dental Research*, **69**, 1240-1243. http://dx.doi.org/10.1177/00220345900690060301

[22] Van Meerbeek, B., Willems, G., Celis, J., Roos, J., Braem, M., Lambrechts, P. and Vanherle, G. (1993) Assessment by Nano-Indentation of the Hardness and Elasticity of the Resin-Dentin Bonding Area. *Journal of Dental Research*, **72**, 1434-1442. http://dx.doi.org/10.1177/00220345930720101401

[23] Swift Jr., E., Perdigao, J. and Heymann, H. (1995) Bonding to Enamel and Dentin: A Brief History and State of the Art. *Quintessence International*, **26**, 95-110.

[24] Chen, R.-S., Liu, C.-C., Tseng, W.-Y. Jeng, J.-H. and Lin, C.-P. (2003) Cytotoxicity of Three Dentin Bonding Agents on Human Dental Pulp Cells. *Journal of Dentistry*, **31**, 223-229. http://dx.doi.org/10.1016/S0300-5712(02)00088-X

[25] Burgess, J.O., Walker, R.S., Porche, C.J. and Rappold, A. (2002) Light-Curing—An Update. *Compendium of Continuing Education in Dentistry*, **23**, 889-892.

[26] Lutz, F., Krejci, I., Luescher, B. and Oldenburg, T. (1986) Improved Proximal Marginal Adaptation of Class II Composite Resin Restoration by Use of Light Refolding Wedges. *Quintessence International*, **17**, 659-664.

[27] Braem, M., Lambrechts, P., Vanherle, G. and Davidson, C. (1987) Stiffness Increase during the Setting of Dental Composite Resins. *Journal of Dental Research*, **66**, 1713-1716. http://dx.doi.org/10.1177/00220345870660120301

[28] Uno, S. and Finger, W. (1995) Function of the Hybrid Zone as a Stress-Absorbing Layer in Dentin Bonding. *Quintessence International*, **26**, 733-738.

[29] Labella, R., Lambrechts, P., van Meerbeek, B. and Vanherle, G. (1999) Polymerization Shrinkage and Elasticity of Flowable Composites and Filled Adhesives. *Dental Materials Journal*, **15**, 128-137. http://dx.doi.org/10.1016/S0109-5641(99)00022-6

[30] Wegdan, B. (2005) Effecting of Cutting Bur on the Bond Strength of Self-Etching and One Bottle Nanofilled to Enamel and Dentin. *Egy Dent*, **51**, 1171-1179.

[31] Van Meerbeek, B., Braem, M., Lambrechts, P. and Vanherle, G. (1993) Evaluation of Two Dentin Adhesives in Cervical Lesions. *Journal of Prosthetic Dentistry*, **70**, 308-314. http://dx.doi.org/10.1016/0022-3913(93)90213-8

[32] Linden, J. and Swift Jr., D. (1994) Microleakage of Two New Dentin Adhesives. *American Journal of Dentistry*, **7**, 31-34.

[33] Yap, A., Stokes, A.N. and Pearson, G.J. (1996) An *in Vitro* Microleakage Study of a New Multi-Purpose Dental Adhesive System. *Journal of Oral Rehabilitation*, **23**, 302-308. http://dx.doi.org/10.1111/j.1365-2842.1996.tb00857.x

[34] Neme, A., Maxson, B., Pink, F. and Aksu, M. (2002) Microleakage of Class II Packable Resin Composite Lined with Flowables: An *in Vitro* Study. *Operative Dentistry*, **27**, 600-605.

World Journal of Nano Science and Engineering, 2016, 6, 70-89
Published Online June 2016 in SciRes. http://www.scirp.org/journal/wjnse
http://dx.doi.org/10.4236/wjnse.2016.62009

Fourth-Order Compact Formulation for the Resolution of Heat Transfer in Natural Convection of Water-Cu Nanofluid in a Square Cavity with a Sinusoidal Boundary Thermal Condition

Mostafa Zaydan, Naoufal Yadil, Zoubair Boulahia, Abderrahim Wakif, Rachid Sehaqui

Mechanical Laboratory, Faculty of Sciences, Hassan II University, Ain Chock Maarif, Casablanca, Morocco
Email: na.zidane@gmail.com

Received 11 April 2016; accepted 18 June 2016; published 21 June 2016

Abstract

In the present work, we numerically study the laminar natural convection of a nanofluid confined in a square cavity. The vertical walls are assumed to be insulated, non-conducting, and impermeable to mass transfer. The horizontal walls are differentially heated, and the low is maintained at hot condition (sinusoidal) when the high one is cold. The objective of this work is to develop a new height accurate method for solving heat transfer equations. The new method is a Fourth Order Compact (F.O.C). This work aims to show the interest of the method and understand the effect of the presence of nanofluids in closed square systems on the natural convection mechanism. The numerical simulations are performed for Prandtl number ($Pr = 6.2$), the Rayleigh numbers varying between $10^3 \le Ra \le 5\times10^5$ and for different volume fractions χ varies between 0% and 10% for the nanofluid (water + Cu).

Keywords

Nanofluid, Heat Transfer, Natural Convection, Fourth-Order Compact (F.O.C) Formulation, Numerical Performance, Sinusoidal Boundary Thermal Condition

How to cite this paper: Zaydan, M., Yadil, N., Boulahia, Z., Wakif, A. and Sehaqui, R. (2016) Fourth-Order Compact Formulation for the Resolution of Heat Transfer in Natural Convection of Water-Cu Nanofluid in a Square Cavity with a Sinusoidal Boundary Thermal Condition. *World Journal of Nano Science and Engineering*, **6**, 70-89.
http://dx.doi.org/10.4236/wjnse.2016.62009

1. Introduction

In a better description, nanofluids are engineered colloidal suspensions of nanoparticles (1 - 100 nm) in a base fluid. Common base fluids include water, oil, and Ethylene Glycol while nanoparticles are typically made of chemically stable metals, metal oxides or carbon in various forms. The use of particles of nanometer dimension was first continuously studied by a research group at the Argonne National Laboratory a decade ago. S. Choi [1] in 1995 was probably the first one who called the fluids with particles of nanometer dimensions "nanofluids". He showed substantial augmentation of heat transported in suspensions of copper or aluminum nanoparticles in water and other liquids. Compared with suspended particles of millimeter or micrometer dimensions, nanofluids show better stability and rheological properties, dramatically higher thermal conductivities and no penalty in pressure drop. Several published literatures have mainly focused on the prediction and measurement techniques in order to evaluate the thermal conductivity of nanofluid. It is noticeable that only a few papers have discussed the convective heat transfer of nanofluids, including the experimental and theoretical investigation.

A numerical study of natural convection of copper-water nanofluide in a two dimensional enclosure was conducted by Khanafer *et al.* [2]. The nanofluid in the enclosure was assumed to be in single phase. It was found in any given Grashof number, heat transfer in the enclosure increased with the volumetric fraction of the copper nanoparticles in water. Lee *et al.* [3] measured the thermal conductivity of Al_2O_3 water and Cu-water nanofluids and indicated that the thermal conductivity of nanofluids increases with solid volume fraction. He concluded that any new models of nanofluide thermal conductivity should contain the effect of surface area and structure dependent behavior as well as the size effect. Xie *et al.* [4] added spherical and cylindrical shaped nano sized SiC particles to water and Ethylene Glycol, separately and found that cylindrical nanoparticles increased thermal conductivity more than spherical ones. The dependence of thermal conductivity of nanoparticles-fluid mixture was estimated by Xie *et al.* [5]. Some of the theoretical and experimental studies have been reported on convective heat transfer coefficient [6]-[9].

Sandeep Naramgari and C. Sulochana [10] analyzed the momentum and heat transfer behavior of MHD nanofluid embedded with conducting dust particles past a stretching surface in the presence of volume fraction of dust particles. They solved equations numerically using Runge-Kutta based shooting technique and showed that the increase in the interaction between the fluid and particle phase enhanced the heat transfer rate and reduced the friction factor. Nader Ben-Cheikh *et al.* [11] studied natural convection in a square enclosure filled with a water based nanofluid (water with Ag, Cu, Al_2O_3 or TiO_2 nanoparticles) with non-uniform (sinusoidal) temperature distribution maintained at the bottom wall. An accurate finite volume scheme along with a multi-grid technique is devised for the purpose of solution of the governing equations. Tiwari *et al.* [12] numerically investigated the behavior of copper-water nanofluid in a two sided lid-driven differentially heated cavity. They considered different cases characterized by the direction of movement of walls and found that both the Richardson number and direction of moving walls influenced the fluid flow and thermal behavior. Yadil *et al.* [13] study the Cu/Water nanofluids filled baffled square cavity.

The effects of Rayleigh number, volume fraction and partitions location on the average Nusselt number are studied. I.El Bouihi and R. Sehaqui [14] she simulate the flow features of nanofluids for a range of solid volume fraction χ and a sinusoidal thermal boundary condition, and we obtained correlations of heat transfer in enclosures for two different thermal boundary conditions on the left wall. Ami-Nossadati and Ghasemi [15] studied natural convection cooling of a localized heat source at the bottom of a nanofluid filled enclosure. Ogut [16] investigated natural convection of water-based nanofluids in an inclined enclosure with a heat source using the expression for calculating the effective thermal conductivity of solid-liquid mixtures proposed by Yu and Choi [17]. Ghasemi and Aminossadati [18] considered periodic natural convection in a nanofluid filled enclosure with oscillating heat flux. Non-uniform heating of surfaces in buoyancy driven flow in a cavity has significant effect of the flow and heat transfer characteristics and finds applications in various areas such as crystal growth in liquids, energy storage, geophysics, solar distillers and others. In a relatively recent study, Sarris *et al.* [19] reported that the sinusoidal wall temperature variation produced uniform melting of materials such as glass in their detailed study on the effect of sinusoidal top wall temperature variations in a natural convection within a square enclosure where the other walls are insulated. Corcione [20] studied natural convection in an air filled rectangular enclosure heated from below and cooled from above for a variety of thermal boundary conditions at the side walls. Roy and Basak [21] studied numerically natural convection flows in a square cavity with non-uniformly (sinusoidal) heated wall(s) using the finite element method. The bottom wall and one vertical wall were heated

(uniformly and non-uniformly) and the top wall was insulated while the other vertical wall was cooled by means of a constant temperature bath. Sathiyamoorthy *et al.* [22] investigated steady natural convection flows in a square cavity with linearly heated side wall(s).

In order to optimize and improve heat transfer by natural convection in closed square cavity. Although extensive research has been given to cases of rectangular cavity filled nanofluid, few studies have focused on the study, theoretical or numerical discretizations high order (≥2). The numerical study of systems of equations in the heat transfer area is usually treated by various methods, sometimes numérical classics like Finite Elements (FE), Volume Finite (VF) and Finite Differences (DF). or using some software adapted as "FLUENT". To solve fluid mechanics problems such as conductive heat transfer, convective or mixed into regular geometries.

More specific order four schemes have been used to solve the Navier-Stokes in enclosures without considering the energy equation by Ecran Erturk et C. Gokcol [2]. The objective of this work is to develop a new method for solving heat transfer equations in convection. The new method is a Fourth Order Compact. This work aims to show the interest of the method and understand the effect of the presence of nanofluids in closed square systems on the natural convection mechanism.

2. Mathematical Formulation

Consider a square cavity filled with a nanofluid. The vertical walls are assumed to be insulated, non-conducting, and impermeable to mass transfer. The horizontal walls are differentially heated, the low is maintained at hot condition (sinusoidal) when the high one is cold (**Figure 1**). The nanofluid in the enclosure is Newtonian, incompressible, and laminar. The nanoparticles are assumed to have a uniform shape and size. Moreover, it is assumed that both the fluid phase and nanoparticles are in thermal equilibrium state and they flow at the same velocity. The thermophysical properties of the nanofluid are assumed to be constant except for the density variation in the buoyancy force, which is based on the Boussinesq approximation.

We have considered the continuity, momentum and energy equations for a Newtonian, Fourier constant property fluid governing an unsteady, two-dimensional flow. It is further assumed that radiation heat transfer among sides is negligible with respect to other modes of heat transfer. Under the assumption of constant thermal properties, the Navier-Stokes equations for an unsteady, incompressible, two-dimensional flow are:

Continuity equation:

$$\frac{\partial u}{\partial x}+\frac{\partial v}{\partial y}=0 \tag{1}$$

x-momentum equation:

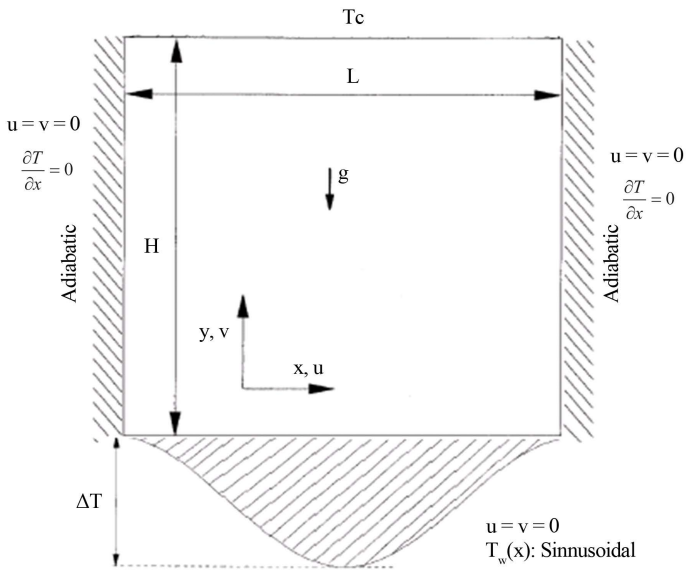

Figure 1. Physical model the coordinate system.

$$\rho_{nf,0}\left(\frac{\partial u}{\partial t}+u\frac{\partial u}{\partial x}+v\frac{\partial u}{\partial y}\right)=-\frac{\partial P}{\partial x}+\mu_{nf}\Delta_2 u \tag{2}$$

y-momentum equation:

$$\rho_{nf,0}\left(\frac{\partial v}{\partial t}+u\frac{\partial v}{\partial x}+v\frac{\partial v}{\partial y}\right)=-\frac{\partial P}{\partial y}+\mu_{nf}\Delta_2 v+\left[\chi\beta_s\rho_s+(1-\chi)\rho_f\beta_f\right]g\cdot T \tag{3}$$

Energy equation:

$$\frac{\partial T}{\partial t}+u\frac{\partial T}{\partial x}+v\frac{\partial T}{\partial y}=\alpha_{nf}\left(\Delta_2 T\right) \tag{4}$$

where $\Delta_2=\frac{\partial^2}{\partial x^2}+\frac{\partial^2}{\partial y^2}$ and $\alpha_{nf}=\frac{\kappa_{eff}}{\left(\rho C_p\right)_{nf}}$.

The viscosity of the nanofluid can be estimated with the existing relations for the two-phase mixture. The equation given by Brinkman [23] has been used as the relation for effective viscosity in this problem, as given by Xuan and Li [24] have experimentally measured the apparent viscosity of the transformer oil-water nanofluid and of the water-copper nanofluid in the temperature range of 20˚C - 50˚C. The experimental results reveal relatively good agreement with Brinkman's theory. The thermophysical properties of fluid and the solid phases are shown in **Table 1**.

The effective density of the nanofluid at reference temperature is

$$\rho_{nf}=\chi\rho_s+(1-\chi)\rho_f \tag{5}$$

The heat capacitance of the nanofluid is expressed as Abu-Nada [25] and Khanafer *et al.* [2]

$$\left(\rho C_p\right)_{nf}=\chi\left(\rho C_p\right)_s+(1-\chi)\left(\rho C_p\right)_f \tag{6}$$

The effective thermal conductivity of the nanofluid is approximated by the Maxwell-Garnetts model [26]

$$\frac{\kappa_{nf}}{\kappa_f}=\frac{\left(\kappa_s+2\kappa_f\right)-2\chi\left(\kappa_f-\kappa_s\right)}{\left(\kappa_s+2\kappa_f\right)+\chi\left(\kappa_{f-}\kappa_s\right)} \tag{7}$$

Equations (1)-(4) can be converted to the dimensionless forms by definition of the following parameters as:

$$X=\frac{x}{H},Y=\frac{y}{H},U=\frac{uH}{\nu_f},V=\frac{vH}{\nu_f},P=\frac{p}{\frac{\rho_f\nu_f^2}{H^2}},\tau=\frac{t}{\frac{H^2}{\nu_f}},\theta=\frac{T-T_c}{T_h-T_c}$$

$$Gr=\frac{\beta_f gH^3\left(T_h-T_c\right)}{\nu_f^2};\ Ra=\frac{\beta_f gH^3\left(T_h-T_c\right)}{\nu_f\alpha}\ \text{and}\ P_r=\frac{\nu_f}{\alpha_f}$$

Hence, the governing equations of continuity, linear momentum and energy for unsteady laminar flow in Cartesian coordinates take the following dimensionless form:

Table 1. Thermophysical properties of water and nanoparticles.

Physical properties	Pure water	Cu
$C_p\left(\mathrm{J/kg\cdot K}\right)$	4179	383
$\rho\left(\mathrm{kg/m^3}\right)$	997.7	8933
$\kappa\left(\mathrm{W/m\cdot K}\right)$	0.613	400
$\beta\left(\mathrm{K^{-1}}\right)$	2.1×10^{-4}	1.67×10^{-5}

$$\frac{\partial U}{\partial X}+\frac{\partial V}{\partial Y}=0 \tag{8}$$

$$\rho_{nf,0}\left(\frac{\partial U}{\partial \tau}+u\frac{\partial U}{\partial X}+V\frac{\partial U}{\partial Y}\right)=-\frac{\partial P}{\partial X}+\mu_{nf}\Delta_2 U \tag{9}$$

$$\rho_{nf,0}\left(\frac{\partial V}{\partial \tau}+U\frac{\partial V}{\partial X}+V\frac{\partial V}{\partial Y}\right)=-\frac{\partial P}{\partial Y}+\mu_{nf}\Delta_2 V+\frac{\left[\chi\beta_s\rho_s+(1-\chi)\rho_f\beta_f\right]}{\beta_f}\frac{Ra}{Pr}\theta \tag{10}$$

$$\frac{\partial \theta}{\partial \tau}+U\frac{\partial \theta}{\partial X}+V\frac{\partial \theta}{\partial Y}=\frac{\alpha_{nf}}{\alpha_f P_r}(\Delta_2\theta) \tag{11}$$

The enclosure boundary conditions consist of no-slip and no penetration walls, $U = V = 0$ on all four walls. The thermal boundary conditions on the bottom wall is such that $\theta_{Y=0}=\theta_h=\sin(\pi X)$. The left and right vertical walls are assumed to be insulated, non-conducting, and impermeable to mass transfer $\left.\frac{\partial\theta}{\partial X}\right|_{X=0}=\left.\frac{\partial\theta}{\partial X}\right|_{X=1}=0$ and the bottom wall are at the cold temperature $\theta_{Y=1}=0$

The governing equations for the present study in (ψ,ω) formulation taking into the account the above mentioned assumptions are written in dimensionless form as:

Kinematics equation:

$$\frac{\partial^2\Psi}{\partial X^2}+\frac{\partial^2\psi}{\partial Y^2}=-\omega \tag{12}$$

Vorticity equation:

$$\left(\frac{\partial\psi}{\partial Y}\right)\left(\frac{\partial\omega}{\partial X}\right)-\left(\frac{\partial\psi}{\partial X}\right)\left(\frac{\partial\omega}{\partial Y}\right)=\frac{\mu_{nf}}{\nu_f\rho_{nf,0}}\left(\frac{\partial^2\omega}{\partial X^2}+\frac{\partial^2\omega}{\partial Y^2}\right)+\eta\left(\frac{\partial\theta}{\partial Y}\right) \tag{13}$$

where: $\eta=\dfrac{\left[\chi\beta_s\rho_s+(1-\chi)\rho_f\beta_f\right]Ra}{P_r\beta_f\rho_{nf,0}}$.

Energy equation:

$$\left(\frac{\partial\Psi}{\partial Y}\right)\left(\frac{\partial\theta}{\partial X}\right)-\left(\frac{\partial\Psi}{\partial X}\right)\left(\frac{\partial\theta}{\partial Y}\right)=\frac{\alpha_{nf}}{\alpha_f P_r}\left(\frac{\partial^2\theta}{\partial X^2}+\frac{\partial^2\theta}{\partial Y^2}\right) \tag{14}$$

Before turning to the application of the method of fourth order in the equations governing our problem we will combine Equations (12) and (13) in a condensed form by introducing a dummy variable Γ, which replace either the temperature θ is the vorticity ω.

$$\left(\frac{\partial\psi}{\partial Y}\right)\left(\frac{\partial\Gamma}{\partial X}\right)-\left(\frac{\partial\psi}{\partial X}\right)\left(\frac{\partial\Gamma}{\partial Y}\right)=\varepsilon\left(\frac{\partial^2\Gamma}{\partial X^2}+\frac{\partial^2\Gamma}{\partial Y^2}\right)+\eta\left(\frac{\partial T}{\partial Y}\right) \tag{15}$$

All these terms are listed in **Table 2**.

Dimensionless boundary conditions for (ψ,ω) are:

For: $X=0, X=1$ and $0\le Y\le 1$, $\psi=0$

For: $Y=0, Y=1$ and $0\le X\le 1$, $\psi=0$.

For vorcicite Störtkuh *et al.* [27] have presented an analytical asymptotic solution near the corners of cavity and using finite element bilinear shape functions they also have presented a singularity-removed boundary condition for vorticity at the corner points as well as at the wall points. For the boundary conditions, in both of the numerical methods described above we follow Störtkuh *et al.* [27] and use the following expression for calculating vorticity values at the wall.

Table 2. Presentation of the different terms of the transport equation.

Quantities transported	Γ	η	ε
Vorticity Equation	ω	$\frac{\left[\chi\beta_s\rho_s+(1-\chi)\rho_f\beta_f\right]Ra}{P_r\beta_f\rho_{nf,0}}$	$\frac{\mu_{nf}}{\nu_f\rho_{nf,0}}$
Equation of Energy	θ	0	$\frac{\alpha_{nf}}{\alpha_f P_r}$

$$\frac{1}{3\Delta h^2}\begin{bmatrix}\cdot & \cdot & \cdot\\ \frac{1}{2} & -4 & \frac{1}{2}\\ 1 & 1 & 1\end{bmatrix}\psi+\frac{1}{9}\begin{bmatrix}\cdot & \cdot & \cdot\\ \frac{1}{2} & 2 & \frac{1}{2}\\ \frac{1}{4} & 1 & \frac{1}{4}\end{bmatrix}\omega=-\frac{V}{\Delta h} \tag{16}$$

For corner points, we again follow Störtkuh *et al.* [27] and use the following expression for calculating the vorticity values:

$$\frac{1}{3\Delta h^2}\begin{bmatrix}\cdot & \cdot & \cdot\\ \cdot & -2 & \frac{1}{2}\\ \cdot & \frac{1}{2} & 1\end{bmatrix}\psi+\frac{1}{9}\begin{bmatrix}\cdot & \cdot & \cdot\\ \cdot & 1 & \frac{1}{2}\\ \cdot & \frac{1}{2} & \frac{1}{4}\end{bmatrix}\omega=-\frac{V}{2\Delta h} \tag{17}$$

where V is the speed of the wall in our case which is equal to 0 for the four stationary walls.

In explicit notation, for the wall points shown in **Figure 2(a)**, the vorticity is calculated as the following:

$$\omega_b=-\frac{3}{2\Delta h^2}\left(\psi_d+\psi_e+\psi_f\right)-\frac{1}{8}\left(2\omega_a+2\omega_c+\omega_d+4\omega_e+\omega_f\right) \tag{18}$$

Similarly, for the corner points also shown in **Figure 2(b)**, the vorticity is calculated as the following:

$$\omega_b=-\frac{3}{2\Delta h^2}\psi_f-\frac{1}{4}\left(2\omega_c+2\omega_e+\omega_f\right) \tag{19}$$

The reader is referred to Störtkuh *et al.* [27] for details on the boundary conditions.

The local and averaged heat transfer rates at the bottom hot wall of the cavity are presented by means of the local and averaged Nusselt numbers, Nu and $\overline{Nu}$, which are, respectively determined as follows:

$$Nu=\frac{h_{nf}L}{k_f}=-\left(\frac{k_{nf}}{k_f}\right)\left.\frac{\partial\theta}{\partial Y}\right|_{Y=0} \tag{20}$$

$$\overline{Nu}=\int_0^1\left(-\left(\frac{k_{nf}}{k_f}\right)\left.\frac{\partial\theta}{\partial Y}\right|_{Y=0}\right)\mathrm{d}X \tag{21}$$

3. Method of the Fourth Order Compact

3.1. Introduction

High-Order Compact (HOC) formulations are becoming more popular in computational fluid dynamics (CFD) field of study. Compact formulations provide more accurate solutions in a compact stencil. In finite differences, a standard three-point discretization provides second-order spatial accuracy and this type of discretization is very widely used. When a high-order spatial discretization is desired, *i.e.* fourth-order accuracy, then a five-point discretization has to be used. However, in a five point discretization there is a complexity in handling the points near the boundaries. High-order compact schemes provide fourth-order spatial accuracy in a 3 × 3 stencil

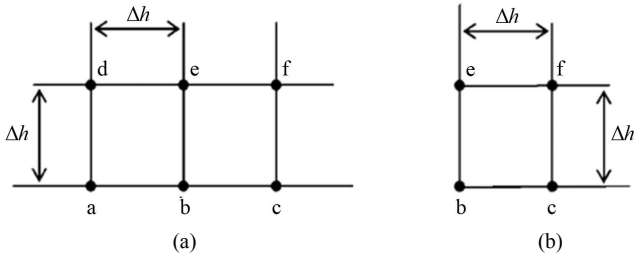

Figure 2. Grid points at the wall and at the corner: (a) wall points and (b) corner points.

and this type of compact formulations does not have the complexity near the boundaries that a standard wide (five- point) fourth-order formulation would have. Dennis and Hudson [28], MacKinnon and Johnson [29], Gupta *et al.* [30], Spotz and Carey [31], Li *et al.* [32], have demonstrated the efficiency of the HOC schemes on the stream function and vorticity formulation of two dimensions. In the literature, it is possible to find numerous different types of iterative numerical methods for the momentum equations. These numerical methods, however, could not be easily used in HOC schemes because of the final form of the HOC formulations used in References [28]-[32]. This fact might be counted as a disadvantage of HOC formulations that the coding stage is rather complex due to the resulting stencil used in these studies. It would be very useful if any numerical method for the solution of momentum equations described in books and papers could be easily applied to HOC formulations. E. Erturk and C. Gokcol [33] present a new Fourth-Order Compact Formulation. The difference of this formulation with References [28]-[32] is not in the way that the Fourth-Order Compact scheme is obtained. The main difference, however, is in the way that the final forms of the equations are written. The main advantage of this formulation is that, any iterative numerical method used for Navier-Stokes equations, can be easily applied to this new FOC formulation, since the final form of the presented FOC formulation is in the same form with the Navier–Stokes equations. Moreover, if someone already has a second-order accurate $O\left(\Delta x^2\right)$ code for the solution of conservation equations the mass and momentum, they can easily convert their existing code to fourth-order accuracy $O\left(\Delta x^4\right)$ by just adding some coefficients into their existing code. In this study, we will applied Using this new compact formulation, we have solved the conservation equations of mass, momentum and energy in square cavity at the Rayleigh number varies in the range $10^3 \le Ra \le 5\times 10^5$ and for different solide volume fractions χ of nanoparticles (Cu) is varied as $0\% \le \chi \le 10\%$, taking water as a base fluid with a Prandtl number equal to $\left(Pr = 6.2\right)$ using a very fine grid mesh to demonstrate the efficiency of this new formulation.

3.2. Principle Method of Fourth Order Compact

We will use the equations of streamlines ψ, vorticity ω and energy θ dimensionless forms are given as follows:

Stream function:

$$\frac{\partial^2\psi}{\partial x^2}+\frac{\partial^2\psi}{\partial y^2}=-\omega \tag{22}$$

General equation of conservation:

$$\left(\frac{\partial\psi}{\partial y}\right)\left(\frac{\partial\Gamma}{\partial x}\right)-\left(\frac{\partial\psi}{\partial x}\right)\left(\frac{\partial\Gamma}{\partial y}\right)=\varepsilon\left(\frac{\partial^2\Gamma}{\partial x^2}+\frac{\partial^2\Gamma}{\partial y^2}\right)+\eta\left(\frac{\partial\theta}{\partial y}\right) \tag{23}$$

For first and second-order derivatives the following discretizations are fourth-order accurate:

$$\frac{\partial\Phi}{\partial x}=\Phi_x-\frac{\Delta x^2}{6}\frac{\partial^3\Phi}{\partial x^3}+O\left(\Delta x^4\right) \tag{24}$$

$$\frac{\partial^2\Phi}{\partial x^2}=\Phi_{xx}-\frac{\Delta x^2}{12}\frac{\partial^4\Phi}{\partial x^4}+O\left(\Delta x^4\right) \tag{25}$$

where Φ_x and Φ_{xx} are standard second-order central discretizations such that

$$\Phi_x = \frac{\Phi_{i+1} - \Phi_{i-1}}{2\Delta x} \tag{26}$$

$$\Phi_{xx} = \frac{\Phi_{i+1} - 2\Phi_i + \Phi_{i-1}}{\Delta x^2} \tag{27}$$

If we apply the discretizations in Equations (24) and (25) to Equations (22) and (23), we obtain the following equation

$$\psi_{xx} + \psi_{yy} - \frac{\Delta x^2}{12}\frac{\partial^4 \psi}{\partial x^4} - \frac{\Delta y^2}{12}\frac{\partial^4 \psi}{\partial y^4} + O\left(\Delta x^4, \Delta y^4\right) = -\omega \tag{28}$$

$$\begin{aligned} &\varepsilon\Gamma_{xx} + \varepsilon\Gamma_{yy} - \varepsilon\frac{\Delta x^2}{12}\left(\frac{\partial^4 \Gamma}{\partial x^4}\right) - \varepsilon\frac{\Delta y^2}{12}\left(\frac{\partial^4 \Gamma}{\partial y^4}\right) + O\left(\Delta x^4, \Delta y^4\right) \\ &= \psi_y\Gamma_x - \psi_x\Gamma_y - \frac{\Delta y^2}{6}\Gamma_x\left(\frac{\partial^3 \psi}{\partial y^3}\right) - \frac{\Delta x^2}{6}\psi_y\left(\frac{\partial^3 \Gamma}{\partial x^3}\right) + \frac{\Delta x^2}{6}\Gamma_y\left(\frac{\partial^3 \psi}{\partial x^3}\right) \\ &+ \frac{\Delta y^2}{6}\psi_x\left(\frac{\partial^3 \Gamma}{\partial y^3}\right) - \eta\theta_y + \eta\frac{\Delta y^2}{6}\left(\frac{\partial^3 \theta}{\partial y^3}\right) + O\left(\Delta x^4, \Delta x^2, \Delta y^2, \Delta y^4\right) \end{aligned} \tag{29}$$

In these equations we have third and fourth derivatives $\left(\partial^3/\partial x^3, \partial^4/\partial x^4, \partial^3/\partial y^3 \text{ et } \partial^4/\partial y^4\right)$ of stream function and general equation of conservation bringing together the equations of vorticity and energy. In order to find an expression for these derivatives we use Equations (22) and (23).

For example, when we take the first and second x-derivative of the stream function Equation (22) we obtain

$$\frac{\partial^3 \psi}{\partial x^3} = -\frac{\partial \omega}{\partial x} - \frac{\partial^3 \psi}{\partial x \partial y^2} \tag{30}$$

$$\frac{\partial^4 \psi}{\partial x^4} = -\frac{\partial^2 \omega}{\partial x^2} - \frac{\partial^4 \psi}{\partial x^2 \partial y^2} \tag{31}$$

And also, by taking the first and second y-derivative of the stream function Equation (22) we obtain

$$\frac{\partial^3 \psi}{\partial y^3} = -\frac{\partial \omega}{\partial y} - \frac{\partial^3 \psi}{\partial y \partial x^2} \tag{32}$$

$$\frac{\partial^4 \psi}{\partial y^4} = -\frac{\partial^2 \omega}{\partial y^2} - \frac{\partial^4 \psi}{\partial y^2 \partial x^2} \tag{33}$$

Using standard second-order central discretizations given in **Table 3**, these equations can be written as

$$\frac{\partial^3 \psi}{\partial x^3} = -\omega_x - \psi_{xyy} + O\left(\Delta x^2, \Delta y^2\right) \tag{34}$$

$$\frac{\partial^4 \psi}{\partial x^4} = -\omega_{xx} - \psi_{xxyy} + O\left(\Delta x^2, \Delta y^2\right) \tag{35}$$

$$\frac{\partial^3 \psi}{\partial y^3} = -\omega_y - \psi_{yxx} + O\left(\Delta x^2, \Delta y^2\right) \tag{36}$$

$$\frac{\partial^4 \psi}{\partial y^4} = -\omega_{yy} - \psi_{xxyy} + O\left(\Delta x^2, \Delta y^2\right) \tag{37}$$

When we substitute Equations (35) and (37) into Equation (28) we obtain the following finite difference equation.

Table 3. Standard second-order central discretizations.

Derivations	Discretizations
Φ_x	$\frac{\Phi_{i+1,j}-\Phi_{i-1,j}}{2\Delta x}$
Φ_y	$\frac{\Phi_{i,j+1}-\Phi_{i,j-1}}{2\Delta y}$
Φ_{xx}	$\frac{\Phi_{i+1,j}-2\Phi_{i,j}+\Phi_{i-1,j}}{\Delta x^2}$
Φ_{yy}	$\frac{\Phi_{i,j+1}-2\Phi_{i,j}+\Phi_{i,j-1}}{\Delta y^2}$
Φ_{xy}	$\frac{\Phi_{i+1,j+1}-\Phi_{i-1,j+1}-\Phi_{i+1,j-1}+\Phi_{i-1,j-1}}{4\Delta x\Delta y}$
Φ_{xxy}	$\frac{\Phi_{i+1,j+1}-2\Phi_{i,j+1}+\Phi_{i-1,j+1}-\Phi_{i+1,j-1}+2\Phi_{i,j-1}-\Phi_{i-1,j-1}}{2\Delta x^2\Delta y}$
Φ_{xyy}	$\frac{\Phi_{i+1,j+1}-2\Phi_{i+1,j}+\Phi_{i+1,j-1}-\Phi_{i-1,j+1}-2\Phi_{i-1,j}+\Phi_{i-1,j-1}}{2\Delta x\Delta y^2}$
Φ_{xxyy}	$\frac{\Phi_{i+1,j+1}-2\Phi_{i,j+1}+\Phi_{i-1,j+1}-2\Phi_{i+1,j}+4\Phi_{i,j}-2\Phi_{i-1,j}+\Phi_{i+1,j-1}-2\Phi_{i,j-1}+\Phi_{i-1,j-1}}{\Delta x^2\Delta y^2}$

$$\Psi_{xx}+\Psi_{yy}=-\omega-\frac{\Delta x^2}{12}\omega_{xx}-\frac{\Delta y^2}{12}\omega_{yy}-\left(\frac{\Delta x^2}{12}+\frac{\Delta y^2}{12}\right)\psi_{xxyy}+O\left(\Delta x^4,\Delta x^2,\Delta y^2,\Delta y^4\right) \tag{38}$$

We note that the solution of Equation (38) is also a solution to stream function Equation (22) with fourth-order spatial accuracy. Therefore, if we numerically solve Equation (38), the solution we obtain will satisfy the stream function equation up to fourth order accuracy.

In order to obtain a fourth-order approximation for the vorticity equation and energy (23), we follow the same procedure. When we take the first and second derivatives of the general equation of conservation (23) with respect to x- and y-coordinates we obtain:

$$\frac{\partial^3\Gamma}{\partial x^3}=\frac{1}{\varepsilon}\frac{\partial^2\psi}{\partial x\partial y}\frac{\partial\Gamma}{\partial x}+\frac{1}{\varepsilon}\frac{\partial\psi}{\partial y}\frac{\partial^2\Gamma}{\partial x^2}-\frac{1}{\varepsilon}\frac{\partial^2\psi}{\partial x^2}\frac{\partial\Gamma}{\partial y}-\frac{1}{\varepsilon}\frac{\partial\psi}{\partial x}\frac{\partial^2\Gamma}{\partial x\partial y}-\frac{\eta}{\varepsilon}\frac{\partial^2\theta}{\partial x\partial y}-\frac{\partial^3\Gamma}{\partial x\partial y^2} \tag{39}$$

$$\begin{aligned}\frac{\partial^4\Gamma}{\partial x^4}=&\frac{1}{\varepsilon}\frac{\partial^3\psi}{\partial x^2\partial y}\frac{\partial\Gamma}{\partial x}+\frac{1}{\varepsilon}\frac{\partial^2\psi}{\partial x\partial y}\frac{\partial^2\Gamma}{\partial x^2}+\frac{1}{\varepsilon}\frac{\partial^2\psi}{\partial x\partial y}\frac{\partial^2\Gamma}{\partial x^2}+\frac{1}{\varepsilon}\frac{\partial\psi}{\partial y}\frac{\partial^3\Gamma}{\partial x^3}-\frac{1}{\varepsilon}\frac{\partial^3\psi}{\partial x^3}\frac{\partial\Gamma}{\partial y}\\&-\frac{1}{\varepsilon}\frac{\partial^2\psi}{\partial x^2}\frac{\partial^2\Gamma}{\partial x\partial y}-\frac{1}{\varepsilon}\frac{\partial^2\psi}{\partial x^2}\frac{\partial^2\Gamma}{\partial x\partial y}-\frac{1}{\varepsilon}\frac{\partial\psi}{\partial x}\frac{\partial^3\Gamma}{\partial x^2\partial y}-\frac{\eta}{\varepsilon}\frac{\partial^3\theta}{\partial x^2\partial y}-\frac{\partial^4\Gamma}{\partial x^2\partial y^2}\end{aligned} \tag{40}$$

$$\frac{\partial^3\Gamma}{\partial y^3}=\frac{1}{\varepsilon}\frac{\partial^2\psi}{\partial y^2}\frac{\partial\Gamma}{\partial x}+\frac{1}{\varepsilon}\frac{\partial\psi}{\partial y}\frac{\partial^2\Gamma}{\partial x\partial y}-\frac{1}{\varepsilon}\frac{\partial^2\psi}{\partial x\partial y}\frac{\partial\Gamma}{\partial y}-\frac{1}{\varepsilon}\frac{\partial\psi}{\partial x}\frac{\partial^2\Gamma}{\partial y^2}-\frac{\eta}{\varepsilon}\frac{\partial^2\theta}{\partial x\partial y}-\frac{\partial^3\Gamma}{\partial x^2\partial y} \tag{41}$$

$$\begin{aligned}\frac{\partial^4\Gamma}{\partial y^4}=&\frac{1}{\varepsilon}\frac{\partial^3\psi}{\partial y^3}\frac{\partial\Gamma}{\partial x}+\frac{1}{\varepsilon}\frac{\partial^2\psi}{\partial y^2}\frac{\partial^2\Gamma}{\partial x\partial y}+\frac{1}{\varepsilon}\frac{\partial^2\psi}{\partial y^2}\frac{\partial^2\Gamma}{\partial x\partial y}+\frac{1}{\varepsilon}\frac{\partial^2\psi}{\partial y^2}\frac{\partial^2\Gamma}{\partial x\partial y}-\frac{1}{\varepsilon}\frac{\partial^3\psi}{\partial x\partial y^2}\frac{\partial\Gamma}{\partial y}\\&-\frac{1}{\varepsilon}\frac{\partial^2\psi}{\partial x\partial y}\frac{\partial^2\Gamma}{\partial y^2}-\frac{1}{\varepsilon}\frac{\partial^2\psi}{\partial x\partial y}\frac{\partial^2\Gamma}{\partial y^2}-\frac{1}{\varepsilon}\frac{\partial\psi}{\partial x}\frac{\partial^3\Gamma}{\partial y^3}-\frac{\eta}{\varepsilon}\frac{\partial^3\theta}{\partial x\partial y^2}-\frac{\partial^4\Gamma}{\partial x^2\partial y^2}\end{aligned} \tag{42}$$

If we substitute Equations (39) and (41) for the third derivatives of the general equation of conservation and into Equations (29), (40) and (42) and also if we substitute Equations (34) and (36), for the third derivatives of stream function into Equations (29), (40) and (42) and finally, if we substitute Equations (40) and (42) for the fourth derivatives of the general equation of conservation into Equation (29), then we obtain the following:

$$\begin{aligned}
&\Gamma_{xx}+\Gamma_{yy}-\frac{1}{\varepsilon}\frac{\Delta x^2}{6}\psi_{xy}\Gamma_{xx}+\frac{1}{\varepsilon}\frac{\Delta y^2}{6}\psi_{xy}\Gamma_{yy}+\frac{1}{\varepsilon^2}\frac{\Delta x^2}{12}\psi_y\psi_y\Gamma_{xx}+\frac{1}{\varepsilon^2}\frac{\Delta y^2}{12}\psi_x\psi_x\Gamma_{yy}\\
&=\frac{1}{\varepsilon}\psi_y\Gamma_x-\frac{1}{\varepsilon}\psi_x\Gamma_y+\frac{1}{\varepsilon}\left(\frac{\Delta x^2}{12}+\frac{\Delta y^2}{12}\right)\psi_{xxy}\Gamma_x-\frac{1}{\varepsilon}\left(\frac{\Delta x^2}{12}+\frac{\Delta y^2}{12}\right)\psi_{xyy}\Gamma_y-\frac{1}{\varepsilon^2}\frac{\Delta x^2}{12}\psi_y\psi_{xy}\Gamma_x\\
&+\frac{1}{\varepsilon^2}\frac{\Delta y^2}{12}\psi_x\psi_{yy}\Gamma_x+\frac{1}{\varepsilon^2}\frac{\Delta x^2}{12}\psi_y\psi_{xx}\Gamma_y-\frac{1}{\varepsilon^2}\frac{\Delta y^2}{12}\psi_x\psi_{xy}\Gamma_y+\frac{1}{\varepsilon}\left(\frac{\Delta x^2}{12}+\frac{\Delta y^2}{12}\right)\psi_y\Gamma_{xyy}\\
&-\frac{1}{\varepsilon}\left(\frac{\Delta x^2}{12}+\frac{\Delta y^2}{12}\right)\psi_x\Gamma_{xxy}-\frac{1}{\varepsilon}\frac{\Delta x^2}{6}\psi_{xx}\Gamma_{xy}+\frac{1}{\varepsilon}\frac{\Delta y^2}{6}\psi_{yy}\Gamma_{xy}+\frac{1}{\varepsilon^2}\left(\frac{\Delta x^2}{12}+\frac{\Delta y^2}{12}\right)\psi_x\psi_y\Gamma_{xy}\\
&-\frac{1}{\varepsilon}\left(\frac{\Delta x^2}{12}-\frac{\Delta y^2}{12}\right)\Gamma_x\Gamma_y-\left(\frac{\Delta x^2}{12}+\frac{\Delta y^2}{12}\right)\Gamma_{xxyy}-\frac{\eta}{\Upsilon_1}\theta_y+\eta\cdot\text{thrust}+O\left(\Delta x^4,\Delta x^2,\Delta y^2\Delta y^4\right)
\end{aligned}\tag{43}$$

where:

$$\begin{aligned}
\text{thrust}=&\frac{\Upsilon_2}{\Upsilon_1}\frac{\Delta y^2}{12}\psi_{xy}\theta_y+\left(\frac{\Upsilon_2}{\Upsilon_1}-\frac{1}{\Upsilon_1^2}\right)\frac{\Delta y^2}{12}\psi_x\theta_{yy}-\frac{\Upsilon_2}{\Upsilon_1}\frac{\Delta x^2}{12}\psi_{yy}\theta_y\\
&+\left(\frac{1}{\Upsilon_1^2}\frac{\Delta x^2}{12}-\frac{\Upsilon_2}{\Upsilon_1}\frac{\Delta y^2}{12}\right)\psi_y\theta_{xy}-\frac{1}{\Upsilon_1}\left(\frac{\Delta x^2}{12}-\frac{\Delta y^2}{12}\right)\theta_{xxy}
\end{aligned}$$

and $\Upsilon_1=\dfrac{\mu_{nf}}{\nu_f\rho_{nf,0}};\Upsilon_2=\dfrac{\alpha_{nf}}{\alpha_f P_r}$.

Again we note that the solution of Equation (43) satisfy the vorticity and energy Equation (23) with fourth-order accuracy.

As the final form of our FOC scheme, we prefer to write Equations (38) and (43) as

$$\psi_{xx}+\psi_{yy}=-\omega+A \tag{44}$$

$$\varepsilon(1+B)\Gamma_{xx}+\varepsilon(1+C)\Gamma_{yy}=(\psi_y+D)\Gamma_x-(\psi_x+E)\Gamma_y+\left(-\frac{\eta}{\Upsilon_1}\theta_y+F\right) \tag{45}$$

where

$$A=-\frac{\Delta x^2}{12}\omega_{xx}-\frac{\Delta y^2}{12}\omega_{yy}-\left(\frac{\Delta x^2}{12}+\frac{\Delta y^2}{12}\right)\Psi_{xxyy}$$

$$B=-\frac{1}{\varepsilon}\frac{\Delta x^2}{6}\Psi_{xy}+\frac{1}{\varepsilon^2}\frac{\Delta x^2}{12}\Psi_y\Psi_y$$

$$C=\frac{1}{\varepsilon}\frac{\Delta y^2}{6}\Psi_{xy}+\frac{1}{\varepsilon^2}\frac{\Delta y^2}{12}\Psi_x\Psi_x$$

$$D=\left(\frac{\Delta x^2}{12}+\frac{\Delta y^2}{12}\right)\Psi_{xxy}-\frac{1}{\varepsilon}\frac{\Delta x^2}{12}\Psi_y\Psi_{xy}+\frac{1}{\varepsilon}\frac{\Delta y^2}{12}\Psi_x\Psi_{yy}$$

$$E=\left(\frac{\Delta x^2}{12}+\frac{\Delta y^2}{12}\right)\Psi_{xyy}-\frac{1}{\varepsilon}\frac{\Delta x^2}{12}\Psi_y\Psi_{xx}+\frac{1}{\varepsilon}\frac{\Delta y^2}{12}\Psi_x\Psi_{xy}$$

$$\begin{aligned}
F=&\left(\frac{\Delta x^2}{12}+\frac{\Delta y^2}{12}\right)\psi_y\Gamma_{xyy}-\left(\frac{\Delta x^2}{12}+\frac{\Delta y^2}{12}\right)\psi_x\Gamma_{xxy}-\frac{1}{\varepsilon}\frac{\Delta x^2}{6}\psi_{xx}\Gamma_{xy}+\frac{\Delta y^2}{6}\psi_{yy}\Gamma_{xy}\\
&+\frac{1}{\varepsilon}\left(\frac{\Delta x^2}{12}+\frac{\Delta y^2}{12}\right)\psi_x\psi_y\Gamma_{xy}-\frac{1}{\varepsilon}\left(\frac{\Delta x^2}{12}-\frac{\Delta y^2}{12}\right)\Gamma_x\Gamma_y-\left(\frac{\Delta x^2}{12}+\frac{\Delta y^2}{12}\right)\Gamma_{xxyy}+\eta\cdot\text{thrust}
\end{aligned}\tag{46}$$

We note that the finite difference Equations (44) and (45) are fourth-order accurate $O\left(\Delta x^4,\Delta x^2,\Delta y^2\Delta y^4\right)$

approximation of the stream function, vorticity and energy Equations (22) and (23). In Equations (44) and (45), however, if A, B, C, D, E and F are chosen to be equal to 0 then the finite difference Equations (44) and (45) simply become

$$\psi_{xx} + \psi_{yy} = -\omega \tag{47}$$

$$\varepsilon\Gamma_{xx} + \varepsilon\Gamma_{yy} = \psi_y \cdot \Gamma_x - \psi_x \cdot \Gamma_y - \frac{\eta}{\Upsilon_1}\theta_y \tag{48}$$

Equations (47) and (48) are the standard second-order accurate $\left(O\left(\Delta x^2, \Delta y^2\right)\right)$ approximation of the stream-function and the general equation of conservation (22) and (23). When we use Equations (44) and (45) for the numerical solution of the stream function and general equation of conservation, we can easily switch between second and fourth-order accuracy just by using homogeneous values for the coefficients A, B, C, D, E and F or by using the expressions defined in Equation (46) in the code.

We note that the numerical solutions of Equations (44) and (45), strictly provided that second-order discretizations in **Table 3** are used and also strictly provided that a uniform grid mesh with and is used, are fourth-order accurate to streamfunction and the general equation of conservation (21) and (22). The only difference between Equations (44) and (45) and Equations (22) and (23) are the coefficients A, B, C, D, E and F. So these equations are of the same form, therefore, all the iterative numerical methods (such as SOR, ADI, factorization schemes, pseudo time iterations, etc.) used to solve stream-function, vorticity and energy Equations (22) and (23) can also be easily applied to fourth-order Equations (44) and (45). In our work we apply the ADI method on the equations of 4th order.

As a measure of convergence to the steady state, during the iterations we monitored three residual parameters. The first residual parameter, RES1, is defined as the maximum absolute residual of the finite difference equations of steady stream function and general Equations (44) and (45). These are, respectively, given as

$$RES1_{\psi} = \max\left(\left|\frac{\psi_{i-1,j}^{n+1} - 2\psi_{i,j}^{n+1} + \psi_{i+1,j}^{n+1}}{\Delta x^2} + \frac{\psi_{i,j-1}^{n+1} - 2\psi_{i,j}^{n+1} + \psi_{i,j+1}^{n+1}}{\Delta y^2} + \omega_{i,j}^{n+1} - A_{i,j}^{n+1}\right|\right) \tag{49}$$

$$\begin{aligned} RES1_{\Gamma} = \max\Bigg(\Bigg|&\varepsilon\left(1 + B_{i,j}^{n+1}\right)\left(\frac{\Gamma_{i-1,j}^{n+1} - 2\Gamma_{i,j}^{n+1} + \Gamma_{i+1,j}^{n+1}}{\Delta x^2}\right) + \varepsilon\left(1 + C_{i,j}^{n+1}\right)\left(\frac{\Gamma_{i,j-1}^{n+1} - 2\Gamma_{i,j}^{n+1} + \Gamma_{i,j+1}^{n+1}}{\Delta y^2}\right) \\ &- \left(\frac{\psi_{i,j+1}^{n+1} - \psi_{i,j-1}^{n+1}}{2\Delta y} + D_{i,j}^{n+1}\right)\left(\frac{\Gamma_{i+1,j}^{n+1} - \Gamma_{i-1,j}^{n+1}}{2\Delta x}\right) + \left(\frac{\psi_{i+1,j}^{n+1} - \psi_{i-1,j}^{n+1}}{2\Delta x} + E_{i,j}^{n+1}\right)\left(\frac{\Gamma_{i,j+1}^{n+1} - \Gamma_{i,j-1}^{n+1}}{2\Delta y}\right) + \left(\frac{\eta}{\Upsilon_1}\frac{\theta_{i,j+1}^{n+1} - \theta_{i,j-1}^{n+1}}{2\Delta y} - F_{i,j}^{n+1}\right)\Bigg|\Bigg) \end{aligned} \tag{50}$$

The magnitude of RES1 is an indication of the degree to which the solution has converged to steady state. In the limit RES1 would be zero. The second residual parameter, RES2, is defined as the maximum absolute difference between two iteration steps in the stream function, vorticity and energy variables. These are, respectively, given as

$$RES2_{\psi} = \max\left(\left|\psi_{i,j}^{n+1} - \psi_{i,j}^{n}\right|\right) \tag{51}$$

$$RES2_{\Gamma} = \max\left(\left|\Gamma_{i,j}^{n+1} - \Gamma_{i,j}^{n}\right|\right) \tag{52}$$

RES2 gives an indication of the significant digit on which the code is iterating. The third residual parameter, RES3, is similar to RES2, except that it is normalized by the representative value at the previous time step. This then provides an indication of the maximum percent change in ψ and Γ in each iteration step. RES3 is defined as

$$RES3_{\psi} = \max\left(\left|\frac{\psi_{i,j}^{n+1} - \psi_{i,j}^{n}}{\psi_{i,j}^{n+1}}\right|\right) \tag{53}$$

$$RES3_{\Gamma} = \max\left(\left|\frac{\Gamma_{i,j}^{n+1} - \Gamma_{i,j}^{n}}{\Gamma_{i,j}^{n+1}}\right|\right) \tag{54}$$

In our calculations, for all Rayleigh numbers we considered that convergence was achieved when both $RES1_{\psi} \le 10^{-6}$ and $RES1_{\Gamma} \le 10^{-6}$ were achieved. Such a low value was chosen to ensure the accuracy of the solution. At these convergence levels, the second residual parameters were in the order of $RES2_{\psi} \le 10^{-10}$ and $RES2_{\Gamma} \le 10^{-11}$, which means that the stream function, vorticity and energy variables are accurate to the 10^{th} and 9^{th} digit accuracy, respectively, at a grid point and even more accurate at the rest of the grids. In addition, at these convergence levels the third residual parameters were in the order of $RES3_{\psi} \le 10^{-10}$ and $RES3_{\Gamma} \le 10^{-9}$, which means that the stream function, vorticity and energy variables are changing with 10% - 9% and 10% - 8% of their values, respectively, in an iteration step at a grid point and even with less percentage at the rest of the grids. These very low residuals ensure that our solutions are indeed very accurate.

4. Results and Discussion

In the present grid independence test, the Prandtl number is set to Pr = 6.2 (pure water). The nanoparticles are chosen to be copper (Cu) with a solid volume fraction $\chi = 0.1$ and a Rayleigh number Ra = 10^5. Numerical computations have been carried on five different grid sizes 32 × 32, 42 × 42, 62 × 62, 82 × 82 and 102 × 102 grid sizes. **Table 4** regroups the values of the averaged Nusselt number through the hot wall and the maximum value of the stream function. Uniform grid has been used for all the computations. The distribution of the u-velocity in the vertical mid-plane and v-velocity in the horizontal mid-plane are shown in **Figure 3**. It is observed that the curves overlap with each other for 82 × 82 and 102 × 102. So a grid number of 82 × 82 is chosen for further computation.

Our code has been tested for natural convection fluid flows in differentially heated cavities and in Rayleigh-Bénard configuration for Rayleigh numbers between 10^3 and 10^6 (**Table 5**) and gave excellent results (see ref. [12] [14] [34]-[36]).

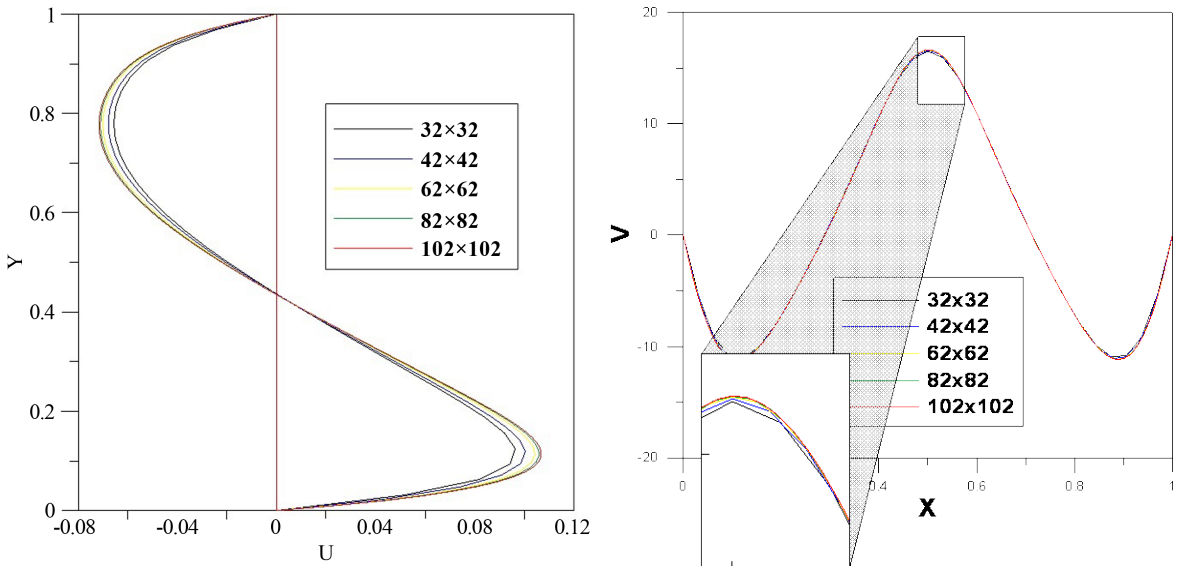

Figure 3. Velocity profiles at mid-sections of the cavity for various meshes sizes (Ra = 10^5 and χ = 0.1).

Table 4. Grid independency results for water-Cu, $Ra = 10^5$ and $\chi = 10\%$.

Grid	32 × 32	42 × 42	62 × 62	82 × 82	102 × 102
$\overline{Nu}$	4.7357	4.6657	4.6072	4.5848	4.5741
$\lvert\Psi_{\max}\rvert$	2.06977	2.0668	2.0621	2.0593	2.0593

Table 5. Comparaison between the present work and other studies for $\overline{Nu}$.

	$Ra=10^3$	$Ra=10^4$	$Ra=10^5$	$Ra=10^6$
G.de Val Davis [34]	1.118	2.243	4.519	8.799
Markatos and perikleous [35]	1.108	2.201	4.430	8.754
G.V.Hadjisophcleous *et al*. [36]	1.141	2.290	4.964	10.390
R.K. Tiwari, M.K. Das [12]	1.087	2.195	4.450	8.803
I. El Bouihi and R. Sehaqui [14]	1.042	2.024	4.520	8.978
Present work	1.012	2.214	4.103	8.293
Difference with I. El Bouihi %	2.87	9.38	9.22	7.62

In this section, the nanofluid-filled enclosure is studied for a range of solid volume fraction $0\% \le \chi \le 10\%$ and the Rayleigh number varies from 10^3 to 10^5. For all simulations the considered base fluid is water ($Pr = 6.2$). In **Figure 4**, we present the streamlines (top) and isotherms (bottom) for $10^3 \le Ra \le 10^5$, for the case of a water-Cu nanofluid and pure water. The value of solid volume fraction is set to $\chi = 0.04$. **Figure 5** represents the same physical quantities but for a volume fraction value of $\chi = 0.1$. Due to the temperature distribution imposed at the bottom wall and to the boundary conditions on vertical walls, we observe a symmetry behavior in both the streamlines and in the contour maps of the isotherms. We can see that whatever the Rayleigh number and value of solid volume fraction, the flow is mainly composed of two counter-rotating circulating cells.

Figure 6 presents the velocity profiles $V(X)$ and $U(Y)$ along the mid-section of the enclosure $X = 0.5$ and $Y = 0.5$ for different values of χ and is in good concordance with the fact that the nanofluid moves slower than a pure water. Indeed, for $Ra = 10^3$, the deviation (relative to $\chi = 0$) between the maximum values of vertical velocity is $\Delta V_{\max} = 18.63\%$ for $\chi = 4\%$ and $\Delta V_{\max} = 38.77\%$ for $\chi = 10\%$. By increasing the Rayleigh number, these deviations decrease. For $Ra = 5 \times 10^4$ and $Ra = 10^5$ these deviations are $\Delta V_{\max}(0.04) = 1.47\%$, $\Delta V_{\max}(0.1) = 22.01\%$, $\Delta V_{\max}(0.04) = 2.08\%$ and $\Delta V_{\max}(0.1) = 8.73\%$ respectively. As far as the temperature distribution is concerned, clear differences are observed in the isotherm contour plots compared to the case $\chi = 0$. These differences are accentuated as the solid volume fraction increases. These differences mean that the presence of nanoparticles affect especially the heat transfer rate through the enclosure.

The heat transfer distribution through the hot wall is displayed in **Figure 7** through the plotted lines of the local Nusselt number for different values of Ra. One can see that for all combinations of Ra and χ, the local Nusselt number behavior is symmetric with respect to the plane $X = 0.5$. For low Rayleigh numbers, ($Ra = 5 \times 10^3$) and $\chi = 0$, the transfer of heat through the hot wall is relatively low with a slight curvature at $X = 0.5$. This curvature is due to relatively higher intensity of the counter rotating cells represented by the highest value of $\psi_{\max}$ when $\chi = 0$. When χ increases to $\chi = 0.1$, the curvature at the center disappears because the fluid velocity decreases. The heat transfer in this case is maximum at $X = 0.5$ and is higher due to the presence of nanoparticles whose thermal conductivity is much greater than that of water. The same phenomena are observed almost on the curves related to $Ra = 5 \times 10^4$ and $Ra = 5 \times 10^5$ with a maximum heat transfer in the vicinity of $X = 0.25$ and $X = 0.75$. For example, for $Ra = 5 \times 10^4$, the maximum Nusselt number value is $Nu_{\max} = 7.374$ and is situated at both locations $X = 0.317$ and $X = 0.682$ for $\chi = 0$. For $\chi = 0.1$, $Nu_{\max} = 10.394$ and is located at $X = 0.317$ and $X = 0.695$.

The variations of average Nusselt number (Nu) with Ra and χ are shown in **Table 6**. For $Ra = 10^3$, there is a substantial increase in Nu as χ is increased above 2%. In general, Nu increases with χ. When χ is 2%, the increase is approximately 9.75%. When χ is 4%, the increase is approximately 19.51%. When χ is 8%, the increase is above 42.07%. For $Ra = 10^4$, as χ is increased to 2%, an increase of 6.03% is observed. A heat transfer augmentation of above 27.63% is obtained for $\chi = 8\%$ compared to $\chi = 0\%$ or more is observed for different Rayleigh number Ra. Thus, one can conclude that the Nusselt number increases with the increase of the volume fraction χ and Rayleigh number Ra.

5. Conclusions

In this study the heat transfer enhancement in a two dimensional enclosure filled with nanofluids is studied

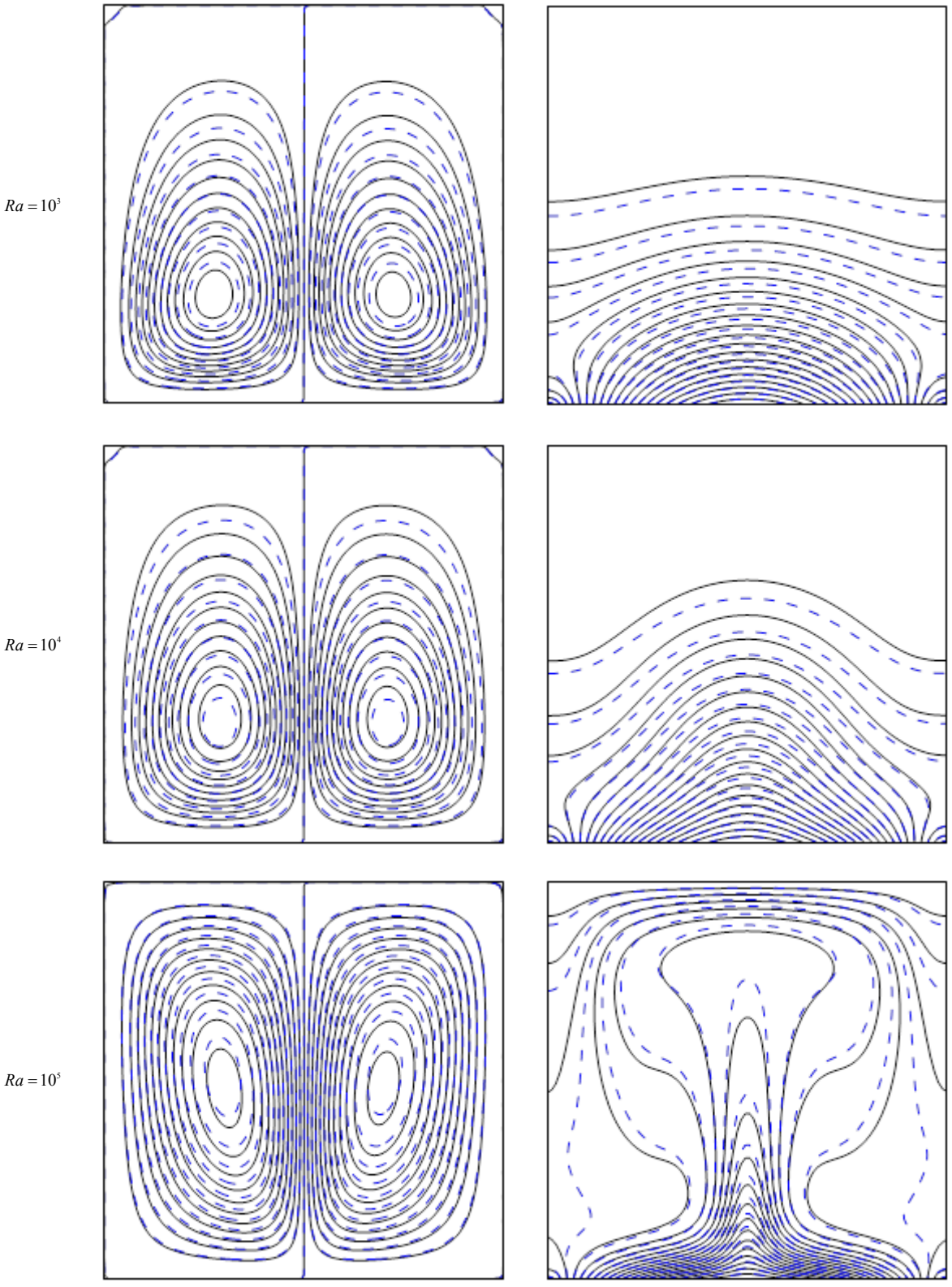

Figure 4. Streamlines and isotherms for the enclosure filled with water-Cu nanofluid (- - -), $\chi = 0.04$ and pure water (—) at different Rayleigh numbers.

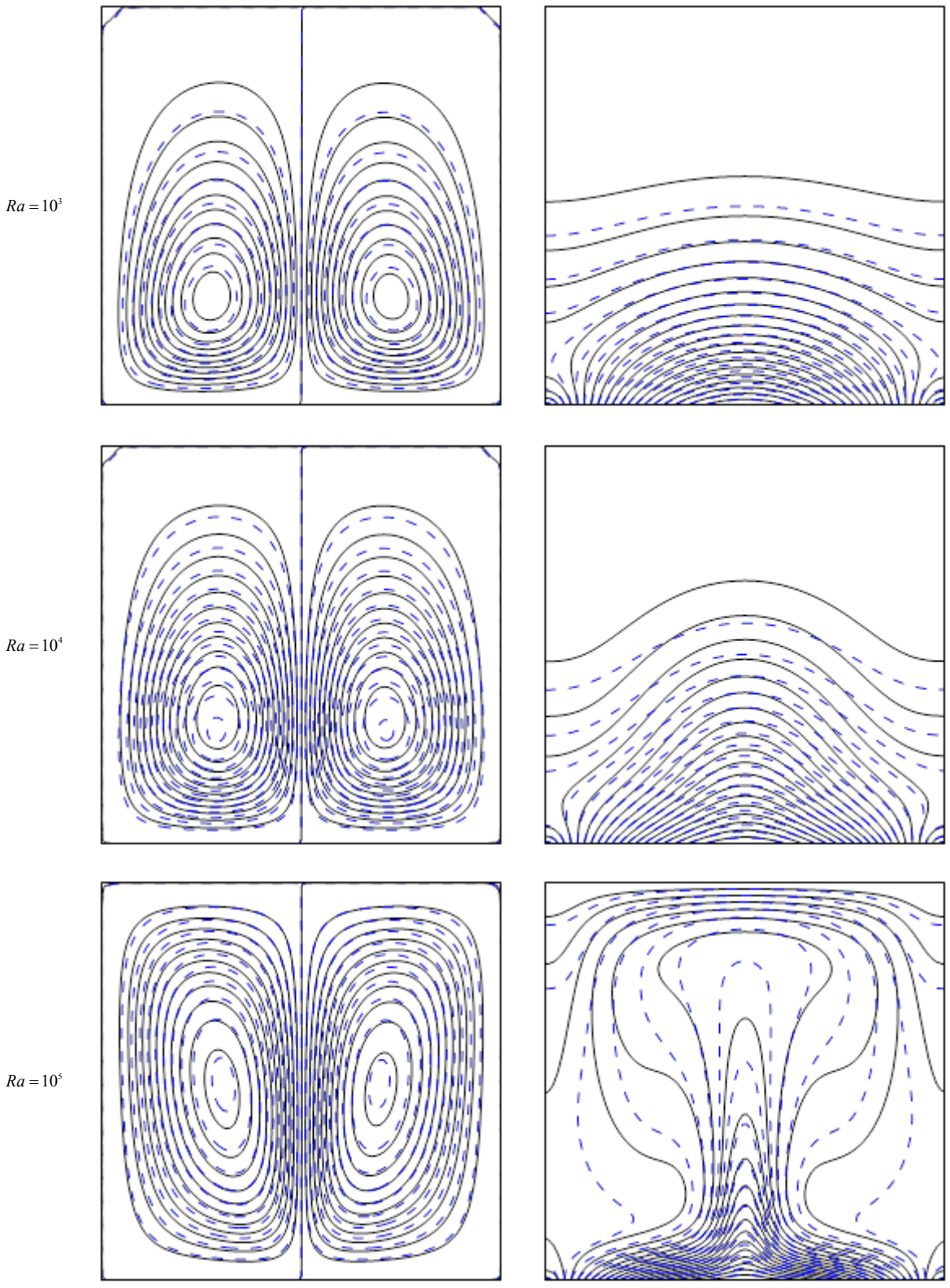

Figure 5. Streamlines and isotherms for the enclosure filled with water-Cu nanofluid (- - -), $\chi = 0.1$ and pure water (—) at different Rayleigh numbers.

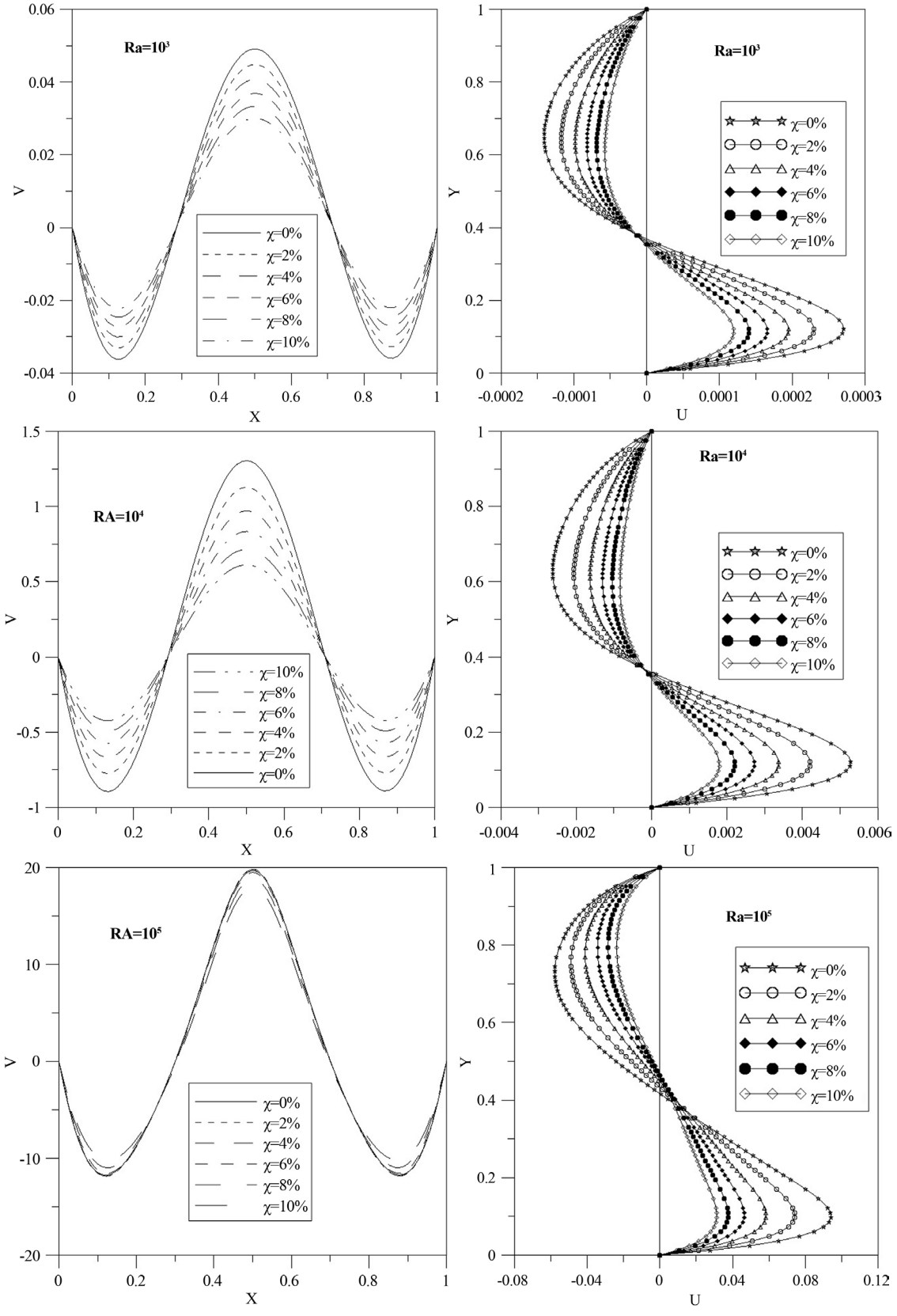

Figure 6. Velocity profiles along the mid-plane for different Ra and different solid volume fractions (Water-Cu).

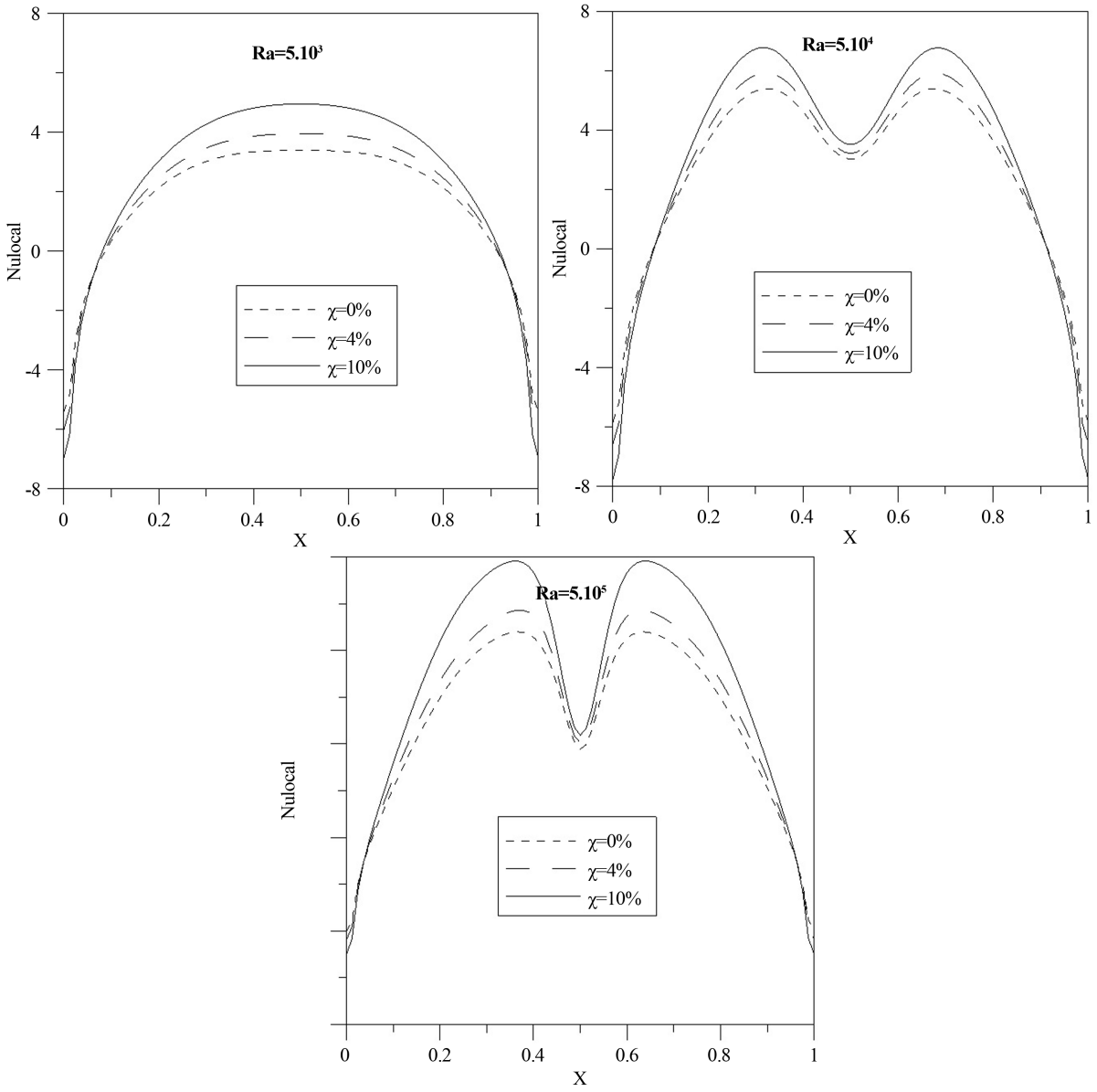

Figure 7. Local Nusselt number through the heated wall for different Ra and solid volume fractions (water-Cu).

Table 6. Comparison of average Nusselt number $\overline{Nu}$ for different Rayleigh number and various solid volume fractions.

	$A(\chi=0\%)$	$B(\chi=2\%)$	$\frac{B-A}{A}\times 100$	$C(\chi=4\%)$	$\frac{C-A}{A}\times 100$	$D(\chi=6\%)$	$\frac{D-A}{A}\times 100$	$E(\chi=8\%)$	$\frac{E-A}{A}\times 100$
$Ra=10^3$	1.64	1.80	9.75	1.96	19.51	2.14	30.48	2.33	42.07
$Ra=5\times10^3$	1.73	1.88	8.67	2.04	17.91	2.21	27.74	2.39	38.15
$Ra=10^4$	1.99	2.11	6.03	2.24	12.56	2.39	20.10	2.54	27.63
$Ra=5\times10^4$	4.42	4.75	7.46	5.09	15.15	5.46	23.52	5.86	32.57
$Ra=10^5$	4.81	5.11	6.23	5.45	13.30	5.83	21.20	6.26	30.14
$Ra=5\times10^5$	6.42	6.73	4.82	7.16	11.52	7.67	19.47	8.22	28.03
$Ra=10^6$	7.61	7.89	3.67	8.29	8.93	8.87	16.55	9.54	25.36

numerically. This study presented a new fourth-order compact formulation and investigated the effect of a sinusoidal thermal boundary condition, for different Rayleigh number *Ra* and volume fractions of nanoparticles. The flow and temperature fields are symmetric near the middle plane of the enclosure due to the imposed symmetry condition on the bottom wall boundary. From the results of this work, the following main conclusions may be drawn:

- The fourth-order accurate compact formulation was developed and was in agree with previous studies.
- Our numerical code has been validated for different Rayleigh number.
- A comparative study illustrates that the suspended nanoparticles substantially increase the heat transfer rate with an increase in the nanoparticles volume fraction for different Rayleigh number *Ra* Rayleigh number. Moreover, the nanofluid flows as well as the cooper nanoparticles increase.

In the near future, this study will be extended for different geometry studies and other types of base fluids and nanoparticles.

References

[1] Choi, S. (1995) Enhancing Thermal Conductivity of Fluids with Nanoparticles. In: Siginer, D.A. and Wang, H.P., Eds., *Developments and Applications of Non-Newtonian Flows*, FED-Vol. 231/MD-Vol. 66, ASME, New York, 99-105.

[2] Khanafer, K., Vafai, K. and Lightstone, M. (2003) Buoyancy-Driven Heat Transfer Enhancement in a Two-Dimensional Enclosure Utilizing Nanofluids. *International Journal of Heat and Mass Transfer*, **46**, 3639-3653. http://dx.doi.org/10.1016/S0017-9310(03)00156-X

[3] Lee, S., Choi, S.U.-S., Li, S. and Eastman, J. (1999) Measuring Thermal Conductivity of Fluids Containing Oxide Nanoparticles. *Journal of Heat Transfer*, **121**, 280-289. http://dx.doi.org/10.1115/1.2825978

[4] Xie, H., Wang, J., Xi, T. and Liu, Y. (2002) Thermal Conductivity of Suspensions Containing Nanosized SiC Particles. *International Journal of Thermophysics*, **23**, 571-580. http://dx.doi.org/10.1023/A:1015121805842

[5] Xie, H., Wang, J., Xi, T., Liu, Y. and Ai, F. (2002) Dependence of the Thermal Conductivity of Nanoparticle-Fluid Mixture on the Base Fluid. *Journal of Materials Science Letters*, **21**, 1469-1471. http://dx.doi.org/10.1023/A:1020060324472

[6] Hwang, K.S., Jang, S.P. and Choi, S.U. (2009) Flow and Convective Heat Transfer Characteristics of Water-Based Al_2O_3 Nanofluids in Fully Developed Laminar Flow Regime. *International Journal of Heat and Mass Transfer*, **52**, 193-199. http://dx.doi.org/10.1016/j.ijheatmasstransfer.2008.06.032

[7] Wen, D. and Ding, Y. (2004) Experimental Investigation into Convective Heat Transfer of Nanofluids at the Entrance Region under Laminar Flow Conditions. *International Journal of Heat and Mass Transfer*, **47**, 5181-5188. http://dx.doi.org/10.1016/j.ijheatmasstransfer.2004.07.012

[8] Xuan, Y. and Li, Q. (2003) Investigation on Convective Heat Transfer and Flow Features of Nanofluids. *Journal of Heat Transfer*, **125**, 151-155. http://dx.doi.org/10.1115/1.1532008

[9] Xuan, Y. and Li, Q. (2000) Heat Transfer Enhancement of Nanofluids. *International Journal of Heat and Fluid Flow*, **21**, 58-64. http://dx.doi.org/10.1016/S0142-727X(99)00067-3

[10] Naramgari, S. and Sulochana, C. (2015) MHD Flow of Dusty Nanofluid over a Stretching Surface with Volume Fraction of Dust Particles. *Ain Shams Engineering Journal*, **7**, 709-716. http://dx.doi.org/10.1016/j.asej.2015.05.015

[11] Ben-Cheikh, N., Chamkha, A.J., Ben-Beya, B. and Lili, T. (2013) Natural Convection of Water-Based Nanofluids in a Square Enclosure with Non-Uniform Heating of the Bottom Wall. *Journal of Modern Physics*, **4**, 147-159. http://dx.doi.org/10.4236/jmp.2013.42021

[12] Tiwari, R.K. and Das, M.K. (2007) Heat Transfer Augmentation in a Two-Sided Lid-Driven Differentially Heated Square Cavity Utilizing Nanofluids. *International Journal of Heat and Mass Transfer*, **50**, 2002-2018. http://dx.doi.org/10.1016/j.ijheatmasstransfer.2006.09.034

[13] Naoufal, Y., Zaydan, M. and Rachid, S. (2015) Numerical Study of Natural Convection in a Square Cavity with Partitions Utilizing Cu-Water Nanofluid. *International Journal of Innovative Research in Science, Engineering and Technology*, **4**, 10354-10367.

[14] El Bouihi, I. and Sehaqui, R. (2012) Numerical Study of Natural Convection in a Two-Dimensional Enclosure with a Sinusoidal Boundary Thermal Condition Utilizing Nanofluid. *Engineering*, **4**, 445-452. http://dx.doi.org/10.4236/eng.2012.48058

[15] Aminossadati, S. and Ghasemi, B. (2009) Natural Convection Cooling of a Localised Heat Source at the Bottom of a Nanofluid-Filled Enclosure. *European Journal of Mechanics-B/Fluids*, **28**, 630-640. http://dx.doi.org/10.1016/j.euromechflu.2009.05.006

[16] Öğüt, E.B. (2009) Natural Convection of Water-Based Nanofluids in an Inclined Enclosure with a Heat Source. *International Journal of Thermal Sciences*, **48**, 2063-2073. http://dx.doi.org/10.1016/j.ijthermalsci.2009.03.014

[17] Yu, W. and Choi, S. (2003) The Role of Interfacial Layers in the Enhanced Thermal Conductivity of Nanofluids: A Renovated Maxwell Model. *Journal of Nanoparticle Research*, **5**, 167-171. http://dx.doi.org/10.1023/A:1024438603801

[18] Ghasemi, B. and Aminossadati, S. (2010) Periodic Natural Convection in a Nanofluid-Filled Enclosure with Oscillating Heat Flux. *International Journal of Thermal Sciences*, **49**, 1-9. http://dx.doi.org/10.1016/j.ijthermalsci.2009.07.020

[19] Sarris, I., Lekakis, I. and Vlachos, N. (2002) Natural Convection in a 2D Enclosure with Sinusoidal Upper Wall Temperature. *Numerical Heat Transfer*, *Part A*: *Applications*, **42**, 513-530. http://dx.doi.org/10.1080/10407780290059675

[20] Corcione, M. (2003) Effects of the Thermal Boundary Conditions at the Sidewalls upon Natural Convection in Rectangular Enclosures Heated from Below and Cooled from Above. *International Journal of Thermal Sciences*, **42**, 199-208. http://dx.doi.org/10.1016/S1290-0729(02)00019-4

[21] Roy, S. and Basak, T. (2005) Finite Element Analysis of Natural Convection Flows in a Square Cavity with Non-Uniformly Heated Wall(s). *International Journal of Engineering Science*, **43**, 668-680. http://dx.doi.org/10.1016/j.ijengsci.2005.01.002

[22] Sathiyamoorthy, M., Basak, T., Roy, S. and Pop, I. (2007) Steady Natural Convection Flows in a Square Cavity with Linearly Heated Side Wall(s). *International Journal of Heat and Mass Transfer*, **50**, 766-775. http://dx.doi.org/10.1016/j.ijheatmasstransfer.2006.06.019

[23] Brinkman, H. (1952) The Viscosity of Concentrated Suspensions and Solutions. *The Journal of Chemical Physics*, **20**, 571-571. http://dx.doi.org/10.1063/1.1700493

[24] Xuan, Y. and Li, Q. (1999) Report of Nanjing University of Sciences and Technology. (In Chinese)

[25] Abu-Nada, E. (2008) Application of Nanofluids for Heat Transfer Enhancement of Separated Flows Encountered in a Backward Facing Step. *International Journal of Heat and Fluid Flow*, **29**, 242-249. http://dx.doi.org/10.1016/j.ijheatfluidflow.2007.07.001

[26] Levin, M. and Miller, M. (1981) Maxwell a Treatise on Electricity and Magnetism. *Uspekhi Fizicheskikh Nauk*, **135**, 425-440. http://dx.doi.org/10.3367/UFNr.0135.198111d.0425

[27] Störtkuhl, T., Zenger, C. and Zimmer, S. (1994) An Asymptotic Solution for the Singularity at the Angular Point of the Lid Driven Cavity. *International Journal of Numerical Methods for Heat & Fluid Flow*, **4**, 47-59. http://dx.doi.org/10.1108/EUM0000000004030

[28] Dennis, S. and Hudson, J. (1989) Compact h^4 Finite-Difference Approximations to Operators of Navier-Stokes Type. *Journal of Computational Physics*, **85**, 390-416. http://dx.doi.org/10.1016/0021-9991(89)90156-3

[29] MacKinnon, R.J. and Johnson, R.W. (1991) Differential-Equation-Based Representation of Truncation Errors for Accurate Numerical Simulation. *International Journal for Numerical Methods in Fluids*, **13**, 739-757. http://dx.doi.org/10.1002/fld.1650130606

[30] Gupta, M.M., Manohar, R.P. and Stephenson, J.W. (1984) A Single Cell High Order Scheme for the Convection-Diffusion Equation with Variable Coefficients. *International Journal for Numerical Methods in Fluids*, **4**, 641-651. http://dx.doi.org/10.1002/fld.1650040704

[31] Spotz, W. and Carey, G. (1995) High-Order Compact Scheme for the Steady Stream-Function Vorticity Equations. *International Journal for Numerical Methods in Engineering*, **38**, 3497-3512. http://dx.doi.org/10.1002/nme.1620382008

[32] Li, M., Tang, T. and Fornberg, B. (1995) A Compact Fourth-Order Finite Difference Scheme for the Steady Incompressible Navier-Stokes Equations. *International Journal for Numerical Methods in Fluids*, **20**, 1137-1151. http://dx.doi.org/10.1002/fld.1650201003

[33] Erturk, E. and Gökçöl, C. (2006) Fourth-Order Compact Formulation of Navier-Stokes Equations and Driven Cavity Flow at High Reynolds Numbers. *International Journal for Numerical Methods in Fluids*, **50**, 421-436. http://dx.doi.org/10.1002/fld.1061

[34] de Vahl Davis, G. (1983) Natural Convection of Air in a Square Cavity: A Bench Mark Numerical Solution. *International Journal for Numerical Methods in Fluids*, **3**, 249-264. http://dx.doi.org/10.1002/fld.1650030305

[35] Markatos, N.C. and Pericleous, K. (1984) Laminar and Turbulent Natural Convection in an Enclosed Cavity. *International Journal of Heat and Mass Transfer*, **27**, 755-772. http://dx.doi.org/10.1016/0017-9310(84)90145-5

[36] Hadjisophocleous, G., Sousa, A. and Venart, J. (1988) Prediction of Transient Natural Convection in Enclosures of Arbitrary Geometry Using a Nonorthogonal Numerical Model. *Numerical Heat Transfer*, **13**, 373-392.

Nomenclature

i	x-direction grid point
j	y-direction grid point
C_p	Specific heat capacity ($J \cdot K^{-1}$)
g	Gravitational cceleration ($m \cdot s^{-2}$)
h	ocal heat transfer coefficient ($m^{-2} \cdot K^{-1}$)
H	Height of cavity (m)
q_w	Heat flux ($W \cdot m^{-2}$)
t	Dimensional time (s)
τ	Non-dimensional time
T	Temperature (K)
p	pressure (pa)
(x, y)	Dimensionless Cartesian coordinates (m)
u, v	velocity components in x, y directions ($m \cdot s^{-1}$)

Greek-Symbols

α	Fluid thermal diffusivity ($m^2 \cdot s^{-1}$)
β	Thermal expansion coefficient (K^{-1})
v	Kinematic viscosity ($m^2 \cdot s^{-1}$)
ρ	Density ($kg \cdot m^{-3}$)
μ	Dynamic viscosity ($N \cdot s \cdot m^{-2}$)
κ	Thermal conductivity ($W \cdot m^{-1} \cdot K^{-1}$)
ψ	dimensional stream function
θ	non-dimensional temperature
ω	dimensionalvorticity
χ	nanoparticle volume fraction

Subscripts

c cold wall
eff effective
h hot wall
s solid
f pure fluid

World Journal of Nano Science and Engineering, 2016, 6, 90-110
Published Online June 2016 in SciRes. http://www.scirp.org/journal/wjnse
http://dx.doi.org/10.4236/wjnse.2016.62010

Therapeutic Potential of Neem Synthesized Silver Nanoparticles on Human Gastric Cancer Cells *in Vitro*

T. Anitha Sironmani

School of Biotechnology, Madurai Kamaraj University, Madurai, India
Email: a_sironmani@yahoo.co.in, asironmani@gmail.com

Received 7 April 2016; accepted 25 June 2016; published 28 June 2016

Abstract

Nanotechnology has shown significant promise in development of drugs and drug delivery systems that can overcome all limitations and address urgent needs to improve efficacy of diagnosis and therapy of various diseases including cancer. The functionalization with neem compounds as synthesis and capping agent had shown very high anticancer activities against Gastric cancer cells *in vitro*. The biochemical factors like albumin, glucose, and DNA concentrations were modulated along with Protease inhibitor and Catalase activates, the various cancer specific proteins like p53, GRD 70 - 78 kDa and other proteins of sizes 35 - 40 kDa corresponding to H+K+ATPase protein etc. The apoptic activity and antiproliferative activity were demonstrated with Gastric cancer cells *in vitro*.

Keywords

Gastric Cancer, Nanotherapy, Silver Nanoparticles, Neem Compounds, *In Vitro* Cancer Treatment, Biochemical Changes in Nanotreatment

1. Introduction

Cancer is a molecularly heterogeneous hyperproliferative disorder marked by metastasis into the vital organs of the body through invasion and angiogenesis. Gastric cancer remains one of the most common cancers worldwide and is typically associated with late-stage diagnosis and high mortality. According to the World Health Organization, 800,000 cancer-related deaths are caused by stomach cancer each year globally [1]. It is the fourth most common cancer worldwide, but the second leading cause of cancer-related deaths in the world.

Cancer therapies are currently limited to surgery, radiation and chemotherapy. All three methods risk damage to normal tissues or incomplete eradication of the cancer. Improved insights into the etiology of cancer have led

How to cite this paper: Sironmani, T.A. (2016) Therapeutic Potential of Neem Synthesized Silver Nanoparticles on Human Gastric Cancer Cells *in Vitro*. *World Journal of Nano Science and Engineering*, **6**, 90-110.
http://dx.doi.org/10.4236/wjnse.2016.62010

to the identification of several novel and highly promising classes of anticancer therapeutics, such as growth factor receptor inhibitors, proteasome inhibitors and anti-angiogenic agents etc. [2]-[11]. Nanotherapies are increasing in importance as vehicles for antineoplastic agents because of their potential for targeting and multifunctionality, the multiple hallmarks of cancer pathogenesis, cellular and molecular alterations and associated targeted therapies [12]-[18].

The development of stimuli-responsive nanomaterials for cancer treatment has been developed [19]-[22]. Surface-enhanced Raman scattering, photoacoustic imaging in lymphangiography [23], photodynamic therapy (PDT) [24] and photothermal therapy (PTT) [25] have been actively investigated as applications in nanomedicine.

However, designing adequate therapies is difficult because of the complexity of cancer biology and the vast heterogeneity of tumors. Only a small fraction of tumor cells is highly sensitive to therapy, and even those cells can develop resistance and progress into a more aggressive disease. The aim of our research program is to develop new Np for therapeutic interventions, and to further enhance of tumor therapy and reduce of clinically relevant side-effects. Molecular and genetic analysis allows physicians to detect, classify, monitor and treat cancer more effectively.

Our results of comparative biochemical screening of green synthesized silver nanoparticles may provide the scientific reality for an optimized therapeutic application and it may also provide the basis to find new template structures for the development of next-generation drugs for patients with resistance to the first generation drugs.

2. Methods

2.1. Synthesis and Characterization of Ag-Nps

One pot green Synthesis of silver nanoparticles (Ag-nps) using Neem leaf extract was done following the method of Kiruba *et al.* [26] The Ag-nps were primarily characterized by UV-visible spectroscopy, Atomic Force Microscopy and FTIR.

2.2. Cell Culture

Human gastric cancer cells AGS were kindly provided by Dr. Kumaresan, SBS, MKU University, and were maintained in Dulbecco's modified Eagle's medium (DMEM) supplemented with 10% fetal bovine serum (FBS) and 1% antibiotic-antimycotic solution. Cells were grown to confluence at 37˚C and 5% CO_2 atmosphere. All experiments were performed in 6-well plates, unless stated otherwise. Cells were seeded onto the plates at a density of 1 × 106 cells per well and incubated for 24 h prior to the experiments. The cells were washed with (phosphate buffered saline, pH 7.4) PBS and incubated in fresh medium containing different concentrations of Ag-nps suspended in water.

2.3. *In Vitro* Cell Viability/Cytotoxicity Assay

To evaluate the cytotoxicity of the Ag-nps, one hundred microliters of AGS cell suspension was dispersed in a 96-well plate, giving a concentration of 5000 cells/well. The plate was pre-incubated for 24 hours in a humidified incubator (37˚C, 5% CO_2), after which 10 µl of various concentrations of Ag-Np were added into the culture media in the plate. After the plate was incubated for a further 24 hours, Cells were harvested and Trypan blue was mixed. Then the blue stained dead cells were counted to see the cytotoxicity and viability. The dye exclusion test is used to determine the number of viable cells present in a cell suspension. Besides, the trypan blue stain is considered as a simple way to evaluate cell membrane integrity and thus assesses cell proliferation or death.

2.4. Invasion Assay

The invasive potential of tumor cells was determined with an *in vitro* invasion assay. Briefly, cells were tested for their ability to penetrate the intestine in organ culture A suspension of tumor cells (1×10^6) in DMEM containing 2% Rhodamine B. After 48 hrs of incubation at 37˚C in 95% air and 5% CO_2, Then the organ culture media was removed and washed and treated with Ag Nps in medium only for experimental plate and plain medium in control plate. Rhodomine staining was analyzed and photographed under an Olympus Fluoview FV

1000 Laser confocal microscope using the 380 nm excitation 560 nm emission.

Antiproliferative efficacy on AGS cell line was determined using Ag-Np-Rhodamin B method after 48 hrs treatment. The fluorescence was measured in spectroflurimeter.

2.5. Biochemical Analysis

For all biochemical tests, following *in vitro* culture for 24 h, the gastric cancer cells, a total amount of 1 × 106, were grown in serum free medium Minimal essential medium without antibiotics with or without Ag-Np were collected, lysed and used for biochemical assays. Estimation of glucose was done following the method of King & Garner [27], The entire DNA was extracted using lysis buffer, phenol chloroform extraction and alcohol precipitation The concentration of the DNA was estimated by reading the absorbance at 260 and 280 nm using the UV spectrophotometer. The methyl orange method of Bracken and Klotz [28] was used for the estimation of albumin. The absorbance of the solution measured photometrically at 480 nm. Catalase activity was estimated by reacting with H_2O_2 measuring the absorbance at 240 nm [29]. Trypsin inhibitor assay was measured using trypsin as substrate in buffer phosphate buffer pH 7.6. The precipitate was pelleted and the absorbance was measured at 410 nm. Trypsin inhibitor activity was represented as unit of tryps in utilized.

2.6. SDS-PAGE

Samples containing 25 mg of protein from homogenized gastric cancer cells with and without nanotreatment were analyzed by SDS-PAGE (12.5%) under reducing conditions according to Laemmli [30].

2.7. Statistics

The results were determined by three independent experiments but with pooled samples.

3. Results and Discussion

Nanotechnology has shown significant promise in development of drugs and drug delivery systems that can overcome all limitations and improve efficacy of diagnosis and therapy of various diseases [31] [32]. Nanotherapies, as carriers for antineoplastic agents with potential for targeting, and multifunctionality are increasing [12]-[18]. Phytochemicals which exhibit anti-carcinogenesis by affecting a spectrum of different cellular signaling pathways have been well recognized in the scientific literature [33] [34].

Nanoparticles functionalized with anticancer phytochemicals, molecular and genetic analysis would help to treat cancer more preciously. Hao *et al.* [35] have reported neem components as potential agents for cancer prevention and treatment. Preliminary experiments with neem synthesized silver nanoparticles (Ag-Np) were performed against gastric cancer cells AGS *in vitro* to study the toxicity and efficiency.

Colloidal Ag-NPs were prepared using Neem leaves to add drug effect to silver nanoparticles following the modified methods of [26] [36] [37]. The color change from yellow to brown suggested the formation of Ag-Nps. Studies indicated that the reducing phytochemicals in the neem (Azadirachta indica) leaf consisted mainly of terpenoids, nimbin and quercetin which served as capping and stabilizing agents in addition to reduction [36] [37].

A strong and broad surface plasmon peak was observed at 420 nm for the Ag-NPs prepared (**Figure 1**) and the particles were well dispersed without aggregation. The diameter by the spectral response of silver nanoparticles was approximately 20 nm which was confirmed by AFM picture (**Figure 2**). Observation of the strong surface plasmon peak has been well known in the case of silver nanoparticles over a wide size range of 2 - 100 nm [26] [38] [39].

Fourier transform infrared spectroscopy (FTIR), of synthesized silver nanoparticles is depicted in **Figure 3**. The broad band corresponding to the presence of the phenolic −OH occurs at 3600 - 3200 cm^{-1}, maybe due to the polyphenols present in the plant extract. The activated neem leaves consist of mainly three dissimilar kinds of phenolic compounds such as 4-chlorophenol (4-CP), 4-nitrophenol (4-NP) [35]. The peaks at 1635 cm^{-1} and 2073 cm^{-1} indicated the presence of aromatic ring C=C stretching alkyne bonds respectively. These bands denote stretching vibrational bands responsible for compounds like flavonoids and terpenoids [35] [40] adsorbed on the surface which are very abundant in Neem plant, while nanoparticles bond shows strong peak at 600 cm^{-1}.

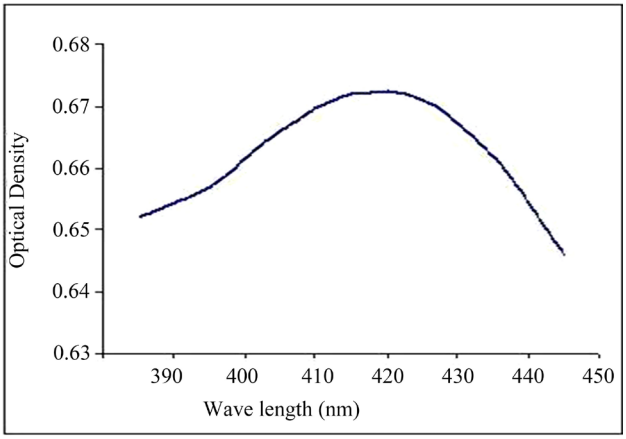

Figure 1. Optical density pattern of neem synthesized silver nanoparticles.

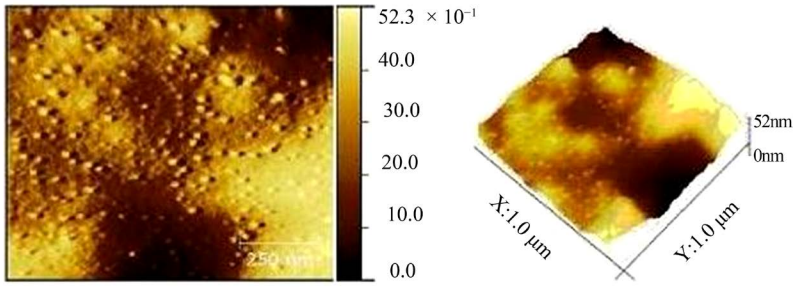

Figure 2. AFM pattern of neem synthesized silver nanoparticles.

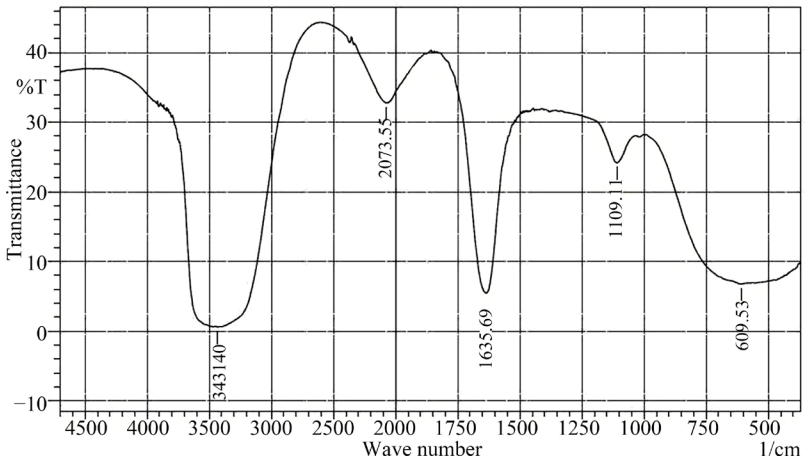

Figure 3. FTIR pattern of neem synthesized silver nanoparticles.

The FTIR spectrum of the un-reacted Azadirachta indica extract showed bands at 1742 and 1636 cm^{-1}. The first band is characteristic of stretching vibrations of the carbonyl functional group in ketones, aldehydes and carboxylic acids. The second absorption at 1636 cm^{-1} corresponded to the amide I band. The intense broad absorbance at 3412 cm^{-1} is attributed to the O-H stretching modes of vibration in hydroxyl functional group in alcohols and N-H stretching vibrations in amides and amines. Moreover, the 1059 cm^{-1} band can be assigned to C-O stretching vibrations. The absorption peak at 2930 cm^{-1} corresponded to C-H stretching vibration modes in the hydrocarbon chains. The main difference between both spectra was that the treated extract exhibits peaks of less intensity for the amide band [35] [40].

In *in vitro* Ag Np viability and antiproliferative analysis (**Figure 4**), these nanoparticles had major effects on

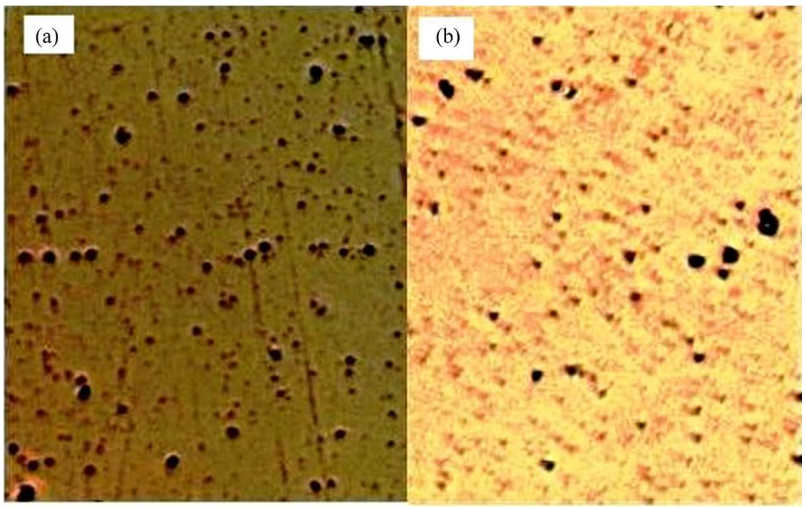

Figure 4. Phase contrast microscopic picture of gastric cancer cells *in vitro* (a) untreated gastric cells (b) Silver nanoparticle treated gastric cancer cells.

the proliferation of Gastric Cancer cells and significantly decreased the viability to 5% - 10%, suggesting good cytotoxicity and antitumor activity. But normal cells treated with Ag-Nps showed no toxicity as observed by our earlier studies as well [26] [38] [39] [41].

Investigation of the antiproliferative effect of Ag-Np in the *in vitro* AGS model system confirmed that the Ag-NP could modulate the sensitivity of the gastric cancer cells. Ag-Np induces cytotoxicity selectively in tumor cells indicating induction of apoptosis. Various nanoparticles were reported to suppress the growth and proliferation of a wide variety of tumor cell lines of different tissue origins [42] [43]. Apoptosis helps to establish a natural balance between cell death and cell renewal in mature animals by destroying excess, damaged, or abnormal cells.

The attachment of nanoparticles to the cell membrane caused aggregation of envelope protein precursors causing dissipation of the protein motive force. Silver nanoparticles also exhibited destabilization of the outer membrane and rupture of the plasma membrane thereby causing depletion of intracellular ATP and rupturing of cell membrane which may lead to cell death. It was also proposed that oxygen associated with silver reacts with the sulphydral (-S-H) groups on the cell membrane to form R-S-S-R bonds causing inhibition of respiration resulting in cell death [44]-[47].

In addition, the anti-proliferative and apoptosis-inducing effects of neem components in which the Ag-nps were prepared are tumor selective as the effects on normal cells are significantly weaker [35].

Over the past decades, albumin has emerged as a versatile carrier for therapeutic and diagnostic agents, primarily for diagnosing and treating diabetes, cancer, rheumatoid arthritis and infectious diseases. Hence in order to understand the role of albumin in cancer therapy, the concentration of albumin in Ag np treated and un treated gastric cancer cells *in vitro* were estimated (**Figure 5**) Serum free minimal essential medium was used for culturing the cells and the whole lysate was used for analysis.

It has also been shown that there is an increase in the albumin flux across the capillary wall, from the intravascular into the extravascular compartments, in patients with cancer and sepsis [48]. There may have been alterations in the rates of albumin turnover with either a decreased or decreased synthesis [49]. Fleck *et al.* [50] have shown that the most important factor in altering serum albumin concentrations is the rate of exchange between blood and the extravascular space. They calculated that this rate of exchange is more than ten times the rate of synthesis and breakdown and suggested variation based on the stage of the tumour, the patient's age, the degree of tumour differentiation [48]-[53]. Those patients with low concentrations of C-reactive protein low concentrations of interleukin 6 (a key cytokine in the induction of hepatic synthesis of acute phase proteins) and higher serum albumin concentrations are more likely to respond to treatment and have a more prolonged survival [54] [55]. Alternatively, tumour necrosis factor may increase the permeability of the microvasculature, thus allowing an increased trans-capilliary passage of albumin [56] and hence a lowering of the serum albumin concentrations.

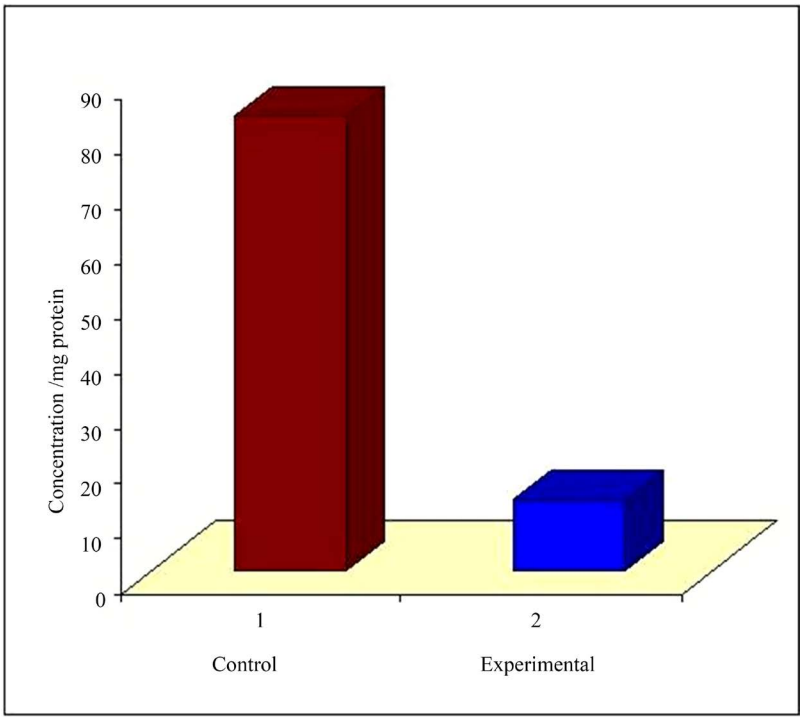

Figure 5. Concentration of albumin in control gastri cancer cells and silver nanoparticle treated cells.

Most human tumors display some forms of genomic instability, including DNA sequence alterations, chromosomal rearrangements, aneuploidy or gene amplifications. These alterations have the potential to affect the function of cell growth-related genes, such as proto oncogenes and tumor suppressor genes, which are associated with the malignant transformation of cells. **Figure 6** shows the DNA content of the Ag np treated and untreated Gastric cancer cells *in vitro*.

Apoptosis is the most important pathway through which many compounds exert their antitumor effects. It has been shown that rhein can induce apoptosis by increasing nuclear condensation and DNA fragmentation [57], activating caspase-8, -9, and -3 [57], increasing the levels of Fas, p53, p21, and Bax, but decreasing the levels of Bcl-2 [58].

The reduction in the DNA level may be due to. the damage in cell function and development which includes oxidative modification of proteins to generate protein radicals [59], initiation of lipid peroxidation [60]-[62], DNA-strand breaks, modification to nucleic acids [63], modulation of gene expression through activation of redox-sensitive transcription factors [64] [65] and modulation of inflammatory responses through signal transduction [66], leading to cell death and genotoxic effects [67]-[72]. The gastric mucosal integrity is maintained through a balance between the proliferation and apoptosis of mucosal cells. DNA damage derived from oxidative stress is another tumorigenic factor attributed to H. pylori infection [73].

Vitamin C is capable of inducing gastric cancer cell growth inhibition, which may be related to the effects on cell protein and DNA synthesis. Extracts of neem has natural substances such as limonin, azadirachtin, kaemferole, beta-carotene and ascorbic acid. In addition to combating oxidative damage in the body, these phytochemicals can help enhance the immune system, reduce inflammation, and interfere with the growth of cancer cells [74]-[77].

The glucose concentration of the Ag-Np treated Gastric cells was three fold higher than the untreated Gastric cancer cells *in vitro* (**Figure 7**). The interactions between cancerous cells and tumor microenvironment during the courses of multistep tumorigenesis play a critical role in modulation of tumor growth, metabolism and metastasis to distant sites [78]-[80].

Enhanced glucose utilization is a prominent and fundamental change in many tumors irrespective of their histological origin and the nature of mutations, first observed by [81]. The extent of increase in glucose utilization measured by FDG-PET has been correlated with the degree of malignancy in some of the tumors [82].

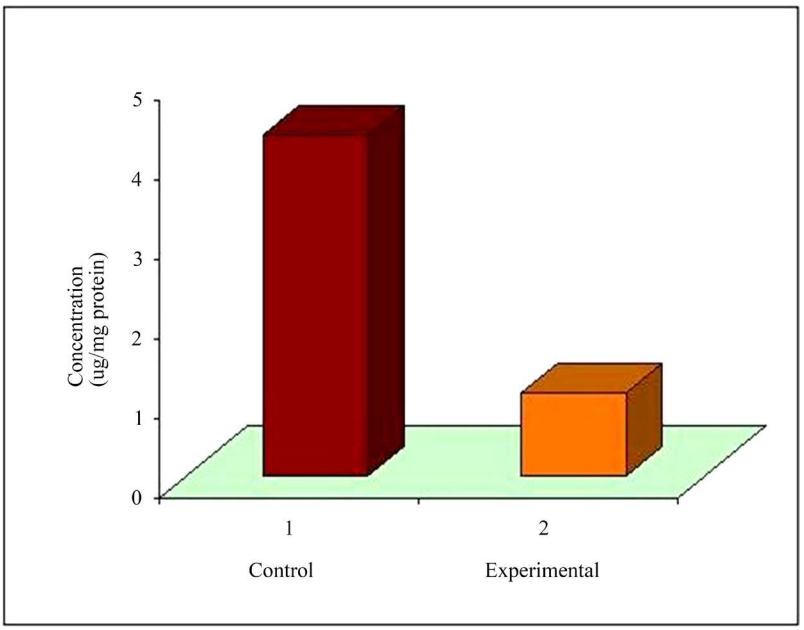

Figure 6. DNA concentration of silver nanoparticle untreated and treated gastric cancer cells.

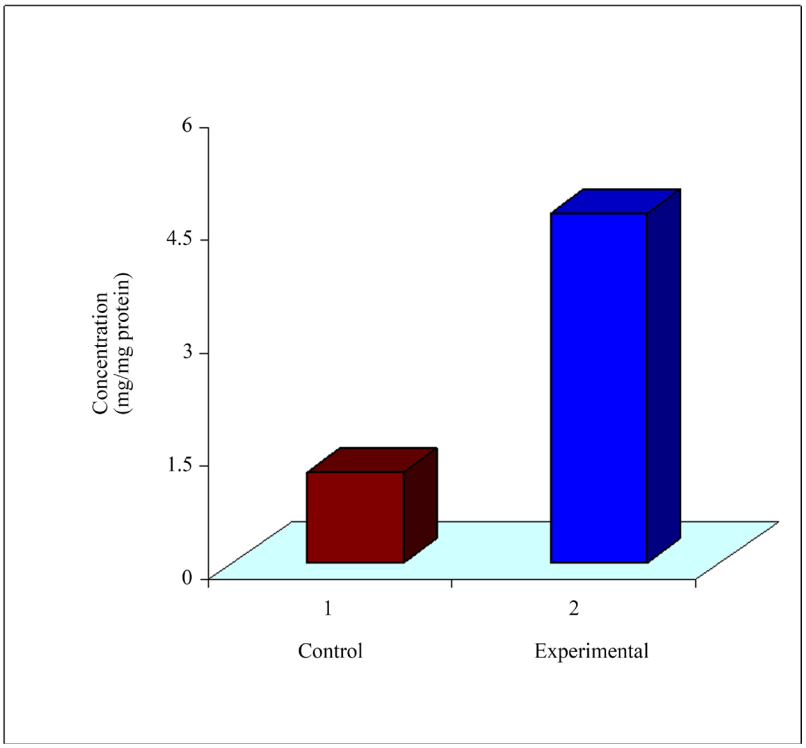

Figure 7. Concentration of glucose in control gastric cancer cells and silver nanoparticle treated cells.

Glucose utilization is also inversely correlated with treatment response in a number of tumors, while changes in tumor glucose utilization during the first weeks of chemotherapy are significantly correlated with patient outcome [83] [84]. Therefore, glucose utilization appears to be a useful metabolic marker for diagnosis, prognosis and prediction of tumor response to a variety of therapies [85].

It was reported that oxidative stress and reactive oxygen species (ROS) were found to be crucial in a variety of diseases such as diabetes, cancer etc. [86]. Catalase is a heme enzyme that has a predominant role in controlling hydrogen peroxide concentration in human cells, by converting H_2O_2 into H_2O and O_2. With superoxide dismutase (SOD) and glutathione peroxidase, catalase constitutes a primary defense against oxidative stress and may provide resistance to the effects of radiation and chemotherapy [87].

To know the effect of Ag-nps in oxidative stress, the catalse activity was measured. As shown in **Figure 8**, the catalase activity was lower in Ag-nps treated cancer cells than the untreated control gastric cancer cells *in vitro* since the antioxidant enzymes are inducible, the levels of the antioxidant enzymes reflect the levels of their substrates, the active oxygen species [88] [89]. Reactive oxygen species (ROS) synthesis in gastric cells [90] [91], and ROS enhances the expression of oncogenes, stimulates cell proliferation and plays an important role in all stages of carcinogenesis [92]. NF-kB was also involved in oxidativestress- mediated cell injury. A variety of antioxidants have been demonstrated to inhibit the activation of NF-κB [93], and micromolar concentrations of H_2O_2 could activate NF-κB, suggesting that reactive oxygen may act as a second messenger in the activation of transcription factor NF-κB [94]. The suppression of NF-κB signaling pathway is, at least partially, involved in the anticancer functions of neem components [35].

Proteases from all catalytic classes positively or negatively affect cancer progression and metastasis through complex and highly regulated processes that involve cleavage of cell adhesion molecules, growth factors, cytokines, or kinases [95]-[99]. The relationship between serum tumor-associated trypsin inhibitor levels with gastri cancer cells with and without Ag Np treatment was studied *in vitro*. **Figure 9** shows more than two fold increased level of protease inhibitor.

The results of this study indicated that trypsin could be considered as a growth factor and the high expression of trypsin inhibitor unravel a new mechanism whereby serine proteases control colon tumours. They are also involved in tissue remodeling during development and in tissue penetration as they induce the migration of monocytes and cancer cells [100]. The lysosomal cysteine proteases, such as cathepsins B, H, and L, are broadly distributed in tissues and believed to be responsible for a major proportion of normal protein turnover and pathological processes.

Upregulation of the protease inhibitor, contributes to cell proliferation inhibition in gastric cancer [101]-[103]. Tumour-associated trypsin inhibitor expression has been associated with impaired survival in several forms of cancer [104]-[106], but not in gastric cancer, where it is believed to have a natural function of protecting the mucosa from proteolytic degradation [107]-[111]. The protease-activated receptor-2 (PAR-2) and trypsin play a

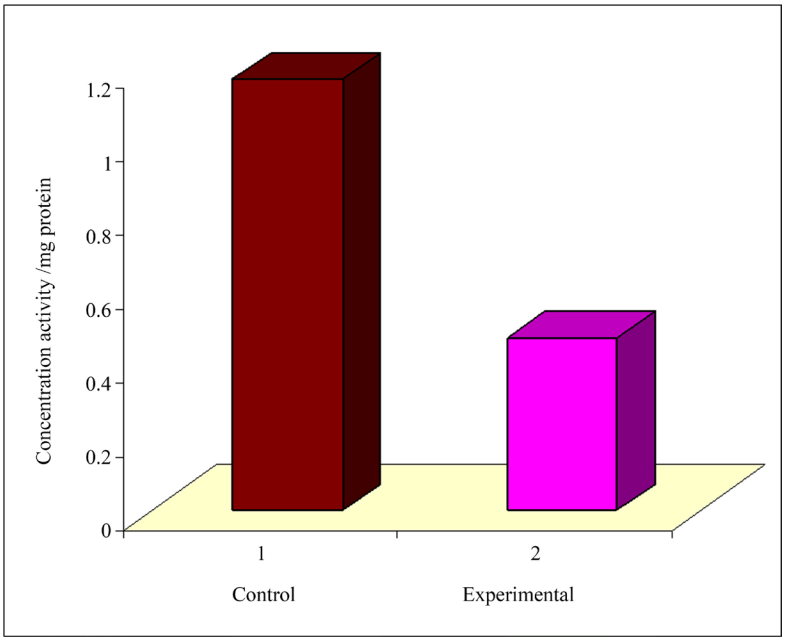

Figure 8. Estimation of catalase activity in control gastric cancer cells and in silver nanopartice treated experimental cells.

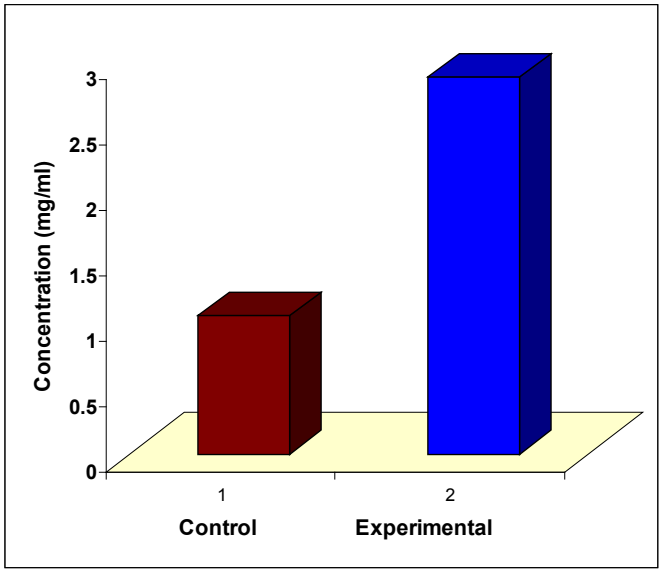

Figure 9. Trypsin inhibitor concentration in Silver nanoparticle untreated and treated gastric cancer cells.

role in cell proliferation in human colon cancer cell lines [112].

Stomach cancer cell lines frequently secreted active trypsin, suggesting that they produced an endogenous activator of trypsinogen, most likely enterokinase. Trypsin (ogen) was frequently expressed at high levels in stomach and colon cancers, but scarcely in breast cancers. In the stomach cancers, the trypsin immunoreactivity was higher. These results support the hypothesis that tumor-derived trypsin is involved in the malignant growth of tumor cells, especially stomach cancer cells [113]. And hence, the level of trypsin inhibitor was found to be high in Ag-Np treated gastric cancer cells.

Knowledge about cancer biomarkers will provide great opportunities for improving the management of cancer patients by enhancing the efficiency of detection and efficacy of treatment. Emerging evidence indicates that most tumor-associated biomarkers are cellular proteins whose aberrant regulation of function could be linked to malignancy [114] [115].

The protein profile of untreated and Ag Np treated Gastric cancer cells were analyzed on 12.5% PAGE and the results are shown in **Figure 10.** The highly expressed proteins of molecular weight 78, 66, 53, 50, 40, 29, 25, 23 and other minor peptides were found to be in high concentration in control untreated gastric cancer cells.

Many stomach, colon, and breast cancer cell lines secreted trypsinogens-1 and/or -2, as well as an unidentified serine proteinase of about 70 kDa, into culture medium. These results support the hypothesis that tumor-derived trypsin is involved in the malignant growth of tumor cells, especially stomach cancer cells [113]. HSPA5 (heat shock 70 kDa protein and glucose-regulated protein 78 kDa) gene is expressed in all nucleated cells, in particular in thyroid-, lung-, smooth muscle-, liver-, and various cells of the immune system [116]. Glucose regulated protein 78 (GRP78) is overexpressed in colorectal carcinoma and regulates colorectal carcinoma cell growth and apoptosis. The HER2 receptor belongs to the epidermal growth factor (EGF) receptor (EGFR) family of tyrosine kinase receptors expressed by a variety of tumor cell lines that appear to drive tumorigenic pathways, including proliferation, invasion, adhesion, and metastatic spread [117] [118]. The 78 - 70 kDa, 25 and 23 kDa protein observed in control untreated gastric cancer cells may be the 70-kDa serine proteinases. 25- and 23-kDa active trypsin observed in various human cancer cell lines [113] p53 protein a tumor suppressor and transcription factor is a 53-kDa protein present in humans and is encoded by the TP53 gene It is a critical regulator in many cellular processes, including cell signal transduction, cellular response to DNA damage, genomic stability, cell cycle control, and apoptosis When tumors develop, point mutations at the TP53 gene can lead to overexpression of p53 proteins, which contribute to continuous cell division and canceration. Overexpression of p53 has been reported in 60% of laryngeal carcinomas, 37% of hypopharyngeal carcinomas, and 52% of tongue carcinomas. With the mortality and disintegration of tumor cells, p53 protein released from cancer cells will enter into the circulation.

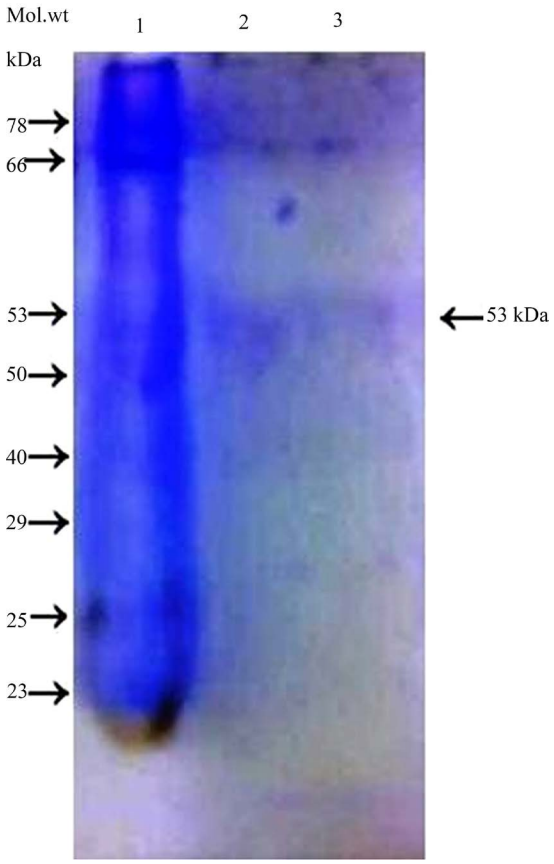

Figure 10. 12.5% SDS-PAGE showing the protein profile of gastric cancer cells (lane 1) and silver nanoparticle treated cells with different concentrations (lanes 2 & 3).

Although p53 is not a typical cancer-specific antigen, its central role in the control of cell growth and apoptosis and frequent mutations in tumours make p53 a unique target for cancer therapy [119]. Curcumin down-regulates the expression of p53 as well as the survival genes egr-1, c-myc, and bcl-XL in B cells [120].

The 40 - 50 kDa glycoprotein was consistently expressed in the intestinal type carcinoma. An albumin associated 40 - 50 kDa glycoprotein was previously shown in mucus gels in gastric cancer. Secreted gastric mucins are large O-glycosylated proteins of crude mucus gels identified as α-1-Acid Glycoprotein which are aberrantly expressed in malignancy [121]. The H+/K+-ATPase enzyme with subunits 35 kDa and 114 kDa of gastric parietal cells exchanges luminal K+ for cytoplasmic H+ and is a specialized proton pump primarily responsible for gastric acidification, leading to the development of gastric enterochromaffin-like (ECL) cell carcinoids in rats [122].

Cancer markers CA 27 - 29 are found on Cancers of the colon, stomach, kidney, lung, ovary, pancreas, uterus, and liver may also raise CA 27 - 29 levels. Noncancerous conditions associated with this substance are first trimester pregnancy, endometriosis, ovarian cysts, benign breast disease, kidney disease and liver disease [119].

The suppression of NF-κB signaling pathway is, at least partially, involved in the anticancer functions of neem components adsorbed with additive effect of Ag-Np Importantly, the anti-proliferative and apoptosis-inducing effects of neem components are tumor selective as the effects on normal cells are significantly weaker. In addition, neem extracts sensitize cancer cells to immunotherapy and radiotherapy, and enhance the efficacy of certain cancer chemotherapeutic agents [35].

To evaluate the effect of Ag Np viability/cytotoxicity assay was done using dissected bit of mice intestine *in vitro* as described in methods and were analysed using confocal microscopy (**Figure 11**). Representative images were selected from the results of one set experiment among three experiments. Higher apoptosis rate, was detected in nanotreated compared with control gut tissue co-cultured with Gastric cancer cells. The gastric mucosal

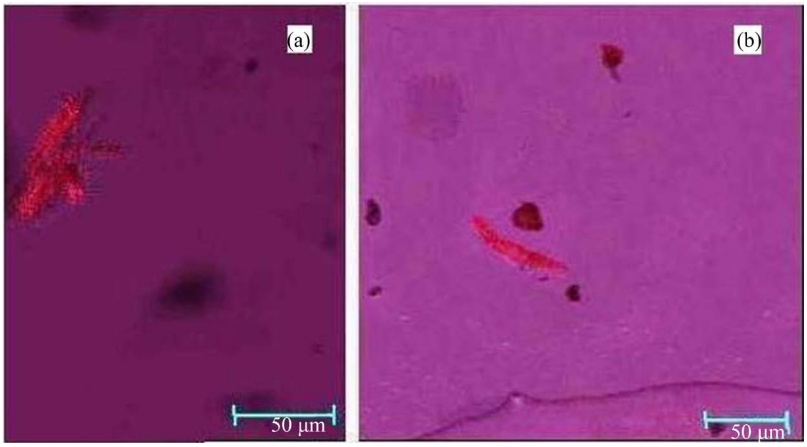

Figure 11. Invasion assay of control and silver nanoparticles treated Rhodamine B labeled gastric cancer cells infected mice intestine in organ culture Confocal microscopic view.

integrity is maintained through a balance between the proliferation and apoptosis of mucosal cells.

Chitosan/heparin nanoparticle-encapsulated CdtB preferentially inhibited the proliferation of cells derived from gastric cancer. Treatment of cells with nanoparticle-encapsulated CdtB enhanced cell-cycle arrest at G2/M, followed by apoptosis. Moreover, our data showed that the mechanism for nanoparticle-encapsulated CdtB-induced cell death was mediated by ATM-dependent DNA damage checkpoint responses [18].

The glandular organization of this tissue, is also critical to its role as a barrier to a range of environmental noxious and immunogenic molecules [123]-[125], During an established infection, the vast majority of H. pylori cells (about 70%) are found in the mucus layer of the superficial gastric mucosa, either motile or adhered to the heavily glycosylated secreted mucins.

Most stomach cancers are adenocarcinomas, which develop in the cells of the mucosa. However, stomach cancer can develop anywhere in the organ and spread to other parts of the body by growing beyond the stomach wall, entering the bloodstream or reaching the lymphatic system.

Gastric cancer cells labeled with rhodamine b was added to mice intestine in organ culture and one set was treated with nanoparticles and the other set served as control (**Figure 12**) The fluoresence spectrometric analysis revealed the reduction in fluorescence and very less accumulation of Ag-nps and less invasion of gastric cancer cells revealing the therapeutic potential of Ag np (**Figure 12**).

The nanoparticle localisation in intestine cultured with and without Gastric cancer cells by the enhanced permeability and retention effect. Ag-nps preferentially accumulated in the tumour mass by extravasation through the fenestrated tumour interstitium Tumor cells, Kupffer cells, and mononuclear phagocyte system have higher phagocytotic rates for uptaking nanoparticles than other tissue cells. Therefore, the Ag-nps could be targeted to tumor, the liver, or spleen [126].

Figure 13 shows the comparison of various factors in gastric cancer cells treated with Ag-nps. Except glucose and antitrypsin concentrations (4 fold and 3 fold respectively) all other biochemical and molecular factors were down regulated in Ag Np treated gastric cancer cells compared to the un treated control gastric cancer cells. Albumin concentration was reduced 6 folds. DNA concentration and catalase activity were down regulated 4 folds and 3 folds respectively (**Figure 13**).

Mechanisms underlying this fundamental alterations in metabolism during carcinogenesis include mutations in the mitochondrial DNA resulting in functional impairment, oncogenic transformation linked upregulation of glycolysis, enhanced expression of metabolic enzymes and adaptation to the hypoxic tumour micro-milieu in case of solid tumours [81]. These abnormalities, which include telomerase activation, genetic instability, and abnormalities in oncogenes, tumor suppressor genes, cell-cycle regulators, cell adhesion molecules, and DNA repair genes, could be effective markers in the molecular diagnosis of gastric cancer.

Apart from being an excellent anti-bacterial agent, Ag-nps had anti-inflammatory properties. The potential anti-inflammatory action of silver nanoparticles has been suggested in various studies described previously (26, 38, 39, 41). Others have also demonstrated the anti-inflammatory effects of silver nanoparticles using a porcine

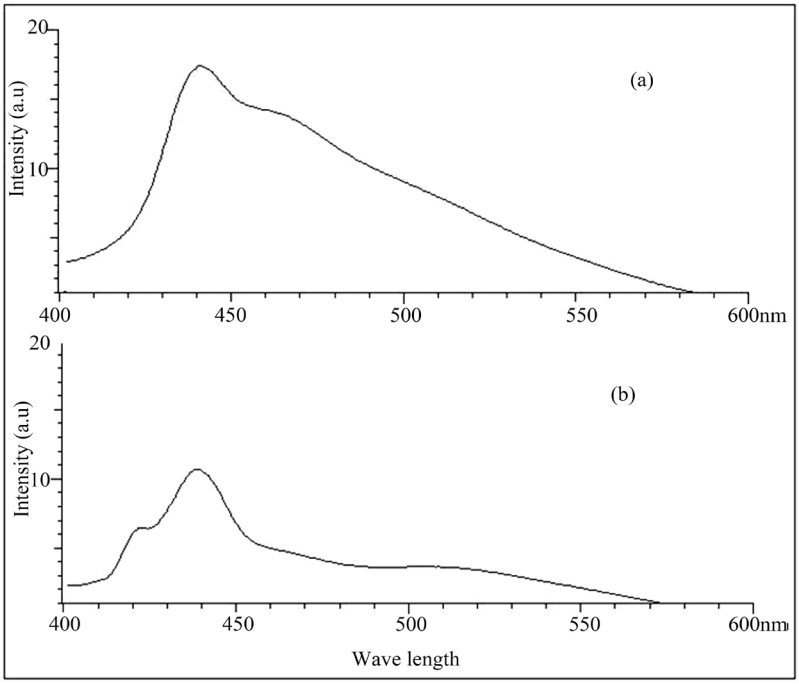

Figure 12. Invasion assay-Fluorescence spectroscopic pattern of Rhodomin B treated control gastric cells (a) and silver nanoparticles treated gastric cancer cells (b) in organ culture.

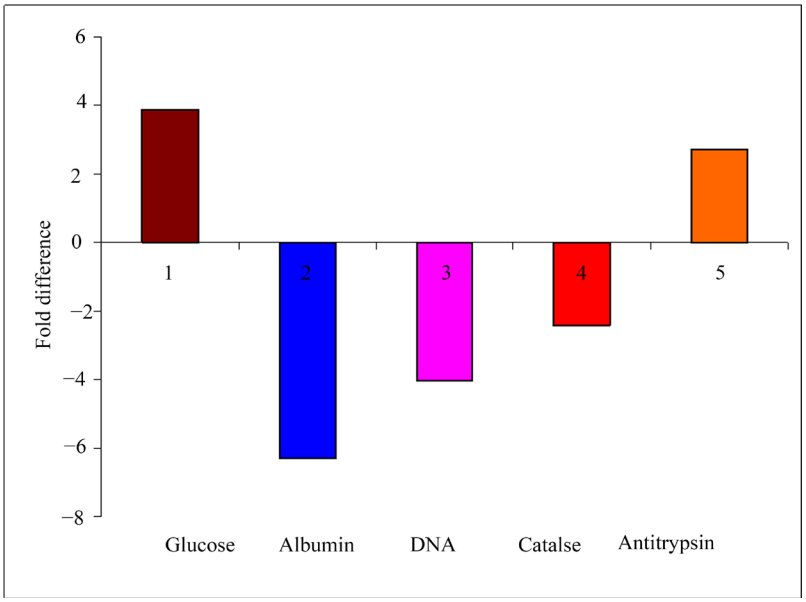

Figure 13. Comparison of various biochemical parameters showing fold difference silver nanoparticle treated gastric cancer cells with un treated control gastric cancer cells.

model of contact dermatitis [127] and in a rat model of ulcerative colitis [128]. Proteins, known as matrix metalloproteinases (MMPs), help cancer cells escape their original locations by cutting through proteins of the extracellular matrix, which normally holds cells in place [129].

Circulating tumour DNA (ctDNA) as a noninvasive modality to assess evolution of solid malignancies, this is DNA originating from cancer cells, carrying tumour-specific genomic alterations, that is present as short cell-

free fragments in body fluids such as blood plasma [130].

Active oxygen species pose a severe threat to cells, and are probably responsible for cellular damage, tissue damage, DNA modifications, and many human diseases [131]. Antioxidant enzymes are the superoxide dismutases (SOD), catalases (CAT), and peroxidases, of which glutathione peroxidase (GPx) appears to be the most important in mammalian cells. free radicals, particularly oxygen radicals, play an important role in the complex course of multistep carcinogenesis. Much of the evidence (**Figure 13**) shows that antioxidants scavenge free radicals directly, or interfere with the generation of free radicals-mediated events, inhibit the neoplastic process [132]-[135]. Overproduction of ROS can induce oxidative stress, resulting in DNA-strand breaks, modification to nucleic acids [49] [63], modulation of gene expression through activation of redox-sensitive transcription factors [64] [65], and modulation of inflammatory responses through signal transduction [66], leading to cell death and genotoxic effects [67] [69].

The protease-activated receptor-2 (PAR-2) and trypsin play a role in cell proliferation in human colon cancer cell lines [112]. Cysteine proteases are released as a response to several normal and pathological processes, including inflammation and tumorigenesis [103] and their proteolytic activities are regulated by potent cystatin inhibitors. Cystatins play a role in the protection of tissues from inappropriate proteolysis, and thus the control of protease activity by cystatins is essential to organisms.

Similar relationship between serum tumor-associated trypsin inhibitor levels and clinicopathological parameters in patients with gastric cancer was reported by Kemik *et al.* [136] Recent exploitation of apoptosis pathways towards re-instating apoptosis induction via caspase re-activation has provided new molecular platforms for the development of therapeutic strategies effective against advanced prostate cancer as well as other solid tumors [137].

Apoptotic cell death induced by Poncirin in AGS cells was mediated by Fas death receptor followed by the caspase-dependent extrinsic apoptosis pathway [138]. In several previous studies, it was found that some phytochemicals induce apoptosis by alteration of MMP in various cancer cells [139] [140].

It can be deduced that upon the microenvironmental stress, such as hypoxia, glucose deprivation and inflammation, the intracellular induced- or extracellular secreted-GRP78 is able to inhibit the function of p53 protein, facilitating genome instability and the related mutations (**Figure 11**).

Glucose regulated protein GRP78 can promote the unfolded or misfolded proteins return to normal conformation, and then protect cells by suppressing oxidative damage and stabilizing calcium homeostasis [72] [116] [134] [141].

Curcumin treatment impairs both Wnt signaling and cell-cell adhesion pathways, resulting in G2/M phase arrest and apoptosis in HCT-116 cells. Curcumin preferentially arrested cells in the G2/S phase of the cell cycle [142] [143].

Poor pharmacokinetic and biodistributional profile upon intravenous administration are the important drawbacks with these second-generation anticancer agents as with the first-generation DNA-damaging counterparts. Multifunctional nano formulations aim to improve the balance between the efficacy and toxicity of systemic anticancer therapy. The currently approved nanoparticle systems have in some cases improved the therapeutic index of drugs by reducing drug toxicity or enhancing drug efficacy. The next generation of nanoparticle systems may have targeting ligands such as antibodies, peptides, or aptamers, which may further improve their efficacy or reduce their toxicities [12] [144] [145].

Gold nanostars (GNSs), as one kind of emerging nanomaterial, have been actively investigated as an application in nanomedicine, including surface-enhanced Raman scattering, photoacoustic imaging in lymphangiography [23] photodynamic therapy (PDT) [33], and photothermal therapy (PTT) [1] [25] [34] [146] [147].

Extracts from the neem tree are packed with beneficial natural substances such as limonin, azadirachtin, kaemferole, beta-carotene and ascorbic acid. In addition to combating oxidative damage in the body, these hytochemicals can help enhance the immune system, reduce inflammation, and interfere with the growth of cancer cells. Neem leaf extracts can cause apoptosis to suppress the proliferation of leukemia and melanoma cell lines [35].

Silver nanoparticles functionalized with anticancer neem phytochemicals would help to treat cancer more preciously in addition to the bactericidal effect, their unique physical, chemical properties, and ease of synthesis and surface modification, biodistribution and biosafety [26] [38] [39] [41]. Ag Nps hold the most promise for achieving optimal targeting all cancers including brain cancer as they can bypass the BBB and improve the distribution within a brain [148]-[150]. Multifunctional therapeutics where a nanoparticle serves as a platform to

facilitate its specific targeting to cancer cells and delivery of a potent treatment, minimizing the risk to normal tissues over coming all problems of cancer therapy.

Acknowledgements

This work was done without any financial support. The help extended by Mr. Brijash, M. Phil student School of Biotechnology, Madurai Kamaraj University in carrying out the experiments is acknowledged.

Conflict of Interest

There is no conflict of interest.

References

[1] Liang, S., Li, C., Zhang, C., Chen, Y., Xu, L., Bao, C., Wang, X., Liu, G., Zhang, F. and Cui, D. (2015) CD44v6 Monoclonal Antibody-Conjugated Gold Nanostars for Targeted Photoacoustic Imaging and Plasmonic Photothermal Therapy of Gastric Cancer Stem-Like Cells. *Theranostics*, **5**, 970-984. http://www.thno.org/v05p0970.htm

[2] Chinnaiyan, A.M., Prasad, U., Shankar, S., *et al.* (2000) Combined Effect of Tumor Necrosis Factor-Related Apoptosis-Inducing Ligand and Ionizing Radiation in Breast Cancer Therapy. *Proceedings of the National Academy of Sciences of the United states of America*, **97**, 1754-1759. http://dx.doi.org/10.1073/pnas.030545097

[3] Matés, J.M. and Sánchez-Jiménez, F.M. (2000) Role of Reactive Oxygen Species in Apoptosis: Implications for Cancer Therapy. *The International Journal of Biochemistry & Cell Biology*, **32**, 157-170. http://dx.doi.org/10.1016/S1357-2725(99)00088-6

[4] Wajant, H., Pfizenmaier, K. and Scheurich, P. (2002) TNF-Related Apoptosis Inducing Ligand (TRAIL) and Its Receptors in Tumor Surveillance and Cancer Therapy. *Apoptosis*, **7**, 449-459. http://dx.doi.org/10.1023/A:1020039225764

[5] Stoklosa, T. and Golab, J. (2005) Prospects for p53-Based Cancer Therapy. *Acta Biochimica Polonica*, **52**, 321-328.

[6] Jedinak, A and Maliar, T. (2005) Inhibitors of Proteases as Anticancer Drugs. *Neoplasma*, **52**, 185-192.

[7] Ip, S.W., Weng, Y.S., Lin, S.Y., Mei, D., Tang, N.Y., Su, C.C. and Chung, J.G. (2007) The Role of Ca^{2+} on Rhein-Induced Apoptosis in Human Cervical Cancer Ca Ski Cells. *Anticancer Research*, **27**, 379-389.

[8] Garrett, M.D. and Collins, I. (2011) Anticancer Therapy with Checkpoint Inhibitors: What, Where and When? *Trends in Pharmacological Sciences*, **32**, 308-316. http://dx.doi.org/10.1016/j.tips.2011.02.014

[9] Borrelli, A., Schiattarella, A., Mancini, R., Morelli, F., Capasso, C., De Luca, V., Gori, E. and Mancini, A. (2011) The Leader Peptide of a Human rec. MnSOD as Molecular Carrier Which Delivers High Amounts of Cisplatin into Tumor Cells Inducing a Fast Apoptosis *in Vitro*. *International Journal of Cancer*, **128**, 453-459. http://dx.doi.org/10.1002/ijc.25334

[10] Smith, D.G., Magwere, T. and Burchill, S.A. (2011) Oxidative Stress and Therapeutic Opportunities: Focus on the Ewing's Sarcoma Family of Tumors. *Expert Review of Anticancer Therapy*, **11**, 229-249. http://dx.doi.org/10.1586/era.10.224

[11] Li, L., Ishdorj, G. and Gibson, S.B. (2012) Reactive Oxygen Species Regulation of Autophagy in Cancer: Implications for Cancer Treatment. *Free Radical Biology and Medicine*, **53**, 1399-1410. http://dx.doi.org/10.1016/j.freeradbiomed.2012.07.011

[12] Kukowska-Latallo, J.F., *et al.* (2005) Nanoparticle Targeting of Anticancer Drug Improves Therapeutic Response in Animal Model of Human Epithelial Cancer. *Cancer Research*, **65**, 5317-5324. http://dx.doi.org/10.1158/0008-5472.CAN-04-3921

[13] Roy, I., *et al.* (2003) Ceramic-Based Nanoparticles Entrapping Water-Insoluble Photosensitizing Anticancer Drugs: A Novel Drug-Carrier System for Photodynamic Therapy. *Journal of the American Chemical Society*, **125**, 7860-7865. http://dx.doi.org/10.1021/ja0343095

[14] Batrakova, E.V. and Kabanov, A.V. (2008) Pluronic Block Copolymers: Evolution of Drug Delivery Concept from Inert Nanocarriers to Biological Response Modifiers. *Journal of Controlled Release*, **130**, 98-106. http://dx.doi.org/10.1016/j.jconrel.2008.04.013

[15] Kratz, F. (2008) Albumin as a Drug Carrier: Design of Prodrugs, Drug Conjugates and Nanoparticles. *Journal of Controlled Release*, **132**, 171-183. http://dx.doi.org/10.1016/j.jconrel.2008.05.010

[16] Egusquiaguirre, S.P., Igartua, M., Hernández, R.M. and Pedraz, J.L. (2012) Nanoparticle Delivery Systems for Cancer Therapy: Advances in Clinical and Preclinical Research. *Clinical and Translational Oncology*, **14**, 83-93. http://dx.doi.org/10.1007/s12094-012-0766-6

[17] Wang, Q., Zhang, C., Shen, G., Liu, H., Fu, H. and Cui, D. (2014) Fluorescent Carbon Dots as an Efficient siRNA Nanocarrier for Its Interference Therapy in Gastric Cancer Cells. *Journal of Nanobiotechnology*, **12**, 58. http://dx.doi.org/10.1186/s12951-014-0058-0

[18] Wang, W., Liu, Z., Sun, P., Fang, C., Fang, H., Wang, Y., Ji, J. and Chen, J. (2015) RGD Peptides-Conjugated Pluronic Triblock Copolymers Encapsulated with AP-2α Expression Plasmid for Targeting Gastric Cancer Therapy *in Vitro* and *in Vivo*. *International Journal of Molecular Sciences*, **16**, 16263-16274. http://dx.doi.org/10.3390/ijms160716263

[19] Slowing, I.I., Vivero-Escoto, J.L., Wu, C.W. and Lin, V.S.-Y. (2008) Mesoporous Silica Nanoparticles as Controlled Release Drug Delivery and Gene Transfection Carriers. *Advanced Drug Delivery Reviews*, **60**, 1278-1288. http://dx.doi.org/10.1016/j.addr.2008.03.012

[20] Descalzo, A.B., Martínez-Máñez, R., Sancenon, F., Hoffmann, K. and Rurack, K. (2006) The Supramolecular Chemistry of Organic-Inorganic Hybrid Materials. *Angewandte Chemie International Edition*, **45**, 5924-5948. http://dx.doi.org/10.1002/anie.200600734

[21] Angelos, S., Liong, M., Choi, E. and Zink, J.I. (2008) Mesoporous Silicate Materials as Substrates for Molecular Machines and Drug Delivery. *Chemical Engineering Journal*, **137**, 4-13. http://dx.doi.org/10.1016/j.cej.2007.07.074

[22] Rosenholm, J.M., Sahlgren, C. and Linden, M. (2010) Towards Multifunctional, Targeted Drug Delivery Systems Using Mesoporous Silica Nanoparticles—Opportunities & Challenges. *Nanoscale*, **2**, 1870-1883. http://dx.doi.org/10.1039/c0nr00156b

[23] Kim, C., Song, H.M., Cai, X., Yao, J., Wei, A. and Wang, L.V. (2011) *In Vivo* Photoacoustic Mapping of Lymphatic Systems with Plasmon-Resonant Nanostars. *Journal of Materials Chemistry*, **21**, 2841-2844. http://dx.doi.org/10.1039/c0jm04194g

[24] Wang, S., Huang, P., Nie, L., Xing, R., Liu, D., Wang, Z., *et al.* (2013) Single Continuous Wave Laser Induced Photodynamic/Plasmonic Photothermal Therapy Using Photosensitizer-Functionalized Gold Nanostars. *Advanced Materials*, **25**, 3055-3061. http://dx.doi.org/10.1002/adma.201204623

[25] Chen, R., Wang, X., Yao, X., Zheng, X., Wang, J. and Jiang, X. (2013) Near-IR-Triggered Photothermal/Photodynamic Dual-Modality Therapy System via Chitosan Hybrid Nanospheres. *Biomaterials*, **34**, 8314-8322. http://dx.doi.org/10.1016/j.biomaterials.2013.07.034

[26] Kiruba Daniel, S.C.G., Kumar, R., Sathish, V., Sivakumar, M., Sunitha, S. and Anitha Sironmani, T. (2011) Green Synthesis (*Ocimum tenuiflorum*) of Silver Nanoparticles and Toxicity Studies in Zebra Fish (*Danio rerio*) Model. *International Journal of NanoScience and Nanotechnology*, **2**, 103-117.

[27] King, E.J. and Garner, R.J. (1947) The Colorimetric Determination of Glucose *Journal of Clinical Pathology*, **1**, 30. http://dx.doi.org/10.1136/jcp.1.1.30

[28] Bracken, J.S. and Klotz, I.M. (1953) A Simple Method for the Rapid Determination of Serum Albumin. *American Journal of Clinical Pathology*, **23**, 1055-1058.

[29] Beers Jr., R.F. and Sizer, I.W. (1952) A Spectrophotometric Method for Measuring the Breakdown of Hydrogen Peroxide by Catalase. *Journal of Biological Chemistry*, **195**, 133-140.

[30] Laemmli, U.K. (1970) Cleavage of Structural Proteins during the Assembly of the Head of Bacteriophage T4. *Nature*, **227**, 680-685. http://dx.doi.org/10.1038/227680a0

[31] Sahay, G., Alakhova, D.Y. and Kabanov, A.V. (2010) Endocytosis of Nanomedicines. *Journal of Controlled Release*, **145**, 182-195. http://dx.doi.org/10.1016/j.jconrel.2010.01.036

[32] Minko, T. (2004) Drug Targeting to the Colon with Lectins and Neoglycoconjugates. *Advanced Drug Delivery Reviews*, **56**, 491-509. http://dx.doi.org/10.1016/j.addr.2003.10.017

[33] Surh, Y.J. (2003) Cancer Chemoprevention with Dietary Phytochemicals. *Nature Reviews Cancer*, **3**, 768-780. http://dx.doi.org/10.1038/nrc1189

[34] Aggarwal, B.B. and Shishodia, S. (2006) Molecular Targets of Dietary Agents for Prevention and Therapy of Cancer. *Biochemical Pharmacology*, **71**, 1397-1421. http://dx.doi.org/10.1016/j.bcp.2006.02.009

[35] Hao, F., Kumar, S., Yadav, N. and Chandra, D. (2014) Neem Components as Potential Agents for Cancer Prevention and Treatment. *Biochimica et Biophysica Acta* (*BBA*)-*Reviews on Cancer*, **1846**, 247-257. http://dx.doi.org/10.1016/j.bbcan.2014.07.002

[36] Shankar, S.S., Rai, A., Ahmad, A. and Sastry, M. (2004) Rapid Synthesis of Au, Ag and Bimetallic Au Core-Ag Shell Nanoparticles Using Neem (*Azadirachta indica*) Leaf Broth. *Journal of Colloid and Interface Science*, **275**, 496-502. http://dx.doi.org/10.1016/j.jcis.2004.03.003

[37] Tripathy, A., Raichur, A.M., Chandrasekaran, N., Prathna, T.C. and Mukherjee, A. (2009) Process Variables in Biomimetic Synthesis of Silver Nanoparticles by Aqueous Extract of *Azadirachta indica* (Neem) Leaves. *Journal of Nanoparticle Research*, **12**, 237-246. http://dx.doi.org/10.1007/s11051-009-9602-5

[38] Kiruba Daniel, S.C.G., Anitha Sironmani, T., Tharmaraj, V. and Pitchumani, K. (2011) Synthesis and Characterization of Fluorophore Attached Silver Nanoparticles. *Bulletin of Materials Science*, **34**, 639-643. http://dx.doi.org/10.1007/s12034-011-0175-4

[39] Nimroth Ananth, A., Kiruba Daniel, S.C.G., Anitha Sironmani, T. and Umapathi, S. (2011) PVA and BSA Stabilized Silver Nanoparticles Based Surface-Enhanced Plasmon Resonance Probes for Protein Detection. *Colloids and Surfaces B*: *Biointerfaces*, **85**, 138-144. http://dx.doi.org/10.1016/j.colsurfb.2011.02.012

[40] Siddiqui, B.S., Afshan, F., Ghiasuddin, Faizi, S., Naqui, S.N.H. and Tariq, R.M. (2000) Two Insecticidal Tetranortriterpenoids from *Azadirachta indica*. *Phytochemistry*, **53**, 371-376. http://dx.doi.org/10.1016/S0031-9422(99)00548-8

[41] Anitha Sironmani, T. and Kiruba Daniel, S.C.G. (2011) Silver Nanoparticles—Universal Multifunctional Nanoparticles for Bio Sensing, Imaging for Diagnostics and Targeted Drug Delivery for Therapeutic Applications. In: Kapetanovic, I.M., Ed., *Drug Discovery and Development—Present and Future*, InTech Publishers. http://dx.doi.org/10.5772/27047

[42] Mukhopadhyay, A., Banerjee, S., Stafford, L.J., Xia, C., Liu, M. and Aggarwal, B.B. (2002) Curcumin-Induced Suppression of Cell Proliferation Correlates with Down-Regulation of Cyclin D1 Expression and CDK4-Mediated Retinoblastoma Protein Phosphorylation. *Oncogene*, **21**, 8852-8861. http://dx.doi.org/10.1038/sj.onc.1206048

[43] Bharti, A.C., Donato, N., Singh, S. and Aggarwal, B.B. (2003) Curcumin (Diferuloylmethane) Down-Regulates the Constitutive Activation of Nuclear Factor-*κ*B and I*κ*B*α* Kinase in Human Multiple Myeloma Cells, Leading to Suppression of Proliferation and Induction of Apoptosis. *Blood*, **101**, 1053-1062. http://dx.doi.org/10.1182/blood-2002-05-1320

[44] Morones, J.R., Elechiguerra, J.L., Camacho, A., Holt, K., Kouri, J.B., Ramírez, J.T. and Yacaman, M.J. (2005) The Bactericidal Effect of Silver Nanoparticles. *Nanotechnology*, **16**, 2346-2353. http://dx.doi.org/10.1088/0957-4484/16/10/059

[45] Lok, C., *et al.* (2006) Proteomic Analysis of the Most of Antibacterial Action of Silver Nanoparticles. *Journal of Proteomic Research*, **5**, 916-924. http://dx.doi.org/10.1021/pr0504079

[46] Lin, Y.E., Vidic, R.D., Strout, J.E., McCartney, C.A. and Yu, V.L. (199) Inactivation of *Mycobacterium avium* by Copper and Silver Ions. *Water Research*, **32**, 1997-2000.

[47] Siva Kumar, V., Nagaraja, B.M., Shaihikala, V., Padmarri, A.H., Madharendra, S.S., Raju, B.D. and Rama Rao, K.S. (2003) Highly Efficient Ag/C Catalyst Prepared and Electrochemical Deposition Method in Controlling Microorganisms in Water. *Journal of Molecular Catalysis A*: *Chemical*, **223**, 313-319. http://dx.doi.org/10.1016/j.molcata.2003.09.047

[48] Christensen, E. (1987) Multivariare Survival Analysis Using Cox's Regression Model. *Hepatology*, **7**, 1346-1358. http://dx.doi.org/10.1002/hep.1840070628

[49] Heys, S.D., Walker, L.G., Deehan, D.J. and Eremin, O.E. (1998) Serum Albumin: A Prognostic Indicator in Patients with Colorectal Cancer. *Journal of the Royal College of Surgeons of Edinburgh*, **43**, 163-168.

[50] Fleck, A., Hawker, F., Wallace, P.I., Raines, G., Trotter, J., Ledingham, I.M. and Calman, K.C. (1985) Increased Vascular Permeability: A Major Cause of Hypoalbuminaemia in Disease and Injury. *The Lancet*, **325**, 781-784. http://dx.doi.org/10.1016/S0140-6736(85)91447-3

[51] Barber, M.D., Ross, J.A. and Fearon, K.C. (1999) Changes in Nutritional, Functional, and Inflammatory Markers in Advanced Pancreatic Cancer. *Nutrition and Cancer*, **35**, 106-110. http://dx.doi.org/10.1207/S15327914NC352_2

[52] Oñate-Ocaña, L.F., Aiello-Crocifoglio, V., Gallardo-Rincón, D., Herrera-Goepfert, R., Brom-Valladares, R., Carrillo, J.F., Cervera, E. and Mohar-Betancourt, A. (2007) Serum Albumin as a Significant Prognostic Factor for Patients with Gastric Carcinoma. *Annals of Surgical Oncology*, **14**, 381-389. http://dx.doi.org/10.1245/s10434-006-9093-x

[53] Lis, C.G., Grutsch, J.F., Vashi, P.G. and Lammersfeld, C.A. (2003) Is Serum Albumin an Independent Predictor of Survival in Patients with Breast Cancer? *Journal of Parenteral & Enteral Nutrition*, **27**, 10-15. http://dx.doi.org/10.1177/014860710302700110

[54] Broom, I., *et al.* (1992) Interleukin 2 Therapy in Cancer: Identification of Responders. *British Journal of Cancer*, **66**, 1185-1187. http://dx.doi.org/10.1038/bjc.1992.433

[55] Simpson, W.G., Heys, S.D., Whiting, P.H., Eremin, O. and Broom, I. (1995) Acute Phase Proteins and Recombinant IL-2 Therapy: Prediction of Response and Survival in Patients with Colorectal Cancer. *Clinical & Experimental Immunology*, **99**, 143-147. http://dx.doi.org/10.1111/j.1365-2249.1995.tb05524.x

[56] Deehan, D.J., Heys, S.D., Simpson, W.G., Herriot, R., Broom, J. and Eremin, O. (1994) Correlation of Serum Cytokine and Acute Phase Reactant Levels with Alterations in Weight and Serum Albumin in Patients Receiving Immunotherapy with Recombinant IL-2. *Clinical & Experimental Immunology*, **95**, 366-372. http://dx.doi.org/10.1111/j.1365-2249.1994.tb07005.x

[57] Lai, W.W., Yang, J.S., Lai, K.C., Kuo, C.L., Hsu, C.K., Wang, C.K., *et al.* (2009) Rhein Induced Apoptosis through the Endoplasmic Reticulum Stress, Caspase- and Mitochondria-Dependent Pathways in SCC-4 Human Tongue Squamous Cancer Cells. *In Vivo*, **23**, 309-316.

[58] Ip, S.W., Weng, Y.S., Lin, S.Y., Mei, D., Tang, N.Y., Su, C.C. and Chung, J.G. (2007) The Role of Ca^{2+} on Rhein-Induced Apoptosis in Human Cervical Cancer Ca Ski Cells. *Anticancer Research*, **27**, 379-389.

[59] Standtman, E.R. and Berlett, B.S. (1997) Reactive Oxygen-Mediated Protein Oxidation in Aging and Disease. *Chemical Research in Toxicology*, **10**, 485-494. http://dx.doi.org/10.1021/tx960133r

[60] Butterfield, D.A. and Kanski, J. (2001) Brain Protein Oxidation in Age-Related Neurodegenerative Disorders That Are Associated with Aggregated Proteins. *Mechanisms of Ageing and Development*, **122**, 945-962. http://dx.doi.org/10.1016/S0047-6374(01)00249-4

[61] Poli, G., Leonarduzzi, G., Biasi, F. and Chiarpotto, E. (2004) Oxidative Stress and Cell Signaling. *Current Medical Chemistry*, **11**, 1163-1182. http://dx.doi.org/10.2174/0929867043365323

[62] Poon, H.F., Calabrese, V., Scapagnini, G. and Butterfield, D.A. (2004) Free Radicals and Brain Aging. *Clinics in Geriatric Medicine*, **20**, 329-359. http://dx.doi.org/10.1016/j.cger.2004.02.005

[63] Evans, M.D., Dizdaroglu, M. and Cooke, M.S. (2004) Oxidative DNA Damage and Disease: Induction, Repair and Significance. *Mutation Research/Reviews in Mutation Research*, **567**, 1-61. http://dx.doi.org/10.1016/j.mrrev.2003.11.001

[64] Crawford, D.R. (1999) Regulation of Mammalian Gene Expression by Reactive Oxygen Species. In: Gilbert, D.L. and Colton, C.A., Eds., *Reactive Oxygen Species in Biological Systems*: *An Interdisciplinary Approach*, Kluwer Academic Publishers, New York, 155-171.

[65] Shi, H., Hudson, L.G. and Liu, K.J. (2004) Oxidative Stress and Apoptosis in Metal Ion-Induced Carcinogenesis. *Free Radical Biology and Medicine*, **37**, 582-593. http://dx.doi.org/10.1016/j.freeradbiomed.2004.03.012

[66] Bodamyali, T., Stevens, C.R., Blake, D.R. and Winyard, P.G. (2000) Reactive Oxygen/Nitrogen Species and Acute Inflammation: A Physiological Process. In: Winyard, P.G., Blake, D.R. and Evans, C.H., Eds., *Free Radicals and Inflammation*, Springer, Basel, 11-16. http://dx.doi.org/10.1007/978-3-0348-8482-2_2

[67] Fu, P.P., Xia, Q., Sun, X. and Yu, H.T. (2012) Phototoxicity and Environmental Transformation of Polycyclic Aromatic Hydrocarbons (PAHs)—Light-Induced Reactive Oxygen Species, Lipid Peroxidation, and DNA Damage. *Journal of Environmental Science and Health*, *Part C*: *Environmental Carcinogenesis and Ecotoxicology Reviews*, **30**, 1-41. http://dx.doi.org/10.1080/10590501.2012.653887

[68] Xia, Q., Boudreau, M.D., Zhou, Y.T., Yin, J.-J. and Fu, P.P. (2011) UVB Photoirradiation of Aloe Vera—Formation of Free Radicals, Singlet Oxygen, Superoxide, and Induction of Lipid Peroxidation. *Journal of Food & Drug Analysis*, **19**, 396-402.

[69] Xia, Q., Chiang, H.M., Zhou, Y.T., *et al.* (2012) Phototoxicity of Kava—Formation of Reactive Oxygen Species Leading to Lipid Peroxidation and DNA Damage. *The American Journal of Chinese Medicine*, **40**, 1271-1288. http://dx.doi.org/10.1142/S0192415X12500942

[70] Xia, Q., Yin, J.J., Cherng, S.H., *et al.* (2006) UVA Photoirradiation of Retinyl Palmitate—Formation of Singlet Oxygen and Superoxide, and Their Role in Induction of Lipid Peroxidation. *Toxicology Letters*, **163**, 30-43. http://dx.doi.org/10.1016/j.toxlet.2005.09.010

[71] Xia, Q., Yin, J.J., Fu, P.P. and Boudreau, M.D. (2007) Photo-Irradiation of Aloe Vera by UVA—Formation of Free Radicals, Singlet Oxygen, Superoxide, and Induction of Lipid Peroxidation. *Toxicology Letters*, **168**, 165-175. http://dx.doi.org/10.1016/j.toxlet.2006.11.015

[72] Fu, P.P., Xia, Q.S., Hwang, H.-M., Ray, P.C. and Yu, H.T. (2014) Mechanisms of Nanotoxicity: Generation of Reactive Oxygen Species. *Journal of Food and Drug Analysis*, **22**, 64-75. http://dx.doi.org/10.1016/j.jfda.2014.01.005

[73] Nardone, G., Holicky, E.L., Uhl, J.R., Sabatino, L., Staibano, S., Rocco, A., Colantuoni, V., Manzo, B.A., Romano, M., Budillon, G., Cockerill III, F.R. and Miller, L.J. (2001) *In Vivo* and *In Vitro* Studies of Cytosolic Phospholipase A_2 Expression in *Helicobacter pylori* Infection. *Infection and Immunity*, **69**, 5857-5863. http://dx.doi.org/10.1128/IAI.69.9.5857-5863.2001

[74] Lupulescu, A. (1991) Vitamin C Inhibits DNA, RNA and Protein Synthesis in Epithelial Neoplastic Cells. *International Journal for Vitamin and Nutrition Research*, **61**, 125-129.

[75] Lupulescu, A. (1992) Ultrastructure and Cell Surface Studies of Cancer Cells Following Vitamin C Administration. *Experimental and Toxicologic Pathology*, **44**, 3-9.

[76] Waring, A.J. and Schorah, C.J. (1998) Transport of Ascorbic Acid in Gastric Epithelial Cells *in Vitro*. *Clinica Chimica Acta*, **275**, 137-149. http://dx.doi.org/10.1016/S0009-8981(98)00079-5

[77] Agus, D.B., Vera, J.C. and Golde, D.W. (1999) Stromal Cell Oxidation: A Mechanism by Which Tumors Obtain Vi-

tamin C. *Cancer Research*, **59**, 4555-4558.

[78] Karnoub, A.E., Dash, A.B., Vo, A.P., Sullivan, A., Brooks, M.W., Bell, G.W., Richardson, A.L., Polyak, K., Tubo, R. and Weinberg, R.A. (2007) Mesenchymal Stem Cells within Tumour Stroma Promote Breast Cancer Metastasis. *Nature*, **449**, 557-563. http://dx.doi.org/10.1038/nature06188

[79] Vermeulen, L., De Sousa E Melo, F., van der Heijden, M., Cameron, K., de Jong, J.H., Borovski, T., Tuynman, J.B., Todaro, M., Merz, C., Rodermond, H., Sprick, M.R., Kemper, K., Richel, D.J., Stassi, G. and Medema, J.P. (2010) Wnt Activity Defines Colon Cancer Stem Cells and Is Regulated by the Microenvironment. *Nature Cell Biology*, **12**, 468-476. http://dx.doi.org/10.1038/ncb2048

[80] Yauch, R.L., Gould, S.E., Scales, S.J., Tang, T., Tian, H., Ahn, C.P., Marshall, D., Fu, L., Januario, T., Kallop, D., Nannini-Pepe, M., Kotkow, K., Marsters, J, C., Rubin, L.L. and de Sauvage, F.J. (2008) A Paracrine Requirement for Hedgehog Signalling in Cancer. *Nature*, **455**, 406-410. http://dx.doi.org/10.1038/nature07275

[81] Dang, C.V. and Semenza, G.L. (1999) Oncogenic Alterations of Metabolism. *Trends in Biochemical Sciences*, **24**, 68-72. http://dx.doi.org/10.1016/S0968-0004(98)01344-9

[82] di Chiro, G., Brooks, R.A., Patronas, N.T., Bairamian, D., Kornblith, P.L., Smith, B.H., Mansi, L. and Barker, J. (1984) Issues in the *in Vivo* Measurement of Glucose Metabolism of Human Central Nervous System Tumors. *Annuals of Neurology*, **15**, S138-S146. http://dx.doi.org/10.1002/ana.410150727

[83] Padma, M.V., Said, S., Jacobs, M., Hwang, D.R., Dunigan, K., Satter, M., *et al.* (2003) Prediction of Pathology and Survival by FDG PET in Gliomas. *Journal of Neuro-Oncology*, **64**, 227-237. http://dx.doi.org/10.1023/A:1025665820001

[84] Spence, A.M., Muzi, M., Graham, M.M., O'Sullivan, F., Link, J.M., Lewellen, T.K., *et al.* (2002) 2-[(18)F]Fluoro-2-Deoxyglucose and Glucose Uptake in Malignant Gliomas before and after Radiotherapy: Correlation with Outcome. *Clinical Cancer Research*, **8**, 971-979.

[85] Weber, W.A. (2006) Positron Emission Tomography as an Imaging Biomarker. *Journal Clinical Oncology*, **24**, 3282-3292. http://dx.doi.org/10.1200/JCO.2006.06.6068

[86] Valko, M., Leibfritz, D., Moncol, J., Cronin, M.T.D., Mazur, M. and Telser, J. (2007) Free Radicals and Antioxidants in Normal Physiological Functions and Human Disease. *The International Journal of Biochemistry & Cell Biology*, **39**, 44-84. http://dx.doi.org/10.1016/j.biocel.2006.07.001

[87] Kim, B. and Lee, B.M. (1997) Oxidative Stress to DNA, Protein, and Antioxidant Enzymes (Superoxide Dismutase and Catalase) in Rats Treated with Benzo(a)pyrene. *Cancer Letters*, **113**, 205-212. http://dx.doi.org/10.1016/S0304-3835(97)04610-7

[88] Yuan, X., Zhou, Y., Wang, W., Li, J., Xie, G., Zhao, Y., Xu, D. and Shen, L. (2013) Activation of TLR4 Signaling Promotes Gastric Cancer Progression by Inducing Mitochondrial ROS Production. *Cell Death & Disease*, **4**, e794. http://dx.doi.org/10.1038/cddis.2013.334

[89] Sun, L., Niu, L., Zhu, X., Hao, J., Wang, P. and Wang, H. (2012) Antitumour Effects of a Protease Inhibitor, Nelfinavir, in Hepatocellular Carcinoma Cancer Cells. *Journal of Chemotherapy*, **24**, 161-166. http://dx.doi.org/10.1179/1973947812Y.0000000011

[90] Bagchi, D., Bagchi, M., Hassoun, E.A. and Stohs, S.J. (1996) Cadmium-Induced Excretion of Urinary Lipid Metabolites, DNA Damage, Glutathione Depletion, and Hepatic Lipid Peroxidation in Sprague-Dawley Rats. *Biological Trace Element Research*, **52**, 143-154. http://dx.doi.org/10.1007/BF02789456

[91] Bagchi, D., Bagchi, M., Stohs, S.J., Das, D.K., Ray, S.D., Kuszynski, C.A., Joshi, S.S. and Pruess, H.G. (2000) Free Radicals and Grape Seed Proanthocyanidin Extract: Importance in Human Health and Disease Prevention. *Toxicology*, **148**, 187-197. http://dx.doi.org/10.1016/S0300-483X(00)00210-9

[92] Trush, M.A. and Kensler, T.W. (1991) An Overview of the Relationship between Oxidative Stress and Chemical Carcinogenesis. *Free Radical Biology and Medicine*, **10**, 201-209. http://dx.doi.org/10.1016/0891-5849(91)90077-G

[93] Schreck, R., Meier, B., Männel, D.N., Dröge, W. and Baeuerle, P.A. (1992) Dithiocarbamates as Potent Inhibitors of Nuclear Factor Kappa B Activation in Intact Cells. *Journal of Experimental Medicine*, **175**, 1181-1194. http://dx.doi.org/10.1084/jem.175.5.1181

[94] Winrow, V.R., Winyard, P.G., Morris, C.J. and Blake, D.R. (1993) Free Radicals in Inflammation: Second Messengers and Mediators of Tissue Destruction. *British Medical Bulletin*, **49**, 506-522.

[95] Mohamed, M.M. and Sloane, B.F. (2006) Cysteine Cathepsins: Multifunctional Enzymes in Cancer. *Nature Reviews Cancer*, **6**, 764-775. http://dx.doi.org/10.1038/nrc1949

[96] Murphy, D.J., Junttila, M.R., Pouyet, L., Karnezis, A., Shchors, K., Bui, D.A., Brown-Swigart, L., Johnson, L. and Evan, G.I. (2008) Distinct Thresholds Govern Myc's Biological Output *in Vivo*. *Cancer Cell*, **14**, 447-457. http://dx.doi.org/10.1016/j.ccr.2008.10.018

[97] Kessenbrock, K., Plasks, V. and Werb, Z. (2010) Matrix Metalloproteinases: Regulators of the Tumor Microenviron-

ment. *Cell*, **141**, 52-67. http://dx.doi.org/10.1016/j.cell.2010.03.015

[98] López-Otín, C. and Hunter, T. (2010) The Regulatory Crosstalk between Kinases and Proteases in Cancer. *Nature Reviews Cancer*, **10**, 278-292. http://dx.doi.org/10.1038/nrc2823

[99] Tang, L. and Han, X. (2013) The Urokinase Plasminogen Activator System in Breast Cancer Invasion and Metastasis. *Biomedicine & Pharmacotherapy*, **67**, 179-182. http://dx.doi.org/10.1016/j.biopha.2012.10.003

[100] Paralkar, V.M., Vail, A.L., Grasser, W.A., *et al.* (1998) Cloning and Characterization of a Novel Member of the Transforming Growth Factor-*β*/Bone Morphogenetic Protein Family. *The Journal of Biological Chemistry*, **273**, 13760-13767. http://dx.doi.org/10.1074/jbc.273.22.13760

[101] Welsh, J.B., Sapinoso, L.M., Kern, S.G., *et al.* (2003) Large-Scale Delineation of Secreted Protein Biomarkers Overexpressed in Cancer Tissue and Serum. *Proceedings of the National Academy of Sciences of the United states of America*, **100**, 3410-3415. http://dx.doi.org/10.1073/pnas.0530278100

[102] Buckhaults, P., Rago, C., St. Croix, B., *et al.* (2001) Secreted and Cell Surface Genes Expressed in Benign and Malignant Colorectal Tumors. *Cancer Research*, **61**, 6996-7001.

[103] Choi, E.H., Kim, J., Kim, J.H., Kim, S.Y., Song, E.Y., Kim, J.W., Kim, S.Y., Yeom, Y., Kim, I.-H. and Lee, H.G. (2009) Upregulation of the Cysteine Protease Inhibitor, Cystatin SN, Contributes to Cell Proliferation and Cathepsin Inhibition in Gastric Cancer. *Clinica Chimica Acta*, **406**, 45-51. http://dx.doi.org/10.1016/j.cca.2009.05.008

[104] Stenman, U.H. (1990) Tumour-Associated Trypsin Inhibitor and Tumour-Associated Trypsin. *Scandinavian Journal of Clinical and Laboratory Investigation*, **50**, 93-101. http://dx.doi.org/10.1080/00365519009085805

[105] Paju, A., Vartiainen, J., Haglund, C., Itkonen, O., von Boguslawski, K., Leminen, A., Wahlström, T. and Stenman, U.H. (2004) Expression of Trypsinogen-1, Trypsinogen-2, and Tumor-Associated Trypsin Inhibitor in Ovarian Cancer: Prognostic Study on Tissue and Serum. *Clinical Cancer Research*, **10**, 4761-4768. http://dx.doi.org/10.1158/1078-0432.CCR-0204-03

[106] Lee, Y.-C., Pan, H.-W., Peng, S.-Y., Lai, P.-L., Kuo, W.-S., Ou, Y.-H. and Hsu, H.-C. (2007) Overexpression of Tumour-Associated Trypsin Inhibitor (TATI) Enhances Tumour Growth and Is Associated with Portal Vein Invasion, Early Recurrence and a Stage-Independent Prognostic Factor of Hepatocellular Carcinoma. *European Journal of Cancer*, **43**, 736-744. http://dx.doi.org/10.1016/j.ejca.2006.11.020

[107] Freeman, T.C., Playford, R.J., Quinn, C., Beardshall, K., Poulter, L., Young, J. and Calam, J. (1990) Pancreatic Secretory Trypsin Inhibitor in Gastrointestinal Mucosa and Gastric Juice. *Gut*, **31**, 1318-1323. http://dx.doi.org/10.1136/gut.31.11.1318

[108] Playford, R.J., Batten, J.J., Freeman, T.C., Beardshall, K., Vesey, D.A., Fenn, G.C., Baron, J.H. and Calam, J. (1991) Gastric Output of Pancreatic Secretory Trypsin Inhibitor Is Increased by Misoprostol. *Gut*, **32**, 1396-1400. http://dx.doi.org/10.1136/gut.32.11.1396

[109] Marchbank, T., Chinery, R., Hanby, A.M., Poulsom, R., Elia, G. and Playford, R.J. (1996) Distribution and Expression of Pancreatic Secretory Trypsin Inhibitor and Its Possible Role in Epithelial Restitution. *The American Journal of Pathology*, **148**, 715-722.

[110] Marchbank, T., Freeman, T.C. and Playford, R.J. (1998) Human Pancreatic Secretory Trypsin Inhibitor: Distribution, Actions and Possible Role in Mucosal Integrity and Repair. *Digestion*, **59**, 167-174. http://dx.doi.org/10.1159/000007485

[111] Wiksten, J.P., Lundin, J., Nordling, S., Kokkola, A., Stenman, U.H. and Haglund, C. (2005) High Tissue Expression of Tumour-Associated Trypsin Inhibitor (TATI) Associates with a More Favourable Prognosis in Gastric Cancer. *Histopathology*, **46**, 380-388. http://dx.doi.org/10.1111/j.1365-2559.2005.02073.x

[112] Darmoul, D., Marie, J.C., Devaud, H., Gratio, V. and Laburthe, M. (2001) Initiation of Human Colon Cancer Cell Proliferation by Trypsin Acting at Protease-Activated Receptor-2. *British Journal of Cancer*, **85**, 772-779. http://dx.doi.org/10.1054/bjoc.2001.1976

[113] Miyata, S., Koshikawa, N., Higashi, S., Miyagi, Y., Nagashima, Y., Yanoma, S., Kato, Y., Yasumitsu, H. and Miyazaki, K. (1999) Expression of Trypsin in Human Cancer Cell Lines and Cancer Tissues and Its Tight Binding to Soluble Form of Alzheimer Amyloid Precursor Protein in Culture. *The Journal of Biochemistry*, **125**, 1067-1076. http://dx.doi.org/10.1093/oxfordjournals.jbchem.a022388

[114] Vogelstein, B. and Kinzler, K.W. (1993) The Multistep Nature of Cancer. *Trends in Genetics*, **9**, 138-141. http://dx.doi.org/10.1016/0168-9525(93)90209-Z

[115] Beckman, R.A. and Loeb, L.A. (2006) Efficiency of Carcinogenesis with and without a Mutator Mutation. *Proceedings of the National Academy of Sciences of the United states of America*, **103**, 14140-14145. http://dx.doi.org/10.1073/pnas.0606271103

[116] Miyake, H., Hara, I., Arakawa, S. and Kamidono, S. (2000) Stress Protein GRP78 Prevents Apoptosis Induced by Calcium Ionophore, Ionomycin, but Not by Glycosylation Inhibitor, Tunicamycin, in Human Prostate Cancer Cells. *Jour-*

nal of Cellular Biochemistry, **77**, 396-408. http://dx.doi.org/10.1002/(SICI)1097-4644(20000601)77:3<396::AID-JCB5>3.0.CO;2-5

[117] Bang, Y.J., Van Cutsem, E., Feyereislova, A., *et al.* (2010) Trastuzumab in Combination with Chemotherapy versus Chemotherapy Alone for Treatment of HER2-Positive Advanced Gastric or Gastro-Oesophageal Junction Cancer (ToGA): A Phase 3, Open-Label, Randomised Controlled Trial. *The Lancet*, **376**, 687-697. http://dx.doi.org/10.1016/S0140-6736(10)61121-X

[118] Yan, B., Yau, E.X., Bte Omar, S.S., *et al.* (2010) A Study of HER2 Gene Amplification and Protein Expression in Gastric Cancer. *Journal of Clinical Pathology*, **63**, 839-842. http://dx.doi.org/10.1136/jcp.2010.076570

[119] Bhatt, A.N., Mathur, R., Farooque, A., Verma, A. and Dwarakanath, B.S. (2010) Cancer Biomarkers—Current Perspectives. *The Indian Journal of Medical Research*, **132**, 129-149.

[120] Han, S.S., Chung, S.T., Robertson, D.A., Ranjan, D. and Bondada, S. (1999) Curcumin Causes the Growth Arrest and Apoptosis of B Cell Lymphoma by Downregulation of *egr*-1, C-*myc*, *Bcl*-XL, NF-*κ*B, and p53. *Clinical Immunology*, **93**, 152-161. http://dx.doi.org/10.1006/clim.1999.4769

[121] Chirwa, N., Govender, D., Ndimba, B., Lotz, Z., Tyler, M., Panieri, E., Kahn, D. and Mall, A.S. (2012) A 40 - 50 kDa Glycoprotein Associated with Mucus Is Identified as *α*-1-Acid Glycoprotein in Carcinoma of the Stomach. *Journal of Cancer*, **3**, 83-92. http://dx.doi.org/10.7150/jca.3737

[122] Yeo, M., Kim, D.K., Park, H.J., Cho, S.W., Cheong, J.Y. and Lee, K.J. (2008) Retraction: Blockage of Intracellular Proton Extrusion with Proton Pump Inhibitor Induces Apoptosis in Gastric Cancer. *Cancer Science*, **99**, 185.

[123] Basque, J.R., Chénard, M., Chailler, P. and Ménard, D. (2001) Gastric Cancer Cell Lines as Models to Study Human Digestive Functions. *Journal of Cellular Biochemistry*, **81**, 241-251. http://dx.doi.org/10.1002/1097-4644(20010501)81:2<241::AID-JCB1039>3.0.CO;2-B

[124] Chailler, P., Beaulieu, J.F. and Ménard, D. (2012) Isolation and Functional Studies of Human Fetal Gastric Epithelium in Primary Culture. In: Mitry, R.R. and Hughes, R.D., Eds., *Human Cell Culture Protocols*, Humana Press, New York, 137-155. http://dx.doi.org/10.1007/978-1-61779-367-7_10

[125] Basque, J.R. and Ménard, D. (2000) Establishment of Culture Systems of Human Gastric Epithelium for the Study of Pepsinogen and Gastric Lipase Synthesis and Secretion. *Microscopy Research and Technique*, **48**, 293-302. http://dx.doi.org/10.1002/(SICI)1097-0029(20000301)48:5<293::AID-JEMT6>3.0.CO;2-A

[126] El-Deeb, N.M., El-Sherbiny, I.M., El-Aassara, M.R. and Hafez, E.E. (2015) Novel Trend in Colon Cancer Therapy Using Silver Nanoparticles Synthesized by Honey Bee. *Journal of Nanomedicine & Nanotechnology*, **6**, 265.

[127] Bhol, K.C., Alroy, J. and Schechter, P.J. (2004) Anti-Inflammatory Effect of Topical Nanocrystalline Silver Cream on Allergic Contact Dermatitis in a Guinea Pig Model. *Clinical and Experimental Dermatology*, **29**, 282-287. http://dx.doi.org/10.1111/j.1365-2230.2004.01515.x

[128] Bhol, K.C. and Schechter, P.J. (2007) Effects of Nanocrystalline Silver (NPI 32101) in a Rat Model of Ulcerative Colitis. *Digestive Diseases and Sciences*, **52**, 2732-2742. http://dx.doi.org/10.1007/s10620-006-9738-4

[129] Zucker, S. and Vacirca, J. (2004) Role of Matrix Metalloproteinases (MMPs) in Colorectal Cancer. *Cancer and Metastasis Reviews*, **23**, 101-117. http://dx.doi.org/10.1023/A:1025867130437

[130] Bettegowda, C., Sausen, M.R., Leary, J., Kinde, I.Y., Wang, Y., *et al.* (2014) Detection of Circulating Tumor DNA in Early- and Late-Stage Human Malignancies. *Science Translational Medicine*, **6**, 224ra24. http://dx.doi.org/10.1126/scitranslmed.3007094

[131] Cross, C.E., Halliwell, B., Borish, E.T., Pryor, W.A., Ames, B.N., Saul, R.L., McCord, J.M. and Harman, D. (1987) Oxygen Radical and Human Disease. *Annuals of Internal Medicine*, **107**, 526-545. http://dx.doi.org/10.7326/0003-4819-107-4-526

[132] Sun, Y. (1990) Free Radicals, Antioxidant Enzymes and Carcinogenesis. *Free Radical Biology & Medicine*, **8**, 583-599.

[133] Casado, A., Torre, R., Fernhdez, M.E.L., Carrascosa, D., Casado, M.C. and Ramirez, M.V. (1995) Superoxide Dismutase and Catalase Blood Levels in Patients with Malignant Diseases. *Cancer Letters*, **93**, l87-192. http://dx.doi.org/10.1016/0304-3835(95)03808-A

[134] Azad, M.B., Chen, Y. and Gibson, S.B. (2009) Regulation of Autophagy by Reactive Oxygen Species (ROS): Implications for Cancer Progression and Treatment. *Antioxidants & Redox Signaling*, **11**, 777-790. http://dx.doi.org/10.1089/ars.2008.2270

[135] Ortega, A.L., Mena, S. and Estrela, J.M. (2011) Glutathione in Cancer Cell Death. *Cancers*, **3**, 1285-1310. http://dx.doi.org/10.3390/cancers3011285

[136] Kemik, O., Kemik, A., Sümer, A., Almali, N., Gurluler, E., Gures, N., Purisa, S., Adas, G., Dogan, Y. and Tuzun, S. (2013) The relationship between serum tumor-associated trypsin inhibitor levels and clinicopathological parameters in patients with gastric cancer. *European Review in Medical Pharmacological Science*, **17**, 2923-2928.

[137] Eid, M.A., Lewis, R.W., Abdel-Mageed, A.B. and Kumar, M.V. (2002) Reduced Response of Prostate Cancer Cells to TRAIL Is Modulated by NFkappaB-Mediated Inhibition of Caspases and Bid Activation. *International Journal of Oncology*, **21**, 111-117.

[138] Choi, H.S., Seo, H.S., Kim, J.H., Um, J.Y., Shin, Y.C. and Ko, S.G. (2012) Ethanol Extract of Paeonia Suffruticosa Andrews (PSE) Induced AGS Human Gastric Cancer Cell Apoptosis via fas-Dependent Apoptosis and MDM2-p53 Pathways. *Journal of Biomedical Sciences*, **19**, 82. http://dx.doi.org/10.1186/1423-0127-19-82

[139] Mouria, M., Gukovskaya, A.S., Jung, Y., Buechler, P., Hines, O.J., Reber, H.A. and Pandol, S.J. (2002) Food-Derived Polyphenols Inhibit Pancreatic Cancer Growth through Mitochondrial Cytochrome C Release and Apoptosis. *International Journal of Cancer*, **98**, 761-769. http://dx.doi.org/10.1002/ijc.10202

[140] Han, M.H., Lee, W.S., Jung, J.H., Jeong, J.H., Park, C., Kim, H.J., Kim, G., Jung, J.M., Kwon, T.K., Kim, G.Y., *et al.* (2013) Polyphenols Isolated from *Allium cepa* L. Induces Apoptosis by Suppressing IAP-1 through Inhibiting PI3K/Akt Signaling Pathways in Human Leukemic Cells. *Food and Chemical Toxicology*, **62**, 382-389. http://dx.doi.org/10.1016/j.fct.2013.08.085

[141] Burk, D. and Woods, M. (1963) Hydrogen Peroxide, Catalase, Glutathione Peroxidase, Quinones, Nordihydroguaiaretic Acid, and Phosphopyridine Nucleotides in Relation to X-Ray Action on Cancer Cells. *Radiation Research Supplement*, **3**, 212-246. http://dx.doi.org/10.2307/3583686

[142] Mehta, K., Pantazis, P., McQueen, T. and Aggarwal, B.B. (1997) Antiproliferative Effect of Curcumin (Diferuloylmethane) against Human Breast Tumor Cell Lines. *Anti-Cancer Drugs*, **8**, 470-481. http://dx.doi.org/10.1097/00001813-199706000-00010

[143] Mulik, R.S., Monkkonen, J., Juvonen, R.O., Mahadik, K.R. and Paradkar, R. (2012) ApoE3 Mediated Polymeric Nanoparticles Containing Curcumin: Apoptosis Induced *in Vitro* Anti-Cancer Activity against Neuroblastoma Cells. *International Journal of Pharmaceutics*, **437**, 29-41. http://dx.doi.org/10.1016/j.ijpharm.2012.07.062

[144] Farokhzad, O.C., *et al.* (2006) Targeted Nanoparticle-Aptamer Bioconjugates for Cancer Chemotherapy *in Vivo*. *Proceedings of the National Academy of Sciences of the United States of America*, **103**, 6315-6320. http://dx.doi.org/10.1073/pnas.0601755103

[145] Raffaghello, L., Zuccari, G., Carosio, R., Orienti, I. and Montaldo, P.G. (2006) *In Vitro* and *In Vivo* Antitumor Activity of the Novel Derivatized Polyvinyl Alcohol-Based Polymer P10(4). *Clinical Cancer Research*, **12**, 3485-3493. http://dx.doi.org/10.1158/1078-0432.CCR-05-2318

[146] Huang, X. and El-Sayed, M.A. (2010) Gold Nanoparticles: Optical Properties and Implementations in Cancer Diagnosis and Photothermal Therapy. *Journal of Advanced Research*, **1**, 13-28. http://dx.doi.org/10.1016/j.jare.2010.02.002

[147] Moorthi, C. and Kathiresan, K. (2013) Curcumin-Piperine/Curcumin-Quercetin/Curcumin-Silibinin Dual Drug-Loaded Nanoparticulate Combination Therapy: A Novel Approach to Target and Treat Multidrug-Resistant Cancers. *Journal of Medical Hypotheses and Ideas*, **7**, 15-20. http://dx.doi.org/10.1016/j.jmhi.2012.10.005

[148] Kiruba Daniel, S.C.G., Tharmaraj, V., Anitha Sironmani, T. and Pitchumani, K. (2010) Toxicity and Immunological Activity of Silver Nanoparticles. *Applied Clay Science*, **48**, 547-551. http://dx.doi.org/10.1016/j.clay.2010.03.001

[149] Kiruba Daniel, S.C.G., Ayyappan, S., Philiphan, N.J.P., Sivakumar, M., Menaga, G. and Anitha Sironmani, T. (2011) Green Synthesis and Transfer of Silver Nanoparticles in a Food Chain through *Chiranamous larva* to Zebra Fish—A New Approach for Therapeutics. *International Journal of Nanoscience and Nanotechnology*, **2**, 159-169.

[150] Anitha Sironmani, T. (2014) Comparison of Nanocarriers for Gene Delivery and Nanosensing Using Montmorillonite, Silver Nanoparticles and Multiwalled Carbon Nanotubes. *Applied Clay Science*, **103**, 55-61. http://dx.doi.org/10.1016/j.clay.2014.11.004

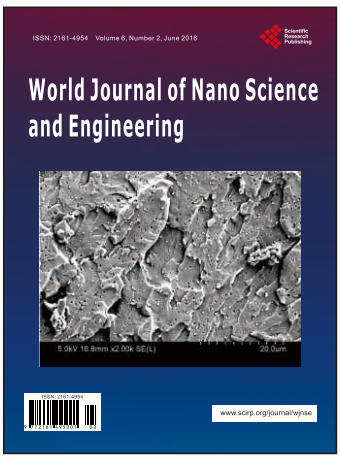

Call for Papers

World Journal of Nano Science and Engineering

ISSN 2161-4954 (Print) ISSN 2161-4962 (Online)
http://www.scirp.org/journal/wjnse

The World Journal of Nano Science and Engineering contains original and innovative research pertaining to the applications of the physical, chemical and biological sciences to engineering at nano scale. The highest priority is given to scientific research that transcends the classical boundaries and introduces cutting-edge frontiers.

Subject Coverage

This journal invites original research and review papers that address the following issues. Fields of interest include, but are not limited to:

- Computational Nanotechnology
- Energy at the Nanoscale
- Molecular Nanotechnology
- Molecular Self-Assembly
- Nanobiotechnology
- Nanodevices
- Nanoelectronics
- Nanoengineering
- Nanolithography
- Nanomachining
- Nanomaterials
- Nanomedicine
- Nano-Optics
- Nanophysics

We are also interested in short papers (letters) that clearly address a specific problem, and short survey or position papers that sketch the results or problems on a specific topic. Authors of selected short papers would be invited to write a regular paper on the same topic for future issues of World Journal of Nano Science and Engineering.

Notes for Intending Authors

Submitted papers should not have been previously published nor be currently under consideration for publication elsewhere. Paper submission will be handled electronically through the website. All papers are refereed through a peer review process. For more details about the submissions, please access the website.

Website and E-mail

http://www.scirp.org/journal/wjnse **E-mail: wjnse@scirp.org**

What is SCIRP?

Scientific Research Publishing (SCIRP) is one of the largest Open Access journal publishers. It is currently publishing more than 200 open access, online, peer-reviewed journals covering a wide range of academic disciplines. SCIRP serves the worldwide academic communities and contributes to the progress and application of science with its publication.

What is Open Access?

All original research papers published by SCIRP are made freely and permanently accessible online immediately upon publication. To be able to provide open access journals, SCIRP defrays operation costs from authors and subscription charges only for its printed version. Open access publishing allows an immediate, worldwide, barrier-free, open access to the full text of research papers, which is in the best interests of the scientific community.

- High visibility for maximum global exposure with open access publishing model
- Rigorous peer review of research papers
- Prompt faster publication with less cost
- Guaranteed targeted, multidisciplinary audience

Scientific Research Publishing

Website: http://www.scirp.org

Subscription: sub@scirp.org

Advertisement: service@scirp.org